

Bifunctional Roles for Two Topological Isoforms of the Cellular Prion Protein

Inaugural-Dissertation

zur

Erlangung des Doktorgrades

der Mathematisch-Naturwissenschaftlichen Fakultät

der Universität zu Köln

vorgelegt von

Sam Saghafi

aus London, GB

San Francisco, 2007

Berichterstatter:

Prof. Dr. Jonathan Howard

Prof. Dr. Thomas Langer

Prof. Dr. Vishwanath Lingappa

Tag der mündlichen Prüfung: 14. Januar 2008

1. Abbreviations	6
2. Introduction	10
2.1 Distinctive roles for PrP ^{Sc} and PrP ^C in prion disease	10
2.2 PrP ^C plays a central role in prion disease pathogenesis	13
2.3 Physiological functions of PrP ^C	14
2.4 Secretory protein biogenesis.....	16
2.5 Quality control mechanisms of protein folding in the secretory pathway	18
2.6 PrP biogenesis and topological heterogeneity	19
2.7 Detecting topological isoforms of PrP	22
2.8 A hypothesis driven study	24
3. Material and Methods	25
3.1 Reagents.....	25
3.2 General procedures	25
3.3 DNA constructs.....	26
3.4 Transgenic mice.....	26
3.5 Inoculation of mice with Sc237 prions	28
3.6 Biochemical analysis of PrP ^C topology in mouse brains	29
3.7 Enhanced detection of C tm PrP in brain homogenates	31
3.8 Glycan maturation analysis of C tm PrP and Sec ^{PrP}	32
3.9 Biochemical detection of PrP ^{Sc}	33
3.10 Measurement of lipid peroxidation in brain homogenates	33
3.11 Analysis of PrP topology in transfected CHO-K1 cells	34
3.12 TUNEL and caspase-3 analysis of transfected CHO-K1 cells	35
3.13 TUNEL analysis of transfected CHO-K1 cells treated with caspase-3 and Bax inhibitors	36
3.14 TUNEL analysis of transfected CHO-K1 cells overexpressing Bcl-2 or Bcl-XL	37
3.15 Viability analysis of Sec ^{PrP} mediated protection to oxidative stress in cultured cells	37
3.16 TUNEL IHC of murine brains	38
3.17 Activated caspase-3 IHC.....	39

3.18 8-hydroxy-2-deoxyguanosine (8-OHdG) IHC	40
3.19 Detection of PrP ^{Sc} by IHC	41
3.20 Internucleosomal DNA -fragmentation analysis	42
3.21 KA treatment and TUNEL analysis of transgenic mice	43
3.22 KA treatment and TUNEL analysis of primary cerebellar granule cell neurons	43
3.23 Image and data analysis	44
3.24 Multi-sequence alignment and dot-plot analysis.....	46
4. Results	47
4.1 Evolutionary analysis of topogenic domains of PrP	47
4.2 PrP ^C is expressed as both ^{Ctm} PrP and ^{Sec} PrP under non-pathologic conditions <i>in vivo</i>	49
4.3 ^{Sec} PrP and ^{Ctm} PrP are recognized as physiologically folded forms.....	52
4.4 Pathologic apoptosis results from ^{Ctm} PrP expression	54
4.5 Physiologic apoptosis as a result of ^{Ctm} PrP expression	57
4.6 Neurodegeneration and ^{Ctm} PrP induction in PrP ^C overexpressing Tg(tTA:mPrP) mice.....	59
4.6.1 Neurodegeneration and apoptosis in Tg(tTA:mPrP) mice	59
4.6.2 Dramatic ^{Ctm} PrP expression in brains of Tg(tTA:mPrP) mice.....	62
4.7 A cell culture model system: ^{Ctm} PrP triggers apoptosis in a dose-dependent manner.....	65
4.8 Characterization of the apoptotic pathway triggered by ^{Ctm} PrP: caspase-3 and Bax dependence	67
4.9 ^{Sec} PrP protects cultured cells from ROS	70
4.10 ^{Sec} PrP protects primary cultured neurons from ROS.....	71
4.11 A model system to probe both PrP ^C functions <i>in vivo</i> : kainic acid-mediated neurodegeneration.....	73
4.12 Probing the bifunctional hypothesis: Infectious prion disease and the role of topology	77
4.13 Gain and loss of PrP ^C functions: Oxidative stress and apoptosis in prion infected mice ..	80
5. Discussion	83
5.1 Conservation of PrP ^C synthesis in multiple topological isoforms	83
5.2 PrP ^C is synthesized as both ^{Sec} PrP and ^{Ctm} PrP under physiological conditions	84

Table of contents

5.3 ^{Ctm} PrP dependent pathophysiological apoptosis	85
5.4 ^{Ctm} PrP dependent physiological apoptosis.....	87
5.5 ^{Sec} PrP protects cells from ROS-mediated cell death.....	88
5.6 Gain and loss of PrP ^C mediated functions in non-Tg wt mice.....	89
5.7 Gain of ^{Ctm} PrP function and loss of ^{Sec} PrP function in transmissible prion disease.....	90
5.8 Bifunctional physiological roles for PrP ^C	93
5.9 Proposed novelties of this study	93
5.10 The world of PrP ^C heterogeneity.....	96
5.11 Protein heterogeneity: A new paradigm?.....	98
6. Summary.....	99
7. Zusammenfassung.....	101
8. References.....	103
9. Acknowledgements.....	125
10. Erklärung	127
11. Lebenslauf	129

1. Abbreviations

8-OHdG	8-hydroxy-2-deoxyguanosine
AR	autoradiography
Bax	Bcl-2-associated x protein
Bcl-2	B-cell lymphoma-2
Bcl-xl	B-cell lymphoma XL
BH2	Bcl-2 homology 2
BIP	binding protein
BME	2-mercaptoethanol
bp	basepair
BSA	bovine serum albumine
C1	proteolytic fragment of PrP ^C
CHO-K1	Chinese hamster ovary cells
CMV	cytomegalo virus
CNS	central nervous system
CO ₂	carbon dioxide
C tm PrP	C-terminal transmembrane PrP (Type II)
DAB	diamino benzidine
DNA	deoxyribonucleic acid
Dox	doxycycline
DTT	dithiothreitol
EDTA	ethylene-diamine-tetra-acetic acid
Endo H	endoglycosidase H

ER	endoplasmatic reticulum
ERAD	ER-associated degradation
FBS	fetal bovine serum
GAPDH	glyceraldehyde 3-phosphate dehydrogenase
GCL	granule cell layer
GCN	granule cell neurons
GPI	glycosylphosphatidyl inositol
GRP94	glucose response protein 94 kD
H ₂ O	water
HEPES	4-(2-hydroxyethyl)-1-piperazineethanesulfonic acid
HRP	horseradish peroxidase
ICC	immunocytochemistry
IgG	immunoglobulin G
IHC	immunohistochemistry
IP	immunoprecipitation
KA	kainic acid
kD	kilo Dalton
KH→II	SHaPrP, K110I, H111I
mAb	monoclonal antibody
MDA	malondialdehyde
mPrP	mouse PrP
NGS	normal goat serum
N tm PrP	N-terminal transmembrane PrP (Type I)

OR	octarepeat
P	postnatal
PAGE	polyacrylamide gel-electrophoresis
PBS	phosphate-buffered saline
PBST	PBS with Tween-20
PCR	polymerase chain reaction
PI	propidium iodide
PK	proteinase K
PMSF	phenylmethylsulfonyl fluoride
<i>Prnp</i>	PrP gene
<i>Prnp</i> ^{-/-}	PrP knockout mice
PrP	prion protein
PrP ^C	cellular prion protein
PrP ^{Sc}	disease causing PrP
ROS	reactive oxygen species
RT	room temperature
SDS	sodium dodecyl sulfate
^{Sec} PrP	secretory PrP
SHaPrP	Syrian hamster PrP
SRP	signal recognition particle
SS	signal sequence
STE	stop transfer effector
TCA	tri-chlor-acetate

Tg	transgenic
TM	transmembrane
TRAM	translocation chain-associated membrane protein
TRAP	tranlocon-associated protein
TRE	tetracycline response element
TRIS	tris-(hydroxymethyl)-aminomethane
tTA	tetracycline transactivator
TUNEL	terminal UDP-mediated nick end labeling
UPS	ubiquitin proteasome system
v/v	volume/ volume
w/v	weight/ volume
wt	wild type
ΔSTE	SHaPrP, Δ104-113

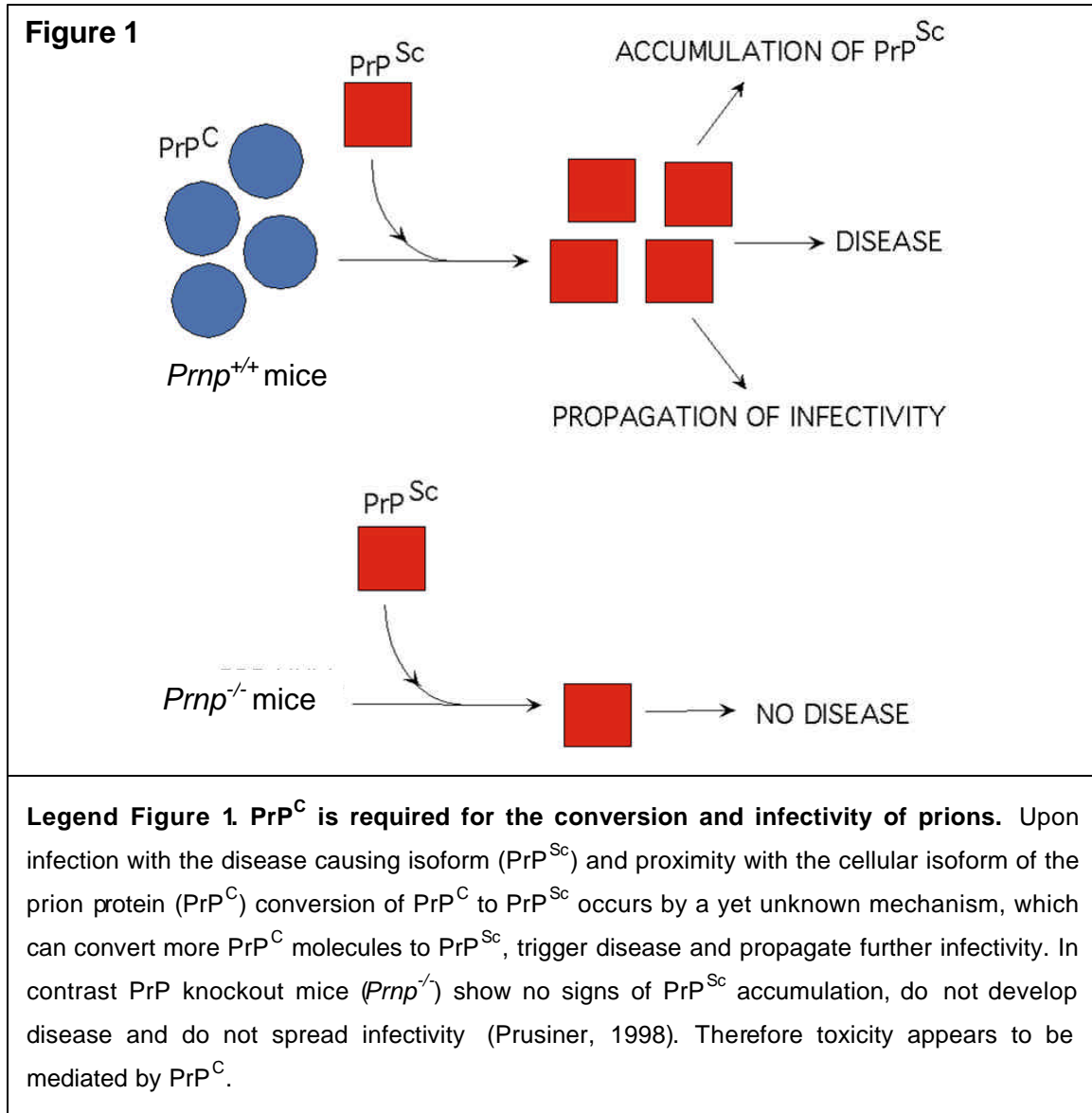
2. Introduction

Prions came to prominence for their involvement in transmissible neurodegenerative disorders including scrapie in sheep and Creutzfeld-Jacob Disease and Kuru in humans (Prusiner, 1998). Interest was further heightened by the development of bovine spongiform encephalitis (BSE) in the United Kingdom which was caused by prion-contaminated bone meal (Kimberlin, 1991; Wilesmith *et al.*, 1991). Prions are proteinaceous infectious particles that are devoid of nucleic acids (Kellings *et al.*, 1992; Kellings *et al.*, 1994; Safar *et al.*, 2005) yet retain and transfer biological information in form of conformation in a non-mendelian fashion causing fatal neurodegenerative disease in mammals. Prion diseases may have an infectious, genetic or sporadic etiology (Prusiner, 1998) that result from changes in the conformation of the normal cellular prion protein (PrP^{C} ; Weissmann, 2004). Great progress has been made in understanding the basis for prion infectivity and conversion to the pathogenic conformation (Prusiner *et al.*, 1998), however very little is understood about the mechanisms that underlie the pathogenesis process.

2.1 Distinctive roles for PrP^{Sc} and PrP^{C} in prion disease

Upon infection with the disease-causing isoform termed PrP^{Sc} , host encoded PrP^{C} which is expressed at high levels in the central nervous system (CNS; Kretschmar *et al.*, 1986) is converted to PrP^{Sc} which in turn stimulates conversion of further PrP^{C} molecules leading to the accumulation of PrP^{Sc} in the CNS (Figure 1; Prusiner, 1998). Two key biochemical properties of prions appear

to be crucial for the manifestation of its infectious nature: First, the extreme conformational stability of PrP^{Sc} makes it highly resistant to chemical, heat or enzymatic degradation thereby facilitating PrP^{Sc} accumulation (Riesner, 2003).



The methods established for the detection of PrP^{Sc} and the discrimination from PrP^C exploit this conformational stability as PrP^{Sc} withstands harsh proteolysis (Caughey *et al.*, 1990) and formic acid treatment (Kitamoto *et al.*, 1987). Second, the ability of PrP^{Sc} to direct the conversion of PrP^C to further PrP^{Sc} molecules

ensures that once even a few PrP^{Sc} molecules reach the host CNS, disease can unfold (Prusiner, 1998). The rate of PrP^{Sc} accumulation and the onset of disease depends on various factors such as host PrP^C expression level (Bueler *et al.*, 1994), titer of PrP^{Sc} inoculum (De Armond *et al.*, 1989), species of host and donor PrP (Bruce *et al.*, 1994), variants of PrP^{Sc} known as strains (Aguzzi *et al.*, 2007) and other less well understood genetic factors (Carlson *et al.*, 1986; Westaway *et al.*, 1987).

Despite the overwhelming evidence in support for the central role of PrP^{Sc} in the infectivity process of prion diseases, evidence suggests that PrP^{Sc} does not itself cause disease directly. Host encoded PrP^C is required for the pathogenesis process as evidenced in PrP knockout mice (*Prnp*^{-/-}) which are immune to infection with PrP^{Sc} (Bueler *et al.*, 1993; Sailer *et al.*, 1994). Transplantation studies with brain tissue from *Prnp*^{+/+} infected donor animals to *Prnp*^{-/-} recipient mice identified pathologic changes only in transplanted cells expressing PrP^C (Blattler *et al.*, 1997). Furthermore, transgenic mice expressing a soluble form of PrP^C lacking the glycosylphosphatidylinositol (GPI) anchor sequence on a *Prnp*^{-/-} background inoculated with prions revealed that conversion and accumulation of PrP^{Sc} in the CNS was not greatly altered, however the onset of symptoms and pathogenesis were vastly delayed (Chesebro *et al.*, 2005). Finally, spatial and temporal correlations between PrP^{Sc} accumulation and neuropathological changes are weak or lacking (Tremblay *et al.*, 1998; Chiesa *et al.*, 2000; Mallucci *et al.*, 2003). All these data indicate that PrP^{Sc} is central to the propagation of infectivity but it is only indirectly involved in disease pathogenesis.

2.2 PrP^C plays a central role in prion disease pathogenesis

Several models have been proposed by which PrP^C can cause neurodegeneration (Wong *et al.*, 2000; Chiesa & Harris, 2001; LeBlanc & Roucou, 2003; Harris & True, 2006). A group of studies suggests that PrP^C normally exerts a neuroprotective function by protecting cells from oxidative stress. Upon infection this function is lost causing increased oxidative stress mediated damage (Milhavet *et al.*, 2000; Wong *et al.*, 2001; Brown, 2005). Consistent with this loss of function hypothesis it has been shown that mice and humans infected with prions reveal increased oxidative stress in brain regions with PrP^{Sc} deposits (Guentchev *et al.*, 2000; Guentchev *et al.*, 2002). It remains however unresolved why *Prnp*^{-/-} mice show no phenotype (Bueler *et al.*, 1992; Manson *et al.*, 1994) if a loss of PrP^C function is the cause of disease.

Also a model by which PrP^C leads to toxicity mediated by a gain of function has been proposed (Chiesa & Harris, 2001; Harris & True, 2006). The induction of a transmembrane form of PrP, termed ^{Ctm}PrP, during prion disease has been implicated in PrP^C-mediated neurotoxicity (Hegde *et al.*, 1998a; Hegde *et al.*, 1999; Stewart *et al.*, 2005). Two lines of evidence suggest ^{Ctm}PrP expression is a determinant of pathogenesis in infectious prion disease. First, the time point of disease onset upon inoculation with prions inversely correlates with the absolute amount of ^{Ctm}PrP expressed in the murine brain. Higher levels of constitutive ^{Ctm}PrP expression at the time point of infection relate to shorter incubation periods (Hegde *et al.*, 1999). Second, upon infection with PrP^{Sc}, an increase in ^{Ctm}PrP expression was detected which closely followed the time course of

pathogenesis (Hegde *et al.*, 1999). Increased expression of ^{Ctm}PrP has been also associated with Gerstmann-Straussler-Scheinker syndrome (GSS) - a human genetic prion disease - where an alanine to valine substitution at amino acid residue 117 (A117V) of PrP renders the potential transmembrane domain of PrP more hydrophobic increasing the propensity of nascent PrP chains to be synthesized during cotranslational translocation in the ^{Ctm}PrP isoform (Hegde *et al.*, 1998a). In conclusion, there is evidence that PrP^C plays a role in the pathogenesis of prion diseases however it remains unclear whether this is due to a loss of protective PrP^C function or a gain of a PrP^C mediated toxic function.

2.3 Physiological functions of PrP^C

While the establishment of $Prnp^{-/-}$ mice has been very valuable for understanding the role of PrP^C in the transmission of prion disease, these mice have been somewhat disappointing in regard to understanding the normal cellular function of PrP^C . $Prnp^{-/-}$ mice seem to develop normally (Bueler *et al.*, 1992; Manson *et al.*, 1994) and show only limited phenotypes such as mild alterations in sleep pattern (Tobler *et al.*, 1997) or synaptic transmission (Collinge *et al.*, 1994; Curtis *et al.*, 2003; Maglio *et al.*, 2004) although this last function has not been observed by all (Lledo *et al.*, 1996). The lack of an obvious phenotype in $Prnp^{-/-}$ mice is puzzling in light of the strong conservation of PrP across mammalian species (van Rheede *et al.*, 2003). Perhaps the normal function of PrP^C is so important that it has a redundant backup mechanism which takes over in $Prnp^{-/-}$

mice. Alternatively, the normal functions of PrP^C may only be revealed under certain conditions.

A growing body of evidence indicates that PrP^C is implicated in cellular survival and neuroprotection. The neuroprotective role of PrP^C as an anti-oxidant protein has been well demonstrated. PrP^C has been shown to have superoxide dismutase activity (Brown *et al.*, 1997; Brown *et al.*, 1999). Cerebellar neurons derived from the *Prnp*^{-/-} mice are more susceptible to oxidative stress than their wild-type (wt) PrP expressing counterparts and the mice themselves show evidence of increased oxidation of proteins and lipid peroxidation (Wong *et al.*, 2001; Brown *et al.*, 2002; McLennan *et al.*, 2004). A neuroprotective function of PrP^C has also been demonstrated for Bcl-2-associated protein X (Bax)-induced apoptosis (Bounhar *et al.*, 2001). Bax is a major neuronal pro-apoptotic member of the Bcl-2 family (Yin *et al.*, 1994). Microinjection of human primary neurons in culture with a cDNA expressing high levels of Bax is sufficient to induce Bax-specific apoptosis (Bounhar *et al.*, 2001), while co-injection with wild type PrP completely protected neurons against Bax-mediated cell death as is observed with the anti-apoptotic protein, Bcl-2. The neuroprotective function of PrP^C is supported by *in vivo* experimental evidence. A single copy of the *Pmp* gene can rescue the ataxic transgenic PrP Δ 32-121 or PrP Δ 32-134 mice from neuronal cell death of the cerebellar granular layer (Shmerling *et al.*, 1998). PrP^C also rescues mice from the prion-like Doppel induced neuronal cell death and neurodegeneration (Moore *et al.*, 1999) which has recently been shown to be Bax-mediated (Heitz *et al.*, 2007). Furthermore, PrP^C protects mice against

seizures and epilepsy-inducing drugs (Walz *et al.*, 1999). Whether these neuroprotective pathways exhibited by PrP^C are all dependent on Bax or share another common pathway remains unresolved.

In contrast, a body of evidence suggests PrP^C exerts a neurotoxic role triggering apoptosis. Cell lines and primary neurons expressing wt PrP^C are susceptible to apoptosis with a low dose of staurosporine which causes caspase-3 activation (Paitel *et al.*, 2004) a key executioner molecule of the apoptotic cascade (Porter & Janicke, 1999), whereas cells derived from *Prnp*^{-/-} mice are less vulnerable to this same treatment. Additionally, overexpression of wt PrP^C has also been shown to trigger caspase-3 activation and apoptosis (Paitel *et al.*, 2002). Another study has shown that PrP^C can trigger cell cycle arrest when overexpressed in cultured cells (Gu *et al.*, 2006). The neurotoxic property of PrP^C has also been demonstrated *in vivo*. Overexpression of PrP^C in transgenic mice can result in ataxia and lead to neurodegeneration (Westaway *et al.*, 1994). Taken together it remains unclear why in some studies PrP^C reveals neuroprotective and in other instances neurotoxic properties.

2.4 Secretory protein biogenesis

Secretory and membrane proteins traverse the secretory pathway which consists of the endoplasmic reticulum (ER), Golgi network and endosomal vesicles. They are initially synthesized in the cytoplasm and rapidly targeted to the ER membrane where the nascent protein while continuing to be synthesized is translocated into the ER lumen (Palade, 1975). Targeting to, and translocation

across, the ER membrane is driven by interaction of the signal sequence of the nascent chain with a series of receptor proteins, first in the cytoplasm (Signal Recognition Particle, SRP) and then at the outer ER membrane with the SRP receptor and the Sec61 complex (Walter & Johnson, 1994). As a result of these interactions a complex protein-conducting channel is opened termed the translocon which consists of the hetero-trimeric Sec61 complex, allowing the nascent chain to cross the ER membrane and enter the ER lumen where it is initially encountered by luminal chaperones like binding protein (BIP) which prevent unintended interactions and shields nascent proteins to facilitate correct folding (Johnson & van Waes, 1999). Transmembrane (TM) and multispanning membrane proteins are synthesized by the partitioning of the translocon and integration of the TM domain within the lipid bilayer by a yet undefined mechanism (Pitonzo & Skach, 2006). In addition to the Sec61 complex the translocation of many substrates requires additional factors such as the translocating-chain associated membrane protein (TRAM; Hegde *et al.*, 1998c), or translocation-associated protein (TRAP; Hegde *et al.*, 1998b, Fons *et al.*, 2003). Contemporaneous with the emergence of the nascent chain to the ER lumen several further covalent modifications such as N-linked glycosylation (Helenius & Aebi, 2004) and disulfide bond formation occur (Fassio & Sitia, 2002).

2.5 Quality control mechanisms of protein folding in the secretory pathway

The cell has developed a stringent quality control mechanism to ensure only *bona fide* folded secretory and membrane proteins leave the ER and that proteins that fail to pass the quality control are rapidly disposed of to maintain the secretory capacity (Molinari & Sitia, 2005). In most cases it seems that control over N-glycan maturation is utilized as a mechanism to sort correctly folded proteins from those that fail to establish a native conformation.

While the nascent chains exits the translocon and enters the ER lumen it is scanned for an asparagine-x-serine/threonine consensus motif by the oligosaccharide transferase complex at which once encountered a pre-assembled, tri-antennary glycan composed of two *N*-acetylglucosamine, nine mannose and three glucose residues are covalently attached to the asparagine residue (Helenius & Aebi, 2004). Subsequently, the two outermost glucose residues are removed by glycosidases I and II (Hebert *et al.*, 2005). The nascent or newly synthesized protein then binds to calreticulin and/or calnexin which together with the oxidoreductase ERp57 shield the nascent protein and assist correct disulfide bond formation (Ellgaard *et al.*, 1999). To release the bound chains from calnexin and calreticulin, glucosidase II removes the remaining glucose residue and the protein can now be shuttled to the Golgi unless recognized by a UDP-glucose glucosyltransferase, which reglucosylates incorrectly folded glycoproteins (Hebert *et al.*, 2005). If reglucosylated the glycoprotein is bound again by calnexin and calreticulin and stays in the cycle until correctly folded or targeted for ER associated degradation (ERAD) by

retrotranslocation to the cytoplasm where degradation by the ubiquitin-proteasome system occurs (Ellgaard & Helenius, 2003).

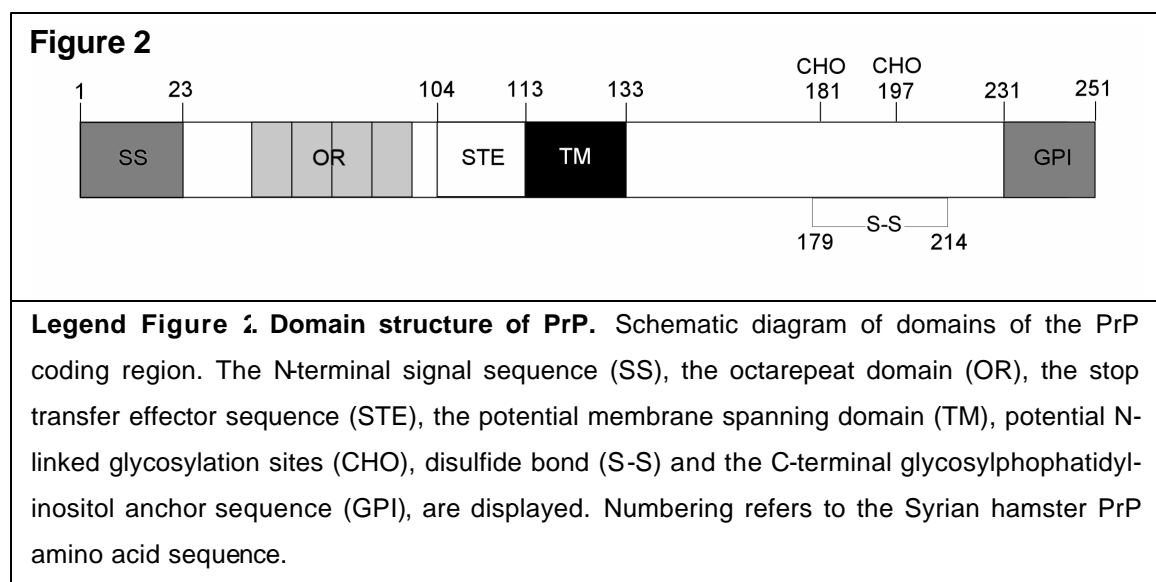
Upon shuttling of correctly folded glycoproteins to the Golgi further processing occurs with the removal of core mannose residues and further protein specific glycan modifications (Herscovics, 1999). Biochemical analysis with Endoglycosidase H (Endo H) is used to detect proteins that have passed quality control and have exited to a post-ER compartment hence enabling detection of *bona fide* folded proteins (Hegde *et al.*, 1998a).

Some proteins appear to have an intrinsic propensity for misfolding leading to a high fraction being degraded, as commonly observed for polytopic membrane proteins like cystic fibrosis transmembrane conductance regulator (Sadlish & Skach, 2004). In the case of PrP, in some instances little misfolding is seen for wt PrP however several mutants including one favoring ^{Ctm}PrP remain Endo H sensitive (Stewart *et al.*, 2001). Yet this observation has at least in part been contested by observations in transgenic (Tg) mice where ^{Ctm}PrP favoring mutants including the same mutant that showed ER-retention reveal resistance to Endo H treatment (Hegde *et al.*, 1998a; Stewart & Harris, 2005). The question why the quality control machinery permits ^{Ctm}PrP to exit the ER *in vivo* despite leading to neurodegeneration remains unresolved.

2.6 PrP biogenesis and topological heterogeneity

PrP is a 27 - 33 kD sialated glycoprotein with two N-linked glycosylation sites, a disulfide bond, an N-terminal cleaved signal sequence (SS), a C-terminal GPI

anchor sequence, an octapeptide motif rich in histidines consisting of 4-5 repeats termed the octarepeat (OR) domain (Figure 2; Prusiner *et al.*, 1998) and a hydrophobic domain of approximately 24 hydrophobic or uncharged residues that could serve to span the lipid bi-layer. It is notable that it is enriched in glycine (7 residues) and alanine (6 residues), resulting in a somewhat diminished hydrophobicity, compatible with transmembrane (TM) domain integration, but significantly lower than is typical for membrane-spanning regions of many other integral membrane proteins which are rich in leucine, isoleucine, and valine (Ott & Lingappa, 2002). Additionally, PrP contains a sequence termed the stop transfer effector (STE) sequence, identified as a charged domain just N-terminal to the hydrophobic domain, which was shown to govern membrane integration of the TM domain (Yost *et al.*, 1990). Other work suggests that the STE concept may apply more generally to conventional integral membrane proteins, as an STE has been defined for transmembrane the immunoglobulin M heavy chain (Falcone *et al.*, 1999).



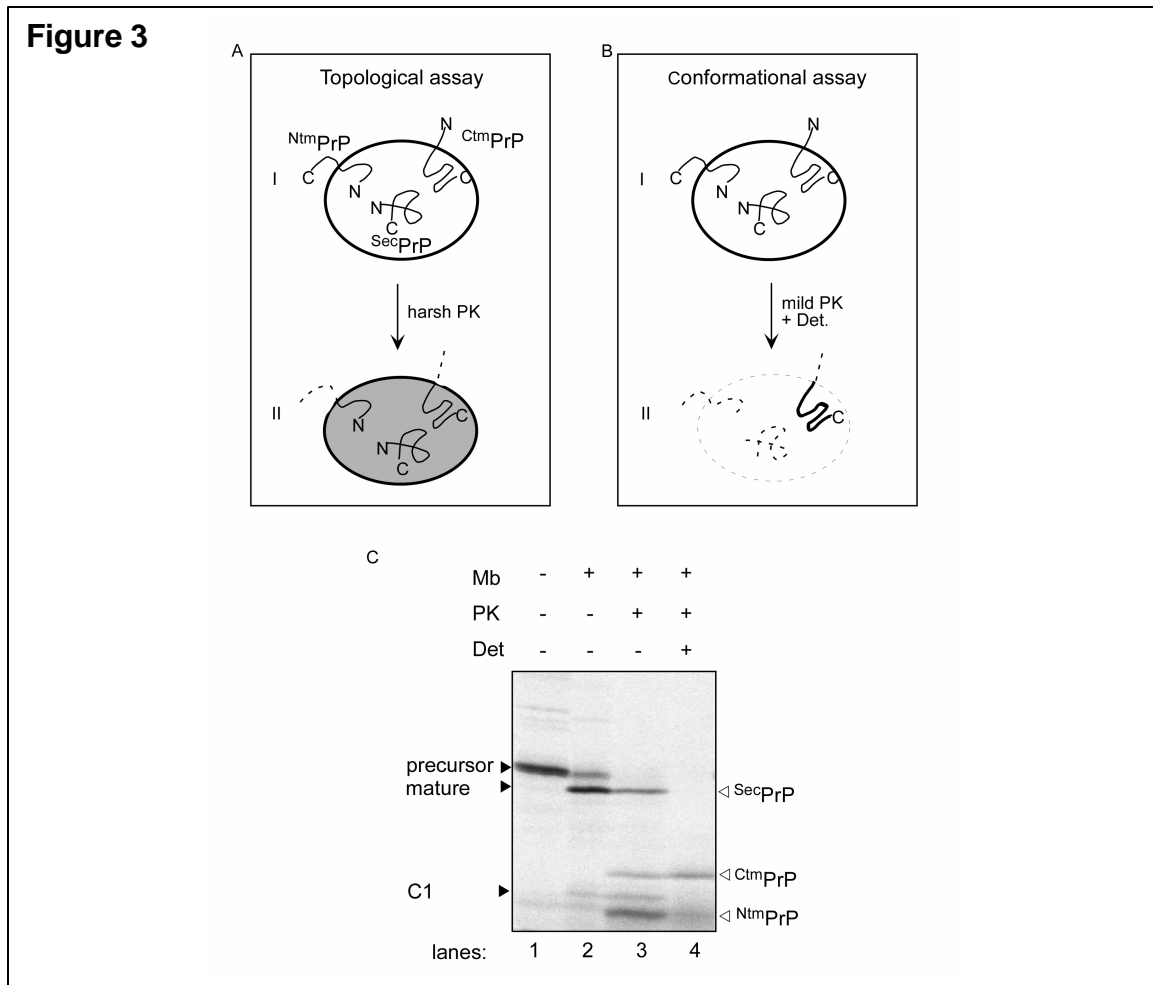
Cell-free translation systems have been shown to faithfully reproduce the luminal localization of classical secretory proteins (Lingappa *et al.*, 1978) and the transmembrane topology of integral membrane proteins (Katz *et al.*, 1977). When studied in these systems however, nascent PrP was unusual in that it gave rise to *both* transmembrane and secretory forms of the full length protein (Hay *et al.*, 1987a; Hay *et al.*, 1987b). Since both N- and C-terminal domains of the transmembrane form were found at the luminal surface, the initial assumption was that the protein spanned the membrane twice. Later, with the development of the monoclonal antibody specific for the STE domain of PrP, it was observed that *both* N- and C-terminal immunoreactive fragments after proteolysis contained this epitope. Hence it was recognized that these domains were derived from separate populations of chains, each spanning the membrane once in one direction or the other (Hegde *et al.*, 1998a; Hegde *et al.*, 1998b; Hegde *et al.*, 1999; Stewart & Harris, 2001). The form that spans the membrane with its C-terminus in the ER lumen was termed ^{Ctm}PrP. The fully translocated form attached to the membrane only by a C-terminal GPI-anchor was termed ^{Sec}PrP. A third form, spanning the membrane with N-terminal domain oriented in the ER lumen, was termed ^{Ntm}PrP.

In vivo the expression of ^{Ctm}PrP has previously been found solely in the context of disease model systems (Hegde *et al.*, 1998a; Hegde *et al.*, 1999; Stewart *et al.*, 2005) whereas the detection of ^{Ntm}PrP has been limited to hematopoietic cells from patients with a genetic GPI-anchoring deficiency (Risitano *et al.*, 2003). ^{Sec}PrP and its N-terminally truncated form, termed C1 (Vincent *et al.*, 2001), are

the only prominently detected forms found under normal physiologic conditions (Hegde *et al.*, 1998a; Stewart *et al.*, 2005).

2.7 Detecting topological isoforms of PrP

The detection of the three topological isoforms of PrP is based on accessibility of exposed residues to proteolysis with Proteinase K (PK, Figure 3A and C; Hegde *et al.*, 1998a), which is henceforth referred to as the *topological assay*. Fully translocated^{Sec}PrP remains shielded from proteolysis whereas^{Ctm}PrP and^{Ntm}PrP are partially cleaved revealing a band shift on autoradiographs (Figure 3C; Hegde *et al.*, 1998a) corresponding to the cleavage of exposed residues to the cytoplasm. Addition of non-denaturing detergents under these conditions completely degrades all topological PrP forms. In addition to the *topological assay* based on orientation across the membrane, it was found that^{Ctm}PrP could be scored by a *conformational assay* involving relatively mild PK resistance in non-denaturing detergent solution, i.e. under conditions where all *topological* differences had been abolished (Figure 3B and C; Hegde *et al.*, 1998a). Thus, the three newly synthesized forms of PrP differ both in topology *and* intrinsic conformation.



Legend Figure 3. Detection of topological isoforms of PrP. (A) Schematic of the topological assay. As shown, vesicles shield proteins from proteolysis, therefore protecting ^{Sec}PrP from proteolysis, whereas the exposed residues of ^{Ctm}PrP and ^{Ntm}PrP are accessible to proteolysis. (B) Schematic of the conformational assay. Addition of non-denaturing detergent abolishes all topological differences, so that mild proteolysis in this scenario is directed towards conformational differences (Hegde *et al.*, 1998a). Treatment with mild protease under these conditions demonstrates intrinsic differences in folded state by protection of a signature fragment of ^{Ctm}PrP . (C) Topological and conformational analysis of PrP in cell-free translation coupled translocation by mild proteolysis with proteinase K (PK). PrP was translated in the absence (lane 1) or presence of rough microsomes (Mb, lanes 2-4). Mb were either left untreated (lane 2) or treated with PK under mild conditions (0.25 mg/ml) in the absence (lane 3) or presence (lane 4) of non-denaturing detergent and resolved by sodium dodecyl sulfate polyacrylamide gel electrophoresis (SDS-PAGE) and autoradiography (AR, Hegde *et al.*, 1998a). Lanes 1-3 demonstrate the *topological assay*, Lane 4, the *conformational assay*. Not shown under harsher PK conditions (>0.5mg/ml) the topological assay remains unaffected whereas the conformational assay reveals a loss of signal (Hegde *et al.*, 1998a).

2.8 A hypothesis driven study

While many studies implicate PrP^C in cellular survival with anti-oxidant (Wong *et al.*, 2001; Brown *et al.*, 2002), neuroprotective (Chiarini *et al.*, 2002; Roucou *et al.*, 2004) and anti-apoptotic (Bounhar *et al.*, 2001) features, other evidence suggests that PrP^C mediates cell death and disease (Westaway *et al.*, 1994; Shmerling *et al.*, 1998; Paitel *et al.*, 2003). Studies on the biogenesis of PrP provide a potential explanation for these dichotomous observations on PrP^C function. It has been shown that PrP can be made in three topologically distinct isoforms: ^{Sec}PrP; ^{Ctm}PrP and ^{Ntm}PrP (Hegde *et al.*, 1998a).

Based on the aforementioned observations the hypothesis was proposed that PrP^C may have both toxic and protective functions depending on changes in relative or absolute expression levels of different topological isoforms of PrP^C.

The aim of this thesis was to test the hypothesis if PrP^C may consist of multiple topological isoforms with potentially distinct roles in physiological or pathological contexts. To dissect the functional roles of ^{Ctm}PrP and ^{Sec}PrP, advantage of mutants was taken which were known to extensively alter the ratio of each topological isoform. A comparative functional analysis of wt PrP expression in relationship to mutants favoring ^{Ctm}PrP or ^{Sec}PrP expression enabled me to determine if both forms are active within PrP^C and to determine what their roles may be.

3. Material and Methods

3.1 Reagents

If not stated otherwise salts, acids, buffers and detergents were purchased from SIGMA (St. Louis, Mo. USA); all inhibitors were purchased from Calbiochem (San Diego, CA, USA). Unless stated otherwise ultrapure water was prepared using reverse osmosis, ultra filtration and UV treatment apparatus Milli-Q (Millipore, Billerica, MA, USA).

Antibodies directed to PrP; mouse monoclonal antibody (mAb) 13A5 (Lowenstein *et al.*, 1990), Humanized Fab '2 D18 (Leclerc *et al.*, 2003), and rabbit polyclonal RO73 (Serban *et al.*, 1990) were kind gifts from Dr. Stanley Prusiner's laboratory (UCSF, San Francisco, CA, USA). TRAP α rabbit anti-sera was kindly provided by Dr. Manu Hegde (NIH, Bethesda, DM, USA). All other antibodies were obtained from commercial sources as stated.

3.2 General procedures

Unless stated otherwise all methods including deoxyribonucleic acid (DNA) cloning and purification, polymerase chain reaction (PCR), sodium dodecyl sulfate (SDS) polyacrylamide gel electrophoresis (PAGE), immunoprecipitation (IP), Western-blotting, immunocytochemistry (ICC) and immunohistochemistry (IHC) were performed according to standard procedures (Celis, 1998; Sambrook & Russell, 2001; Hayat, 2004).

3.3 DNA constructs

DNA constructs for cell culture experiments were engineered by subcloning the open reading frame of SHaPrP (SWISS-PROT: P04273; Basler *et al.*, 1986) and its mutants which have been previously characterized (Hegde *et al.*, 1998a) from pSP64 (Promega, Madison, WI, USA) into pcDNA3.1 Zeo+ (Invitrogen, Calsbad, CA USA) by utilizing Bam HI and Eco RI sites. Three mutants were mainly used throughout this study, two favoring the expression of ^{C_{tm}}PrP by substitutions K110I, H111I, termed KH→II and A117V albeit the A117V favors C_{tm}PrP expression to a much lesser extent than the KH→II mutant. Another mutant with a deletion of the STE domain, Δ103-114, termed ΔSTE diminishes the capacity of PrP to be expressed as ^{C_{tm}}PrP, however greatly favors the expression of ^{Sec}PrP (Hegde *et al.*, 1998a).

Human Bcl-2 and human Bcl-XL were kind gifts from Dr. Andrea LeBlanc (McGill University, Montreal, Canada) and were engineered into pcDNA 3.1 zeo + using Kpn I/ Xho I and Eco RI/ Bam HI sites respectively. All DNA sequences were verified by DNA-sequencing.

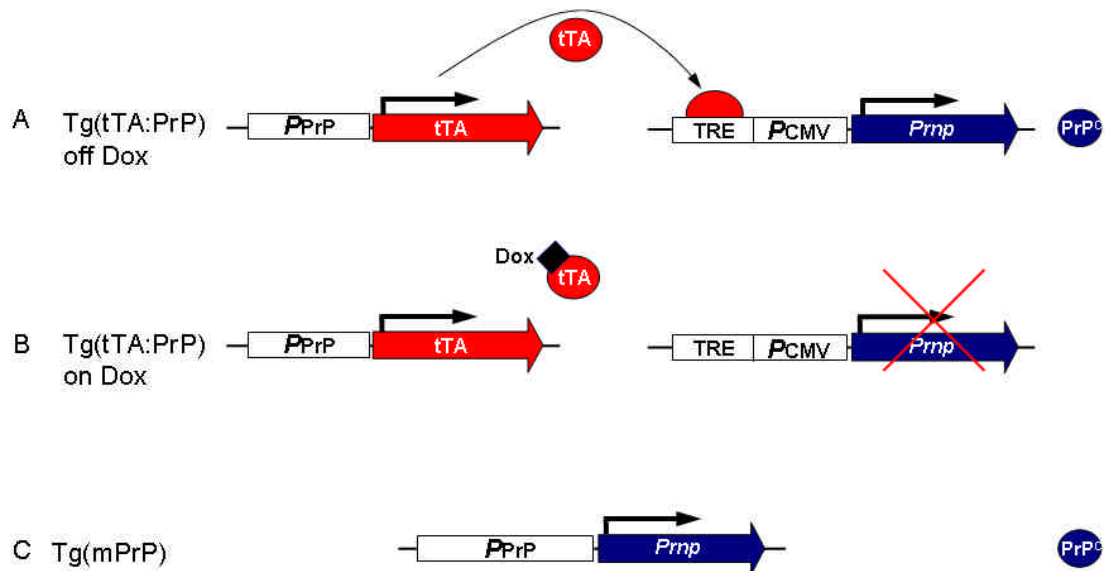
3.4 Transgenic mice

Transgenic mice used in this study—Tg(SHaPrP,KH→II)F1198; Tg(SHaPrP, ΔSTE)F1788; Tg(SHaPrP)A3922—have been previously described (Hegde *et al.*, 1998a) and were constructed on a *Prnp*^{-/-} background (Bueler *et al.*, 1992).

Double Tg(tTA:mPrP) and Tg(mPrP), 4053 mice on a *Prnp*^{-/-} background have also previously been described (Tremblay *et al.*, 1998) and were made by

crossing parental lines Tg(Prnp-tTA)F595 with Tg(tetO-PrP)E6740 to make bigenic Tg(Prnp-tTA:tetO-PrP)E6740/F595, which were then bred to homozygosity and termed Tg(tTA:mPrP). Temporal regulation of PrP expression in these mice was achieved by facilitating a reverse tetracycline-controlled transactivator (tTA) driven by the PrP gene control elements to ensure tissue-specific expression of PrP on a *Prnp*^{-/-} background as has been previously described (for details, see legend to Figure 4; Tremblay *et al.*, 1998). Systemic administration of doxycycline (dox), an analogue of tetracycline, in the drinking water of Tg(tTA:mPrP) mice results in suppression of PrP expression, whereas its withdrawal enables PrP expression. Dox was provided at 0.02 mg/ml in drinking water supplemented with 5% sucrose in light-protected bottles.

All mice were maintained on an inbred FVB background, were provided food and water *ad libitum* and were cared for according to the guidelines provided by the University of California. Euthanasia was performed by placing mice in a gas chamber saturated with CO₂ for a few minutes until mice were no longer responsive. After cervical dislocation mice were decapitated, brains carefully dissected and further processed according to experimental demands described in the appropriate sections.

Figure 4

Legend Figure 4. Transgenic mice. Tetracycline-dependent, tissue-specific expression of PrP^{C} in transgenic (Tg) mice, termed Tg(tTA:mPrP), have been previously described (Tremblay *et al.*, 1998) and were engineered on a $\text{Prnp}^{-/-}$ background. (A) In the absence of doxycycline (dox), a tetracycline analogue, the transactivator (tTA) is expressed from the Syrian hamster (SHa) PrP gene control elements (*PPrP*) binds to the tet response element (TRE), which facilitates transcription of the mouse PrP gene (*Prnp*) from a minimal Cytomegalovirus promoter (*PCMV*). (B) Administration of dox (black rectangle) leads to the silencing of PrP^{C} expression, by binding to the tTA and inducing a conformational change, reducing affinity for TRE and thus silencing *Prnp* transcription. (C) All other Tg mice used in this study were made by placing the *Prnp* gene (including mutants) under direct control of *PPrP*.

3.5 Inoculation of mice with Sc237 prions

Tg mice were inoculated with hamster Sc237 prions as previously described (Hegde *et al.*, 1999). Briefly, intracerebral inoculation was performed with 30 μl of 1% (w/v) hamster brain homogenate prepared in PBS that had been derived from terminally sick hamsters inoculated with hamster prions Sc237. Mice were

maintained under normal conditions and provided food and water *ad libitum*. When clinical symptoms typical of neurodegeneration were first observed data was recorded and mice were killed. Brains were carefully extracted and half brains placed in 10% buffered formalin for IHC while the other half was homogenized, frozen in liquid nitrogen and stored at -80 °C until needed for the detection of PK resistant PrP^{Sc}.

3.6 Biochemical analysis of PrP^C topology in mouse brains

Ten-percent (w/v) whole brain homogenates were prepared from fresh tissue in ice-cold homogenization buffer composed of 0.25 M sucrose (Fisher Scientific, Pittsburg, PA, USA), 100 mM KCl, 5 mM MgAc₂ and 50 mM HEPES (pH 7.5) by 10 strokes with a teflon pestle homogenizer (Wheaton, Millville, NJ, USA), rapidly frozen in liquid nitrogen and stored at -80°C until further use. *Topological and conformational assays* were performed in principle as previously described (Hegde *et al.*, 1998a). Brain homogenates were rapidly thawed, placed on ice and diluted in cold homogenization buffer to a final concentration of 2% (w/v). Each sample was aliquoted into three tubes on ice: the first remained untreated, the second was treated with 0.25-1 mg/ml PK (Merck) for topological analysis and the third tube was treated with 0.5% (v/v) TritonX-100 and 0.25 mg/ml PK for the conformational analysis. Samples were incubated for 1 hour (h) on ice at 4°C upon which the PK reaction was terminated with 1 mM phenylmethanesulfonyl fluoride (PMSF, Sigma, St. Louis, MO, USA), was further incubated for 5 min on ice and transferred to 4 volumes of denaturation buffer consisting of 1% SDS, 50

mM Tris-Ac pH 8.0 which had been heated in a boiling water bath and incubated for 5 min. After cooling down to room temperature (RT) samples were diluted with 1 volume 2% 2-mercaptoethanol (BME, Sigma), 50 mM Tris-Ac pH 8.0, incubated for 15 min at 37°C and then 2 min at 99°C, cooled to RT and TritonX-100 added to a final concentration of 0.5% (v/v). After thorough mixing deglycosylation was performed with 200 Units PNGase F (New England Biolabs, Ipswich, MA, USA) overnight at 37°C. The following day samples were placed on ice and precipitated with a final concentration of 10% (w/v) tri-chloroacetate (TCA), sedimented for 5 min at 10,000 g. The supernatant was aspirated and washed with 1 volume ice-cold ethanol and ether (1:1), pellets were left to air dry for ~10 min and resuspended in 1x SDS samples buffer 1% (w/v) SDS, 25mM Tris pH6.8, 0.01% (w/v) bromphenolblue (Sigma), 25% (v/v), glycerol, 100 mM dithiothreitol (DTT) in a three fold greater volume than the initial 10% homogenate. Typically 20 µl of 10% homogenate was used per tube treated with PK and one-fourth there of was resolved by 0.75 mm thick 12.5% Tris-Tricine SDS-PAGE. Gels were transferred to nitrocellulose in 1.3 l transfer buffer containing 156 mM Glycine, 80 mM Tris, 20% (v/v) Methanol (VWR, West Chester, PA, USA) for 90 min at 50 volts with a Criterion tank transfer apparatus containing plate electrodes (Biorad). Quality of transfer was assessed by staining nitrocellulose membrane with 0.01% (w/v) Imidio black for 10 min. Only membranes with ensured even transfer lacking any obvious artifacts were further processed. Membranes were blocked for 30 min in 5% (w/v) fat-free dry milk (Carnation, Nestle, Vervy, Switzerland) in phosphate buffered saline (PBS) with

0.025% (v/v) Tween 20 (PBST) at RT on a rocking platform. The membrane was cut at the 50 kD marker (Precision, Biorad). The top section was probed against GRP94 (Stressgen, Ann Arbor, MI, USA) at 1:10,000 to control for loading and ER integrity. The bottom part of the membrane was probed against PrP with mAb 13A5 or humanized Fab'2 D18 at 1:1,000 overnight at 4°C on a rocking platform. Subsequentially, blots were washed 4 times at 5 min each with 1% fat-free dry milk with PBST and then incubated 1-4 h at RT with the corresponding anti-rabbit, mouse or human Fab'2 secondary antibody conjugated to horseradish peroxidase (HRP) (all Pierce, Rockford, IL, USA) at 1 µg/ml. Membranes were then washed 6 times with PBS and developed with chemiluminescent Super Signal Substrate West Pico or Femto (Pierce) according to the manufactures guide lines and exposed to Biomax XR film (Kodak, Rochester, NY, USA).

3.7 Enhanced detection of ^{Ctm}PrP in brain homogenates

The enhanced detection of ^{Ctm}PrP in non-Tg FVB mice was in principle performed as described above (3.6) for the topological assay however PrP was further enriched prior to SDS-PAGE by IP. After denaturation samples were diluted to a final concentration of 0.2% SDS, 0.75% Triton X100, 0.375% deoxycholate, 37.5 mM KCl, 50mM Tris-Ac pH 8.0 supplemented with EDTA-free Protease Inhibitor Cocktail Tablets (Roche, Palo Alto, CA, USA) according to the manufacturer's instructions. Samples were then thoroughly mixed, 200 U PNGase F was added and incubated overnight at 37 °C. The following day after deactivation of enzymes by heating samples 10 min at 90 °C, samples were left

to cool for ~10 min at RT then were placed on ice and 30 μ l (50%) Protein A (Biorad) that had been preequilibrated with IP buffer was added and tubes placed for 1-6 h on a top-to bottom rotation wheel at 4°C after which samples were sedimented for 10 min at 16,000 g. 90% of the supernatant typically 1.8 ml was transferred to a new tube and IP performed with 10 μ l anti-PrP polyclonal RO73 and 60 μ l (50%) Protein A overnight with top to bottom rotation at 4°C. Samples were washed 3 times in 1 volume IP buffer and once in 50 mM Tris-Ac pH 8.0. After drying beads for 15 min at 99°C they were resuspended in 60 μ l sample buffer; 30 μ l was resolved by 12.5% Tris-Tricine SDS-PAGE, then transferred to nitrocellulose and probed overnight at 4°C. Below the ~50 kD marker membranes were probed with D18 directly conjugated to HRP (kindly provided by Hana Serban, Prusiner laboratory) at 0.2 μ g/ml and above ~50 kD with anti-Rabbit-HRP (Pierce) at 1:10,000. Membranes were washed and developed as described above (3.6). The use of directly conjugated HRP to anti-PrP D18 was proved an imperative step to obtain a sufficient signal to noise ratio to detect ^{Ctm}PrP in wild-type non-transgenic FVB mice. It should be noted that despite extensive optimization attempts with secondary antibodies that supposedly only detect non-reduced forms of IgG (Trueblot, eBioscience, San Diego, CA, USA) the background 25 kD IgG light chain cross reactivity could not be eliminated from *Prnp*^{-/-} negative control samples (data not shown).

3.8 Glycan maturation analysis of ^{Ctm}PrP and ^{Sec}PrP

Brain homogenates that had been processed by the topological assay (See 3.6) and denatured in denaturation buffer were reduced with 1 volume 2% BME (BME, Sigma), 100 mM Tris-Ac pH 8.0 incubated for 15 min at 37°C and 2 min at 99°C. After cooling to RT, TritonX-100 was added to a final concentration of 0.5% (v/v) and sodium citrate pH 5.5 was added to a final concentration of 100 mM. After thorough mixing the sample was divided into three tubes. One was left untreated, the second was treated with 200 Units PNGase F and the third was treated with 300 U Endoglycosidase H (Endo H, NEB). Samples were incubated overnight at 37°C, precipitated with TCA and Western-blotted as describe above. In addition to PrP and GRP94, blots were also probed with anti-TRAP α at 1:5,000 which being an ER-resident glycoprotein served as a positive control for Endo H treatment.

3.9 Biochemical detection of PrP^{Sc}

PrP^{Sc} was detected by proteolysis with PK as previously described (Hegde *et al.*, 1999). Briefly, 2% (w/v) brain homogenates were treated with 0.5 mg/ml PK for 1 h at 37 °C in buffer containing a final concentration of 10 mM Tris-Ac (pH 8.0), 150 mM NaCl, 0.5% TritonX-100 and 0.5% deoxycholic acid. The reaction was terminated with 4 volumes ice cold methanol precipitation, sedimented for 5 min at 10,000 g and air dried pellets resuspended in SDS sample buffer, resolved by 15% Tris-Glycine SDS-PAGE, transferred to nitrocellulose and probed with anti-PrP 13A5 as described above (3.6).

3.10 Measurement of lipid peroxidation in brain homogenates

Lipid peroxidation was measured using a BIOXYTECH MDA-586 assay kit (Oxis International) by assessing the level of malondialdehyde (MDA) following the manufacturer's protocol with minor modifications. Dissected hippocampi were homogenized in 0.1 M phosphate buffer (pH 7.4) and centrifuged at 20,000 g at 4 °C for 30 min. Protein concentrations of the supernatants were determined with the BCA kit (Pierce) and 75 µg of protein (50 µl) was incubated with 2.5 µl probucol, 160 µl diluted R1 reagent and 37.5 µl of R2 at 45 °C for 60 min. The reaction mixture was then centrifuged at 10,000 g for 10 min and optical density of the supernatant was determined at 586 nm using a Beckman Spectrophotometer. MDA concentration was calculated based on TMOP standard curve.

3.11 Analysis of PrP topology in transfected CHO-K1 cells

CHO-K1 cells (ATCC: CCL-61) were maintained in Ham's F12 (UCSF, cell culture facility, CCF), 10% Fetal bovine serum (FBS, Hyclone, Logan, UT, USA) supplemented with penicillin and streptomycin (CCF) in a humidified incubator with 5% CO₂ at 37°C. 24 h prior to transfection 4x10⁵ cells were plated in 35-mm wells (6-well plate) and transfection was performed with Lipofectamine Plus (Invitrogen) according to the manufacturer's guidelines with 3 µg DNA, 5 µl Lipofectamine and 7.5 µl Plus reagent per well and cells harvested 24 h thereafter. 4.5 h prior to harvesting the media was changed to cysteine and methionine free Hams' F12 (CCF) with dialyzed FBS (Hyclone). ~0.25 mCi S35

labeled cysteine and methionine (Easy Tag, Perkin Elmer, Costa Mesa, CA, USA) was added and cells were incubated for 4 h prior to harvest. Cell culture plates were placed for 10 min on ice and then mechanically detached by scraping cells in media, washed 2 times with ice cold PBS by sedimentation at 1,000 g and resuspended in 600 μ l hypotonic lysis buffer consisting of 10 mM HEPES pH 7.4 and incubated 20 min on ice prior to lysis by 10 passages through a 30 gauge syringe (BD Biosciences, San Jose, CA, USA). Samples were adjusted to a final concentration of 50 mM KCl, 5 mM MgAc₂, 50 mM HEPES (pH 7.4). Proteolysis of samples with PK was performed as described above (see 3.6). After PNGase F treatment and heat deactivation samples were pre-cleared and immunoprecipitated with 2 μ l mAb13A5 and 30 μ l (50%) Protein G (ImmunoPure, Pierce). Samples were then washed and resuspended in 60 μ l sample buffer; 15 μ l was resolved by SDS-PAGE on 12.5% Tris-Tricine gels and visualized by AR by exposing to Biomax XR film.

3.12 TUNEL and caspase-3 analysis of transfected CHO-K1 cells

CHO-K1 cells were maintained and transfected as described above (3.11) however transfection was performed with 0.6 μ g DNA, 1 μ l Lipofectamine and 1.5 μ l Plus reagent per well. Cells were plated in 15-mm wells with glass coverslips (Fisher Scientific) at 5×10^4 cells per well. After 48 h, cells were fixed on ice for 15 min with 4% paraformaldehyde in PBS. The cells were then washed twice and blocked for 30 min with 5% (w/v) BSA, 0.5% (w/v) saponin in PBS and washed 3 times with PBS then stained for TUNEL by the In Situ Death Detection

kit (Roche, Palo Alto, CA, USA) according to the manufacturer's instructions using 17 μ l of a 20 fold diluted enzyme solution and incubated 1 h at 37 °C in a humidified chamber. Alternatively, fixed cells were stained for activated caspase-3 by probing with rabbit polyclonal specific for the activated form (Cell Signaling, Billerica, MA, USA) according to the manufacturer's guideline by probing at 1:20 diluted in 1% BSA in PBS overnight at 4 °C. After washing four times with PBS, subsequently all cells were stained for PrP by probing with mAb 13A5 at 1:100 for 1 h at RT, washed 4 times with PBS, followed by incubation for 30 min at RT in the dark with secondary goat anti-mouse antibody conjugated to Alexa 594 and/or anti-rabbit conjugated to Alexa 488 (Molecular Probes) diluted at 1:500 in PBS with 1% BSA. Coverslips were then washed four times in PBS counterstained with DAPI (Molecular Probes, Eugene, OR, USA) and coverslips mounted on slides with aqueous mounting medium (Pro Long, Molecular Probes).

3.13 TUNEL analysis of transfected CHO-K1 cells treated with caspase-3 and Bax inhibitors

Caspase-3 and Bax are two pro-apoptotic molecules known to participate in the execution of apoptosis that leads to the fragmentation of DNA (Korsmeyer, 1995; Porter & Janicke, 1999). Hence by blocking their activation with pharmacological inhibitors permits the study of their participation in PrP mediated apoptosis. Experiments were conducted exactly as stated above under 3.12 however with the exception that cells were treated 30 min prior to transfection with either

10 μ M Z-DEVD-FMK (caspase-3 inhibitor), 100 μ M V5 (Bax inhibitor) or an equal volume of the solvent dimethylsulfoxide (DMSO) alone.

3.14 TUNEL analysis of transfected CHO-KI cells overexpressing Bcl-2 or Bcl-XL

Bcl-2 and Bcl-XL belong to the Bcl-2 homology (BH) family of proteins just like Bax however with anti-apoptotic properties which have also been shown to offset the pro-apoptotic effect of Bax (Korsmeyer, 1995). The protective effect of Bcl-2 and Bcl-XL against ^{Ctm}PrP mediated apoptosis was tested by preparing CHO-KI clonal cell lines that were expressing either Bcl-2 or Bcl-XL or an empty pcDNA 3.1 Zeo+ plasmid (Mock) which had been selected and maintained with 0.25 mg/ml Zeocin (Invitrogen) in complete media. Screening of Bcl-2 and Bcl-XL cell lines was performed by Western-blot. Clones with the highest expression level were used for experiments with two independent clones tested for each candidate. Experiments were then performed as described above (3.12) by transfection with KH \rightarrow II and then probing for apoptosis by TUNEL.

3.15 Viability analysis of ^{Sec}PrP mediated protection to oxidative stress in cultured cells

Stable CHO-KI cell lines expressing Δ STE, wt PrP or mock were isolated by clonal selection in media containing 0.25 mg/ml Zeocin (Invitrogen, Carlsbad, CA, USA). Cell lines expressing similar levels of PrP were selected for this study. Cells were seeded in 24-well plates at 2×10^4 cells per well 24 h before treatment

with 1.5 mM hydrogen peroxide (Sigma) in serum-free media for 5 h. Cell viability was assessed by staining with 3 μ M propidium iodide (PI) and Hoechst 5 μ M (Molecular Probes) 15 min prior to collecting images from live cells.

3.16 TUNEL IHC of murine brains

Terminal UTP-mediated nick end-labeling (TUNEL) was performed using the Apoptag Kit (Chemicon, Billerica, MA, USA) according to the guidelines of the manufacturer. Half-brains were immersion-fixed in 10% formalin for 3 days before being embedded in paraffin, cut into 8 μ m sections, and mounted on glass slides (Superfrost/Plus, Fisher Scientific). Sections were deparaffinized in xylene and were rehydrated by emerging slides through serial grades of ethanol from 100% - 50%, and then rinsing in H₂O. Sections were then quenched with 0.3% hydrogen peroxide for 30 min, at RT, in the dark. Sections were washed in PBS with 0.05% Tween 20 (PBST) 3 times for 3 min each. Sections were treated with 20 μ g/ml PK (Invitrogen) in PBS at RT for 30 min. Slides were washed as described above and then covered with equilibration buffer (for 10 min at RT, followed by incubation with terminal deoxynucleotide transferase (TdT) in reaction buffer (3:7) at 37 °C in a hydration box for 1 h. The enzyme labeling was stopped with pre-warmed stop/wash buffer (stock:water, 1:35) at 37 °C for 40 min. Sections were washed and then incubated with anti-digoxigenin antibody at RT for 30 min. Sections were washed again and developed with diaminobenzidine (DAB, Invitrogen) for 12 min at RT, then washed twice with PBST and once with PBS prior to counterstaining with Methyl Green (Vector,

Burlingame, CA, USA) at 55 °C for 10 min. Slides were washed once in PBS and twice in H₂O before a 5-second stain in eosin (Fisher Scientific). Then slides were dehydrated by taking through a series of graded alcohols (50% -100%) with changes every 5 min followed by to two 5 min incubations in xylene (Fisher Scientific). Coverslips were mounted on slides with Permount (Fisher Scientific). TUNEL-positive nuclei, which are dark reddish-brown and spherical, were counted in the same location of cerebellum in each brain within a defined area using a Microbright field measurement grid and averaged. At least three coronal brain sections with similar bregma were quantified from at least three mice per line.

3.17 Activated caspase-3 IHC

Paraffin-embedded coronal brain sections were prepared as described above (3.16). Before staining, sections were deparaffinized, rehydrated, and endogenous peroxidases blocked in the same way as performed for TUNEL staining (3.16). For antigen retrieval, slides were submerged in 1 mM EDTA (pH 8) in a closed container and microwaved to reach and hold a temperature of 95 °C for 15 min; the temperature was checked every 5 min. Sections were allowed to cool to RT for 30 min, then washed in water once and PBST twice, each for 3 min. Non-specific antibody binding was blocked with 5% normal goat serum (NGS) in PBST for 30 min at RT. Sections were incubated with the primary antibody, anti-activated caspase-3 (9661, Cell Signaling), was diluted 1:500 in 5% NGS/PBST overnight at 4 °C. The sections were washed in PBST,

3 × 3 min, and incubated with biotinylated secondary goat anti-rabbit (Vector) in 5% NGS/PBST for 30 min at RT. Afterwards, slides were incubated with 1% ABC mixture (Vector Laboratories) for 30 min at RT, washed with PBS and stained with the DAB chromagen according to the manufacturer's protocol and stopped by placing slides under running tap water then counter stained with methyl green, gradually dehydrated and coverslipped in Permount (Fisher Scientific).

3.18 8-hydroxy-2-deoxyguanosine (8-OHdG) IHC

8-OHdG is a well recognized ROS marker which has been linked with oxidative damage and neurodegeneration in the brain (Floyd & Carney, 1992; Won *et al.*, 1999). 8 µm coronal brain sections were cut from paraffin embedded brains and transferred to glass slides (Superfrost, Fisher Scientific). Sections were deparaffinized, rehydrated and rinsed in H₂O as described above (3.16). Antigen retrieval was performed by incubating slides for 5 min in 10 mM citrate buffer pH 6.4. Sections were then sequentially incubated with a blocking buffer containing 5% mixed NGS and rabbit sera (1:1), goat anti-mouse IgG anti-Fc F(ab')₂ fragment (Covalab, Villeurebanne, France) at 1:5,000 and 20 mM L-lysine in PBS to block endogenous IgG and other non-specific interactions. After washing with PBS, brain sections were incubated with primary mouse monoclonal IgG against 8-OHdG at 1:200 (Clone 4E9, Trevigen, Gaithersburg, MD, USA) for overnight at 4 °C, then washed with 3 times with PBS and incubated with biotinylated goat anti-mouse IgG (Fc) (Vector Laboratories, 1:200). Then treated with the ABC Kit

and developed with DAB before dehydrating and mounting slides with Permount as described above (3.16).

3.19 Detection of PrP^{Sc} by IHC

PrP^{Sc} was detected by IHC treatment with formic acid as previously described (Kitamoto *et al.*, 1987). Half-brains were fixed in 10% buffered formalin (Fisher Scientific) for 5 days, processed, and embedded in paraffin according to standard procedures. Sections 8 µm thick were cut and mounted on glass slides (Superfrost Plus, Fisher Scientific) and dried overnight. Tissues were deparaffinized by heating at 60 °C for 30 min followed by two changes of xylene for 5 min each and rehydrated in graded alcohols from 100-50%. After rinsing with H₂O endogenous peroxidases were blocked with 3% hydrogen peroxide in methanol for 10 min at RT. Tissue sections were washed in water and then autoclaved for 5 min in 10 mM sodium citrate buffer, pH 6.0 at 121 °C and cooled for 30 min after removal from the autoclave. The sections were then treated with 90% formic acid for 2 min exactly at RT, and washed for 10 min in a constant flow of H₂O. Sections were then washed with PBST 3 times for 3 min (all additional washing steps performed the same). Non-specific antibody binding was blocked with 5% NGS in PBST for 30 min at RT. Sections were incubated with primary antibody 13A5 at 1:500 in PBST with 5% NGS for overnight at 4 °C. After which sections were washed and incubated with HRP-conjugated secondary anti-mouse (Invitrogen) at 1:5,000 in PBST for 1 h at RT. After washing, the HRP reactivity was detected with DAB, dehydrated. Sections were

briefly washed twice in PBST and once in PBS and then were counterstained for 1 minute in hematoxylin (Fisher Scientific).

3.20 Internucleosomal DNA-fragmentation analysis

Internucleosomal DNA-fragmentation or DNA-laddering is recognized as a hallmark of apoptosis (Kerr *et al.*, 1972). To distinguish fragmentation of DNA that occurs from necrotic processes (smear) rather apoptotic ones (laddering) it is important to validate the observations made by TUNEL to rule out necrotic mechanisms (Stadelmann & Lassmann, 2000). Brain homogenates that had been prepared as described above (3.6) were used to extract DNA with the Wizard Genomic Purification Kit (Promega, Madison, WI, USA) according to the manufacturer's instructions. Extracted DNA was normalized according to standard spectrometric measurement at 260 nm which had been corrected by the 280 nm extinction. Purified DNA samples were subject to a sensitive detection method for DNA-laddering by ligation-mediated PCR (Staley *et al.*, 1997) with the LM-PCR kit (Maxim Biotech, South San Francisco, CA, USA) performed according to the manufacturer's instructions. Briefly, normalized DNA from cerebellar brain homogenates was ligated to adaptors and then amplified by PCR. Adapter oligonucleotides (kit) were ligated to terminally available ends of 100 ng extracted DNA overnight at 16 °C. 5 ng DNA was used as a template for the PCR with primers (kit) complementary to the ligated adapters and amplification was performed for 15 cycles according to the guidelines of the manufacturer. To control for the template concentration in the PCR,

Glyceraldehyde-3-phosphate dehydrogenase (GAPDH) primers were included instead of adaptor primers in a parallel PCR. Samples were then resolved by gel electrophoresis and stained with SYBR green I (Molecular Probes, Eugene, OR, USA) at 1:10,000 in H₂O for 10 min in the dark followed by rinsing for 10 min in H₂O and visualized with an ultraviolet transilluminator.

3.21 KA treatment and TUNEL analysis of transgenic mice

Six to nine week old mice were treated with subcutaneous injections of 10 mg/ml kainic acid (KA) prepared in PBS (25–30 mg/kg) and sacrificed 24 h after the onset of intermittent but generalized tonic-clonic seizures which appeared in different degrees and extents among the various lines of mice compared. Untreated mice served as controls and showed no seizure activity or cell death. TUNEL was performed on frozen coronal brain sections using the In Situ Cell Death Detection kit (Roche) according to the manufacturer's protocol and coverslips applied with VECTASHIELD mounting medium containing PI as nuclear counter stain (Vector Laboratories, Burlingame, CA, USA).

3.22 KA treatment and TUNEL analysis of primary cerebellar granule cell neurons

Primary cultures from the cerebellum were prepared from 7-day-old mice. After decapitation brains were quickly removed and placed in ice cold dissection solution containing 8 g/l NaCl, 0.3 g/l KCl, 0.5 g/l NaH₂PO₄, 0.25 g/l KH₂PO₄, 4 mg/ml NaHCO₃, 2 g/l glucose. All further steps were performed on ice unless

stated otherwise. Cerebelli were dissected, the meninges removed and transferred to a solution with Hank's balanced salt solution (BSS) containing 20% FBS then further transferred to serum free Hank's BSS, minced into $\sim 1 \text{ mm}^3$ sections and incubated for 5 min at 37 °C in 0.5 mg/ml trypsin (Invitrogen). After quenching the reaction by addition of FBS to a final concentration of 10%, the tissue was washed 3 times in Hank's BSS by letting tissue settle and aspirating off the supernatant. The tissue was then resuspended in the dissociation solution containing Hank's BSS, 12 mM MgCl_2 , 0.02 mg/ml DNase I (Sigma) and single cell suspensions prepared by trituration through several fire-polished glass Pasteur pipettes (Fisher Scientific) of decreasing tip diameters. Cell suspensions were then washed 3 times with Hank's BSS with 20% FBS. An aliquot of cells was then taken, from which the proportion of viable cells was determined (typically over 75%) by staining with trypan blue (Sigma) and visualizing with a hemacytometer under a light microscope. After counting, cells were resuspended in the appropriate volume of culturing media consisting of minimal essential medium, 10% FBS (Invitrogen), 2% B-27 (Invitrogen), 0.025 mg/ml insulin, 0.1 mg/ml transferrin, 5 mg/ml glucose and 2 mM glutamine that had been preequilibrated at 37 °C with 5% CO_2 and plated at a density 1×10^5 per 15 mm well of a 24 well plate coated with poly-D-lysine and laminin coverslips (BD-Biosciences). 24 h after plating cells, Arabidonase C (Sigma) was added to a final concentration of 4 μM to suppress non-neuronal proliferation. After 72 h *in vitro*, cells were treated for 48 h with 100 μM KA, prior to fixation and TUNEL-

staining was performed as described above (3.12) with the In Situ Death Detection Kit (Roche).

3.23 Image and data analysis

Fluorescent micrographs were captured with an inverted microscope, Nikon TE-200 (Melville, NY, USA) equipped with a cooled CCD Retiga 900 (QImaging, Surrey, BC, Canada) and excitation and emission filters corresponding to DAPI, fluorescein or Texas Red were used (Chroma, Rockingham, VT, USA). Monochrome images were acquired with the software Image Pro 4.5 at 8 bit resolution (Media Cybernetics, Bethesda, MD, USA).

Bright field microscopy was performed using the Leica DM/IRB microscope and imaging using a Spot Flex digital camera and Spot Advanced software.

All images taken part of the same experiment were acquired with the same exposure parameters. Monochrome images, part of multi-channel fluorescent sets were colored according to their original excitation wavelength and merged for further quantification.

Statistical analysis was performed with Prism 4 (Graph Pad, San Diego, CA, USA). For pair wise comparisons T-Test were used to assess significance set to $P < 0.05$ in all cases. For comparison of multiple data sets ANOVA was used to assess the significance of the data set. For *post hoc* data analysis comparing the significance of each pair within data set with more than three data groups, Turkey's multi comparison test was used. For non-parametric pair wise comparison Fisher's exact test was used.

Densitometric quantification of digitalized autoradiographs was performed with Photoshop 7 (Adobe, San Francisco, CA, USA) by determining the average pixels of a given band of interest corrected for the background.

Presented data such as autoradiographs, Western blots and micrographs were all edited in Photoshop 7 by only applying the brightness, contrast and cropping to whole image or in case of data consisting of multiple images the same modifications were equally applied to the entire set acquired from one experiment.

3.24 Multi-sequence alignment and dot-plot analysis

The open reading frames of PrP were retrieved from the SwissProt data base in FASTA format and aligned with the ClustalW multi-alignment program (Thompson *et al.*, 1994) found at <http://www.ebi.ac.uk/Tools/clustalw/> with the following parameters: BLOSUM 30 matrix series, a gap opening penalty of 10 residues, a gap separation penalty of 4 and gap extension penalty of 0.2.

Dot plot analysis was performed with Vector NTI 6.0 (Invitrogen) with a window set to 15 and a stringency set to 11 (73%) with human PrP amino acid sequence probed against the turtle sequence.

4. Results

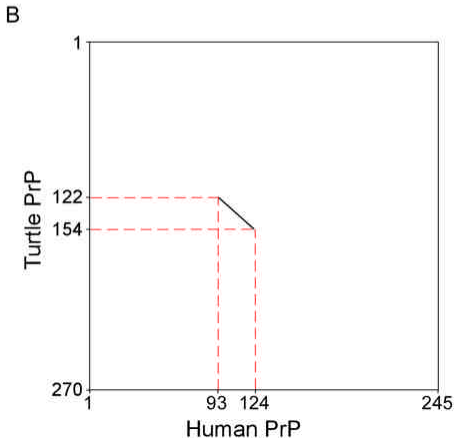
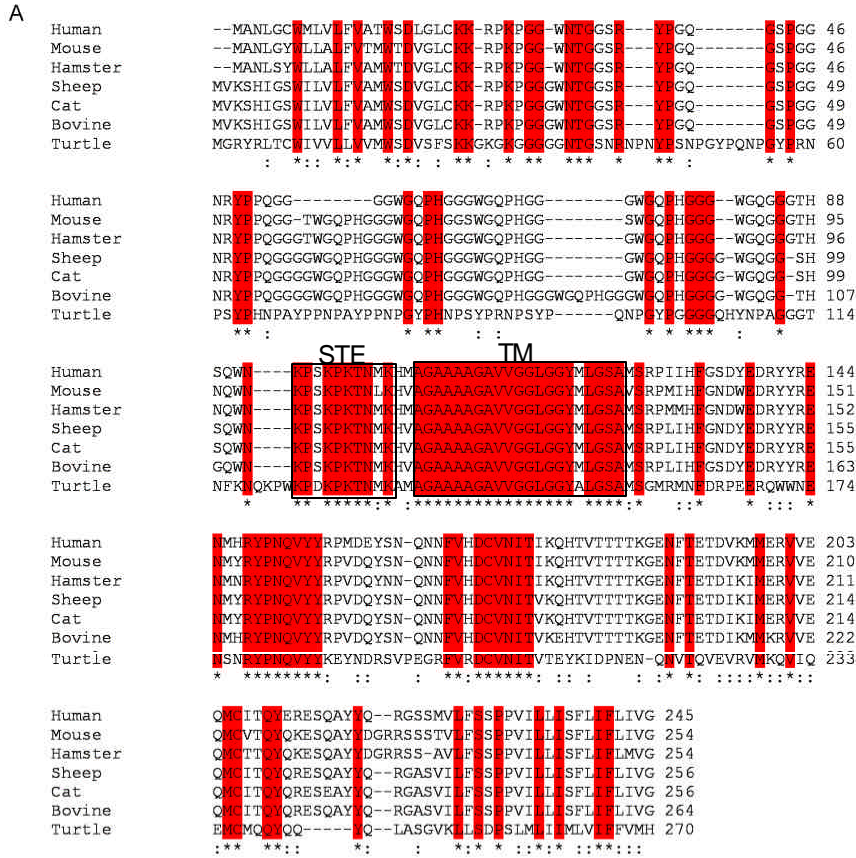
4.1 Evolutionary analysis of topogenic domains of PrP

Multi-sequence alignments can be helpful to highlight conserved domains that may be important for protein structure and/or its corresponding function. It is generally assumed that conservation of domains is an indication of selection pressure imposed on that particular domain resulting in no or few amino acid changes (Graur & Li, 2000).

Previous multi-sequence analysis of mammalian PrP has demonstrated the high degree of conservation (van Rheede *et al.*, 2003). Nevertheless, further multi-sequence analysis was performed in this study with emphasis on the topogenic domains. Sequence analysis was performed by multi-sequence alignment of not too distant species to determine if topogenic STE and TM domains of PrP are subject to evolutionary conservation and if the capacity of PrP to be made in multiple topological isoforms bears weight on organismal selection pressure. A multi-sequence alignment was performed with six mammalian and one reptile sequence using the ClustalW algorithm which highlighted several conserved segments of PrP including STE and TM domains (Figure 5A). Further sequence analysis was performed by dot plot comparing human and turtle amino acid residues with the window set to 15 residues the stringency set to 11 only STE and TM domains were highlighted (Figure 6A). In conjunction with the notion that single point mutations in these domains can dramatically alter the ratio of expressed topological forms (Kim & Hegde, 2002) suggest that the capacity of PrP^C to be expressed in multiple topological forms has been maintained

throughout vertebrate evolution. However the detection of PrP^C under normal physiological conditions has been limited to SecPrP and its truncated form (Vincent *et al.*, 2001) and it remains unexplored if the physiological relevance of CtmPrP or NtmPrP may account for the conservation of the STE and TM domains.

Figure 5



Legend Figure 5. *In silicio* analysis of topogenic domains. (A) The conservation of PrP domains was assessed by performing multi-sequence alignments of 7 vertebrate amino acid sequences with human, mouse, Syrian hamster, cat, sheep, bovine and turtle with Clustal W (Thompson *et al.*, 1994) as described under *Material and Methods*. Conserved residues are denoted by an asterisk or red marked text; conservative substitutions are denoted by a colon. STE and TM domains are marked by a frame. (B) Selection pressure on STE and TM domain endures thorough out vertebrate evolution. Dot plot analysis of human PrP and turtle PrP amino acid sequences as described under *Material and Methods*. With the given window of residues and stringency the STE and TM domains were revealed to be the most conserved domains within PrP.

4.2 PrP^C is expressed as both ^{C_{tm}}PrP and ^{Sec}PrP under non-pathologic conditions *in vivo*

To test the hypothesis that PrP^C may consist of multiple topological isoforms, brains of wt PrP expressing mice were analyzed by the *topological* and *conformational* assays.

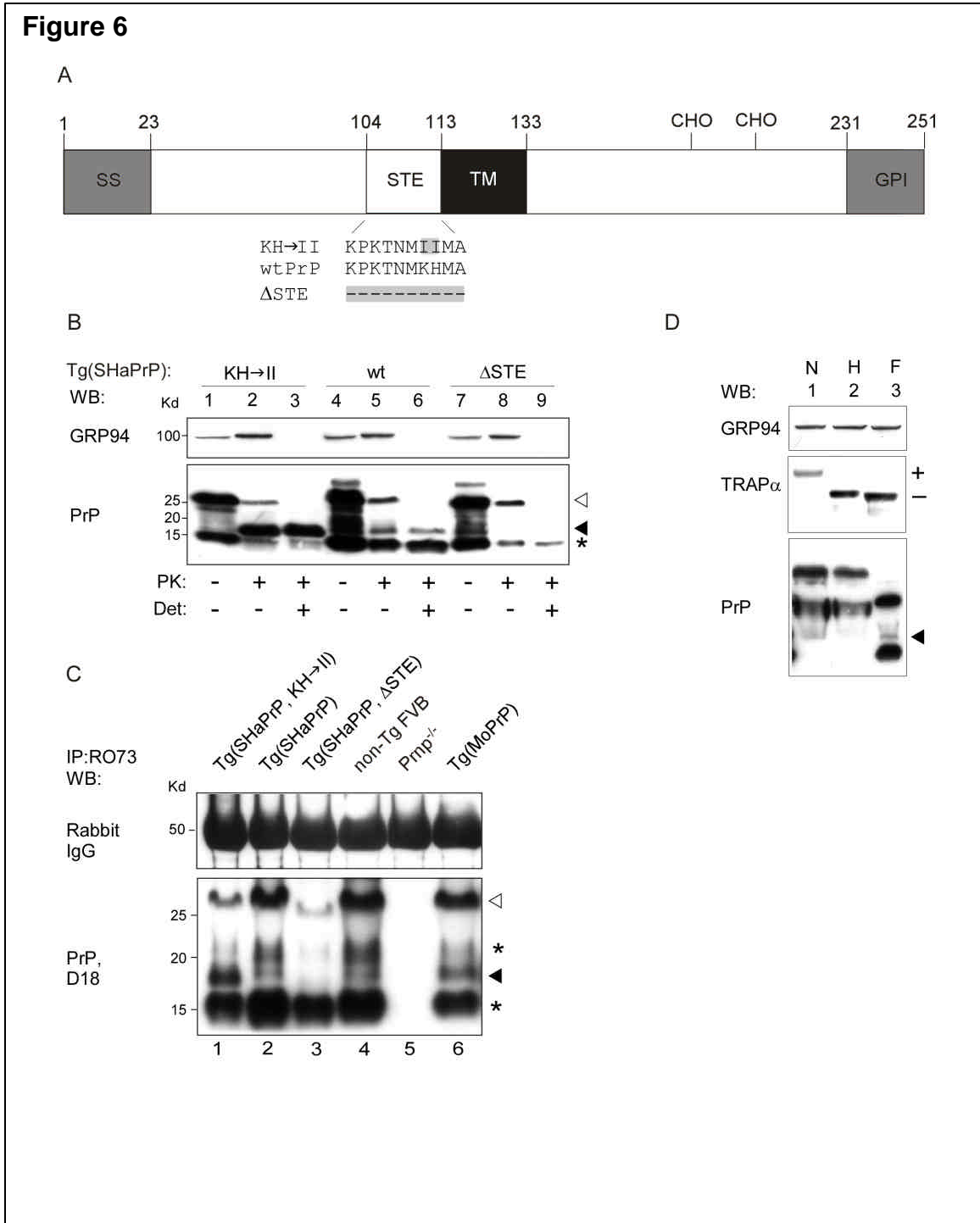
The detection of topological forms of PrP has been previously established (Hegde *et al.*, 1998a) and is based on the accessibility of membrane shielded PrP domains to limited proteolysis with proteinase K (PK) in the absence of any detergents (Figure 3A). Additionally, it has been shown ^{C_{tm}}PrP is more protease resistant compared to ^{Sec}PrP in the presence of non-denaturing detergent therefore displaying conformational variations among the two topological forms (Figure 3B).

Expression of ^{C_{tm}}PrP and ^{Sec}PrP was examined in brain homogenates of asymptomatic transgenic (Tg) mice overexpressing wt Syrian hamster PrP (SHaPrP) on a *Pmp*^{-/-} background, designated Tg(SHaPrP) mice, by both topological and conformational analysis. Tg(SHaPrP) mice were compared to Tg

mice expressing a mutant that favors either ^{Ctm}PrP expression as a result of mutations (K110I, H111I) in the topogenic STE domain, termed Tg(SHaPrP,KH→II) mice, or compared to a mutant that is predominantly expressed in the ^{Sec}PrP form as a result of a deletion of the STE domain $\Delta 104-113$, termed Tg(SHaPrP Δ STE) mice (Figure 6A; Yost *et al.*, 1990; Hegde *et al.*, 1998a).

To increase the likelihood of detecting ^{Ctm}PrP , the topological and conformational analyses were performed with whole brain homogenates rather than with ER-derived microsomal membranes (Hegde *et al.*, 1998a; Stewart *et al.*, 2005), as it represents only 1-5% of the total expressed PrP. Upon overexposure of the Western-blots, ^{Ctm}PrP was detected in the brains of Tg(SHaPrP) mice and at much higher levels in Tg(SHaPrP,KH→II) mice (Figure 6B, black arrowhead). ^{Sec}PrP and C1 were detected in all Tg mice (Figure 6B, white arrowheads). In no instance could ^{Ntm}PrP be detected.

To substantiate the physiological relevance of the findings in Tg(SHaPrP) mice the occurrence of ^{Ctm}PrP and ^{Sec}PrP were further analyzed in brains of non-Tg wt mice. With further enhancements to the detection method by immunoprecipitation of samples that were processed by the topological assay ^{Ctm}PrP was detected in non-Tg wt FVB mice (Figure 6C, black arrowhead), corroborating the findings in Tg(SHaPrP) mice and excluding the likelihood that the detection of ^{Ctm}PrP in Tg(SHaPrP) mice is a mere result of overexpression. Therefore the detection of ^{Ctm}PrP and ^{Sec}PrP in the healthy murine brains expressing wt PrP^C provides a line of evidence in support of the proposed hypothesis.



Legend Figure 6 Analysis of PrP topology *in vivo*. (A) Schematic diagram of topogenic PrP domains. Two mutants, KH→II and Δ STE, were chosen that favor expression in the Ctm PrP and Sec PrP form, respectively. SS, Nterminal signal sequence; STE, stop-transfer-effector domain; TM, transmembrane domain; CHO, Nlinked glycosylation sites; GPI, glycolipidation sequence. Amino acid numbering refers to the SHaPrP sequence. (B) Wild-type PrP^C is expressed as Ctm PrP and Sec PrP. Topological (lanes 2, 5 and 8) and conformational (lanes 3, 6 and 9) analyses of PrP expressed in Tg(SHaPrP,KH→II), Tg(SHaPrP) and Tg(SHaPrP, Δ STE) mice, as indicated. Brain homogenates were left untreated (lanes 1, 4, 7) or digested with PK (0.25 mg/ml) in the absence (lanes 2, 5 and 8) or presence (lanes 3, 6 and 9) of Triton-X100 (det) for 60 min at 0 °C. Samples were deglycosylated prior to Western-blotting with anti-SHaPrP 13A5 and anti-GRP94 (control for vesicle integrity and loading). Black arrowhead indicates Ctm PrP; white arrowhead depicts Sec PrP or full-length PrP in untreated samples; asterisk denotes truncated PrP, termed C1. (C) Ctm PrP and Sec PrP are detected in non-Tg wt mice (lane 4). Brain homogenates from indicated mice were processed by the *topological* assay, deglycosylated, immunoprecipitated, and PrP was detected by Western-blotting with Fab'2 D18 which recognizes mouse PrP with a higher affinity than SHaPrP therefore SHa controls are underrepresented (lanes 1-3). Tg mice overexpressing mouse PrP (MoPrP) to a similar extent than Tg(SHaPrP) mice were used to account for the difference in antibody affinity. Rabbit IgG heavy chain was probed to normalize loading. Black arrowhead indicates Ctm PrP; white arrowhead depicts Sec PrP; asterisk shows truncated PrP forms C1 and C2. (D) Mature Ctm PrP is expressed in Tg(SHaPrP) mice. Brain homogenates were subject to the *topological* assay, then left untreated (lane 1), treated with EndoH (lane 2) or treated with PNGaseF (lane 3). Anti-TRAP α is a control for EndoH treatment; GRP94 is a control for loading. Comparing amounts of deglycosylated Ctm PrP was used to assess the fraction of matured chains, revealing that Ctm PrP remains mostly resistant to EndoH treatment. Glycosylation is indicated by + or -. Black arrowhead indicates deglycosylated Ctm PrP.

4.3 Sec PrP and Ctm PrP are recognized as physiologically folded forms

Proteins that fail to pass the quality control machinery due to misfolding are subject to the endoplasmic reticulum (ER)-associated degradation (ERAD), which involves retrotranslocation to the cytoplasm and degradation by the ubiquitin proteasome system. Misfolded proteins are initially retained in the ER with untrimmed mannose units until being transported to the cytoplasm where

glycans are removed prior to degradation by UPR (Ellgaard *et al.*, 1999). Therefore, PrP molecules targeted for degradation are expected to show either an increase in mannose-containing glycans or completely deglycosylated chains. To determine if the Ctm PrP molecules detected in Tg(SHaPrP) brains were *bona fide* folded forms or if they were misfolded and destined for degradation the maturation of glycans was probed.

Previous studies have shown mutants favoring the expression of Ctm PrP mature to a post-ER compartment in some cases (Hegde *et al.*, 1998a; Stewart & Harris, 2005). However, these analyses were performed with untreated lysates and therefore maturation could not be attributed specifically to the subfraction of Ctm PrP. To overcome this limitation and determine the maturation of the fraction of Ctm PrP detected in Tg(SHaPrP) mice, the glycosylation maturation of brain lysates that had been processed by the *topological assay* followed by treatment with either Endoglycosidase H (Endo H), which deglycosylates immature N-linked glycans, or by PNGase F, which deglycosylates all N-linked glycans was analyzed. To control for Endo H activity a known ER glycoprotein, TRAP α was analyzed in parallel. Most of the detected PK-resistant Ctm PrP molecules appeared to be resistant to Endo H treatment and sensitive to PNGase F treatment (Figure 6D), suggesting that Ctm PrP had matured to a post-ER compartment. Sec PrP was equally Endo H resistant and appeared indistinguishable from Ctm PrP with respect to maturation. Taken together, the data suggest both Ctm PrP and Sec PrP are topological isoforms of PrP^C and are both processed by the folding machinery of the ER in a similar fashion.

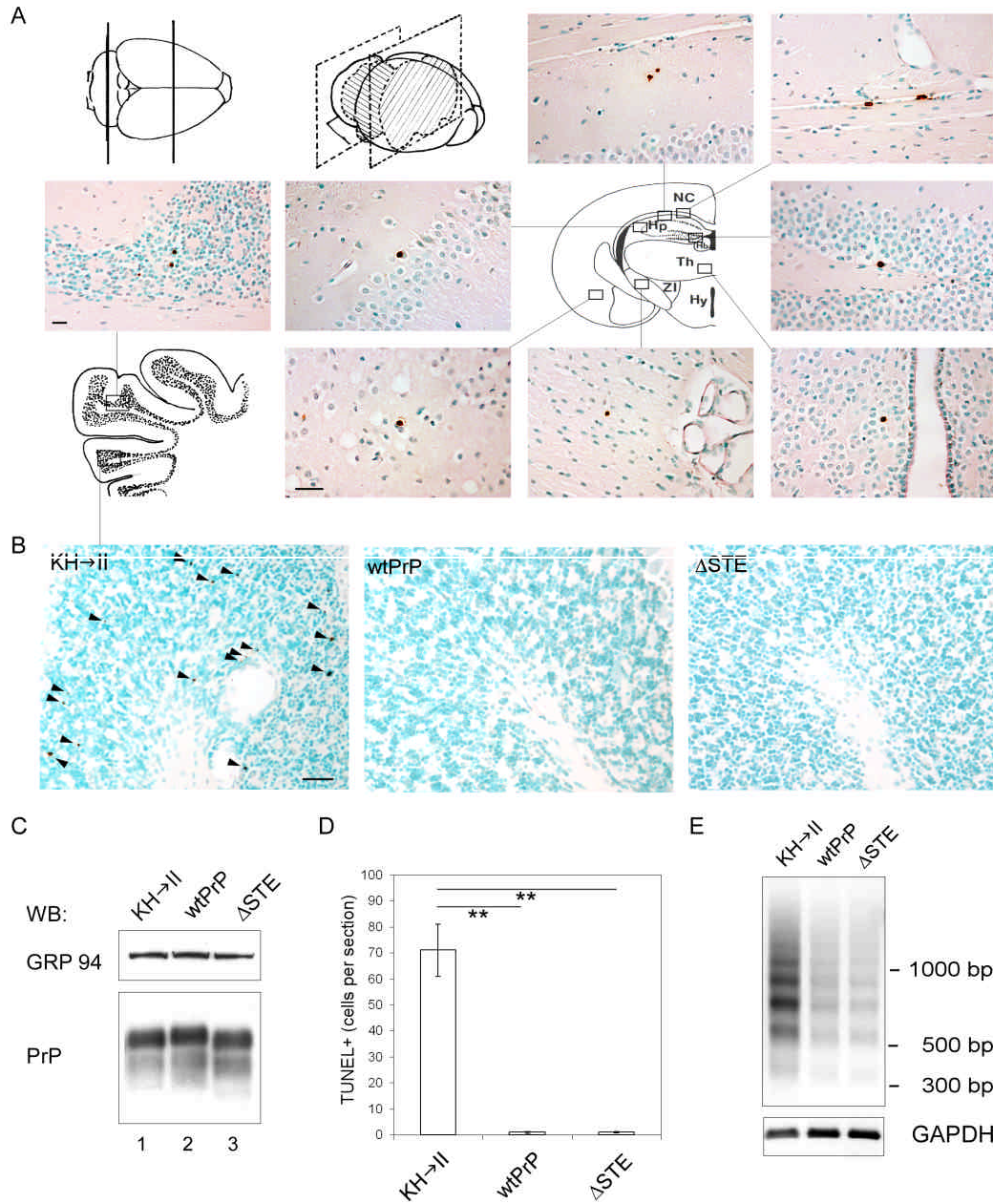
4.4 Pathologic apoptosis results from ^{Ctm}PrP expression

Initial evidence suggests PrP^C may naturally consist of both ^{Ctm}PrP and ^{Sec}PrP therefore it was next examined if each isoform exhibited independent functions. The physiologic impact and cellular response of ^{Ctm}PrP and ^{Sec}PrP expression were investigated by taking advantage of mutations biasing the fraction of each isoform, which enabled me to segregate and amplify the function attributed to each isoform upon which the activity of each isoform could be assessed in non-Tg wt mice.

Increased expression of ^{Ctm}PrP has been associated with both transmissible and some genetic prion diseases (Hegde *et al.*, 1998a; Hegde *et al.*, 1999). However, the causative mechanisms underlying ^{Ctm}PrP mediated disease and its potential cellular function remains unclear. The potential neurotoxic gain-of-function associated with ^{Ctm}PrP expression was investigated in Tg mice. Tg(SHaPrP,KH→II) mice develop ataxia at ~90 days of age and show profound astrogliosis and vacuolation which are common neuropathological features also observed in other prion diseases (Hegde *et al.*, 1998a). Upon neuropathologic analysis, neuronal loss and pyknotic nuclei were evident in the granule cell layer (GCL) of the cerebellum (data not shown), raising the possibility of apoptotic cell loss. Using terminal dUTP nick end-labeling (TUNEL) to evaluate apoptosis, brains of symptomatic Tg(SHaPrP,KH→II) mice were examined and TUNEL-positive (+) cells were detected throughout the brain, however extensive levels were only observed in the cerebellum (Figure 7A). Quantitative analysis of TUNEL+ cells in the cerebellum was performed. As controls, age-matched

Tg(SHaPrP) and Tg(SHaPrP, Δ STE) mice were analyzed, which expressed total PrP at comparable levels in all Tg lines (Figure 7C). Tg(SHaPrP, KH \rightarrow II) mice displayed increased TUNEL+ nuclei in the GCL of the cerebellum (Figure 7B). Quantitative analysis revealed ~50-fold more TUNEL+ nuclei in Tg(SHaPrP, KH \rightarrow II) mice compared to Tg(SHaPrP) and Tg(SHaPrP, Δ STE) mice (Figure 7D). *Prnp*^{-/-} mice also showed no abnormal cell death (data not shown), excluding the likelihood that apoptosis is due to loss of PrP^C function. To confirm nuclear fragmentation resulted from apoptosis, brains were further analyzed for internucleosomal DNA-fragmentation, a hallmark of apoptosis (Kerr *et al.*, 1972). Higher levels of internucleosomal DNA-fragmentation was detected in Tg(SHaPrP, KH \rightarrow II) mice compared to Tg(SHaPrP, Δ STE) and Tg(SHaPrP) mice (Figure 7E) which appears consistent with the observation made by TUNEL analysis. Together, these findings suggest that neurodegeneration observed in Tg(SHaPrP, KH \rightarrow II) mice occurs through apoptosis and concomitant loss of cerebellar GCL neurons.

Figure 7

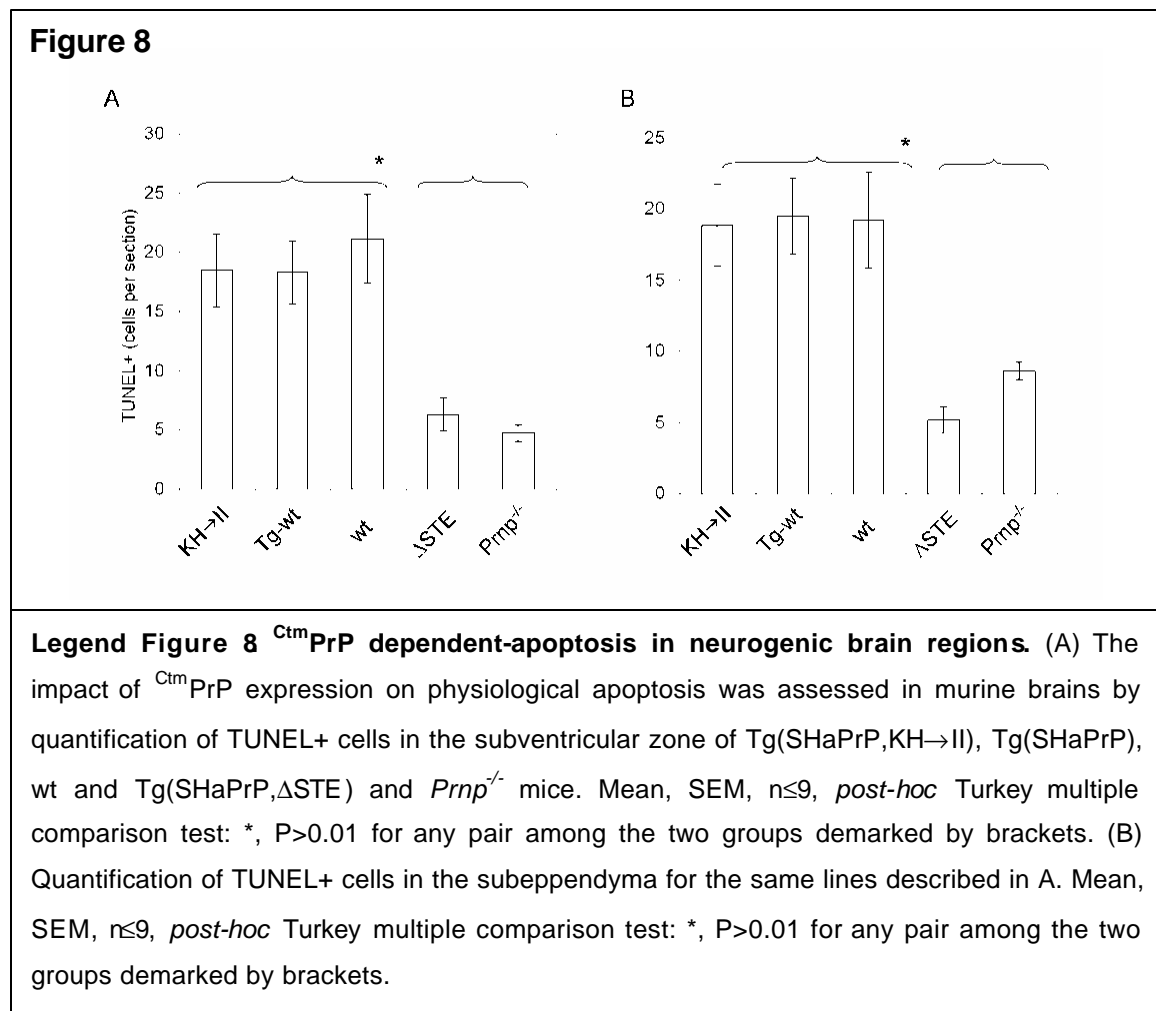


Legend Figure 7. Analysis of ^{Ctm}PrP-mediated apoptosis *in vivo*. (A) Coronal brain sections from Tg(SHaPrP, KH→II) mice were evaluated at ~90 days of age by TUNEL. TUNEL+ cells are shown from representative fields in the cerebellum (bottom left) and seven fields from a single brain section encompassing the hippocampus. Hp=hippocampus, Th=thalamus, Hy=hypothalamus, NC=neocortex, and ZI=zona incerta. Scale bars, 25 μ m. (B) Cerebellar brain sections (coronal) from Tg(SHaPrP,KH→II), Tg(SHaPrP), and Tg(SHaPrP, Δ STE), mice were evaluated at ~90 days of age by TUNEL. Images displayed are from representative matched fields with similar bregma. Arrowheads point to TUNEL+ nuclei. Scale bars, 25 μ m. (C) Western-blotting of brain homogenates shows that all Tg mice expressed similar levels of PrP^C, normalized against GRP94. Under these conditions PrP^C from different Tg mice appears similar. (D) Quantitative analysis in the cerebella of the Tg mice indicates significantly greater TUNEL+ cells in Tg(SHaPrP,KH→II) mice. Mean, SEM, n=7, one-way ANOVA (P>0.0001), *post-hoc* Turkey multiple comparison test (**, P>0.001). (E) DNA was isolated from brains of ^{Ctm}PrP-expressing mice and analyzed for internucleosomal DNA-fragmentation. GAPDH levels were assessed to control for amount of genomic DNA.

4.5 Physiologic apoptosis as a result of ^{Ctm}PrP expression

Systematic analysis for apoptosis was also performed on other brain regions from Tg(SHaPrP,KH→II), Tg(SHaPrP, Δ STE), Tg(SHaPrP), non-Tg wt and *Prnp*^{-/-} mice. Surprisingly, significantly more TUNEL+ cells (~3-fold) was observed in the subventricular zone (SVZ) and subependyma (SE) of Tg(SHaPrP,KH→II), Tg(SHaPrP) and non-Tg wt mice, compared to Tg(SHaPrP, Δ STE) mice and *Prnp*^{-/-} mice (Figure 8E and F). Considering that both Tg(SHaPrP, Δ STE) and *Prnp*^{-/-} mice displayed similar counts in the SVZ and SE indicates that the reduction of TUNEL+ cells is not a consequence of ^{Sec}PrP expression and argues lack of ^{Ctm}PrP expression is the proximal cause for the reduced apoptosis

observed, suggesting the apoptosis observed in the SVZ and SE of non-Tg wt mice is likely associated with the expression of $C^{tm}PrP$. The SVZ and SE are well characterized stem cell niches, also with the highest densities of physiologic apoptosis in the murine brain which has been attributed to the loss of progenitor cells that fail to establish a niche during maturation (Biebl *et al.*, 2000). Taken together, the data presented here provide evidence $C^{tm}PrP$ may have a normal physiologic role triggering apoptosis in the SVZ and SE as part of the natural elimination process of superfluous-repopulating progenitor cells.



4.6 Neurodegeneration and ^{Ctm}PrP induction in PrP^C overexpressing Tg(tTA:mPrP) mice

An alternative approach was sought to demonstrate ^{Ctm}PrP mediated apoptosis and neurodegeneration in the absence of any mutations to rule out a contribution of the mutation to the phenotype itself. Previous studies in Tg mice have revealed that the relative amount of ^{Ctm}PrP increases with the expression level (Hegde *et al.*, 1998a). Therefore it was plausible that extensive overexpression of wt PrP could facilitate increased production of ^{Ctm}PrP. To avoid embryonic lethality which has been described when overexpressing PrP (Tremblay *et al.*, 1998) a reverse-tetracycline tissue specific inducible Tg model system was employed (Tremblay *et al.*, 1998), termed Tg(tTA:mPrP) mice.

4.6.1 Neurodegeneration and apoptosis in Tg(tTA:mPrP) mice

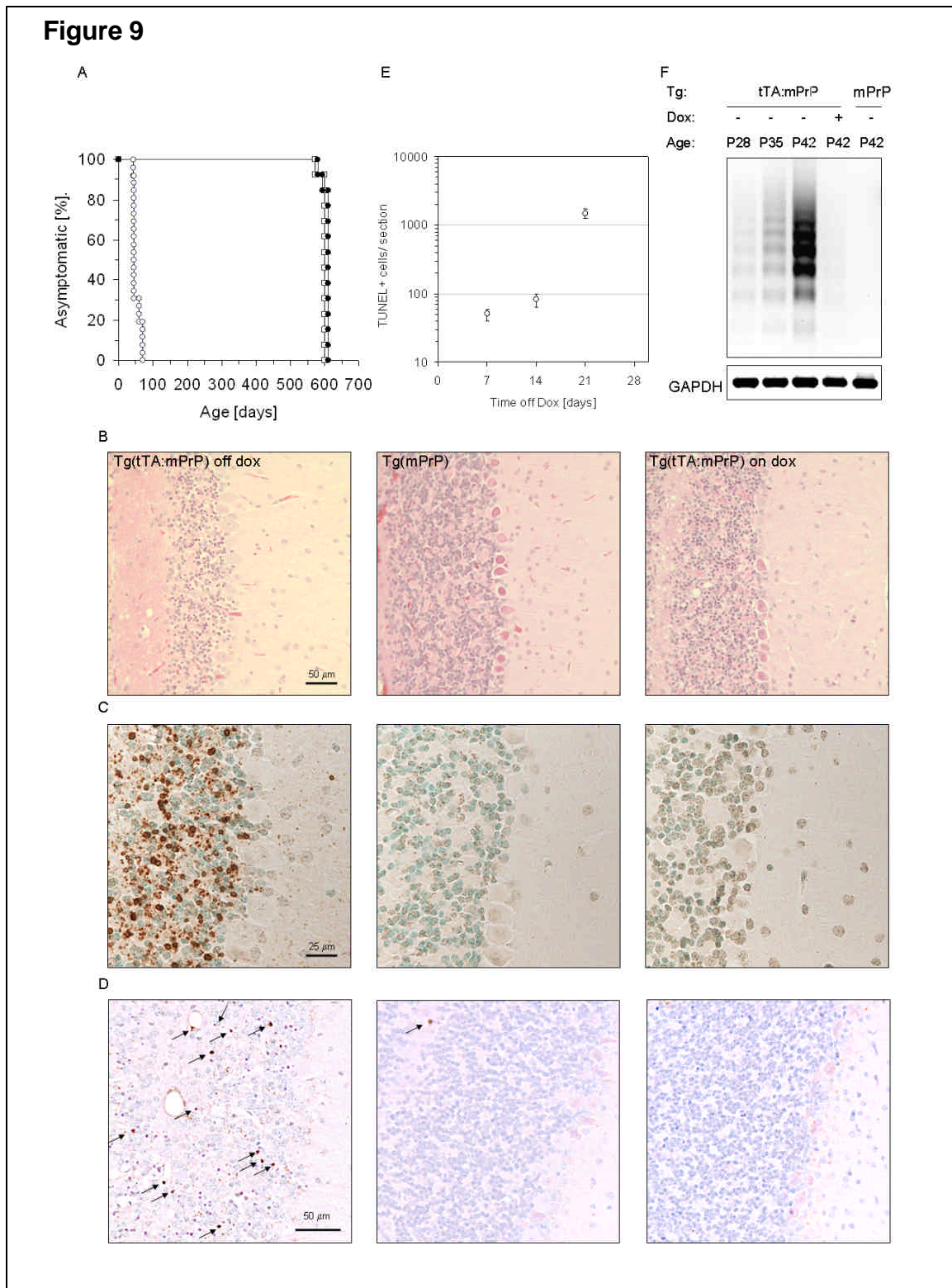
At postnatal day 21 (P21), dox was withdrawn and the mice were weaned. Within three to four weeks, most Tg(tTA:mPrP) mice develop severe ataxia and circling (Figure 9A), at which time they were sacrificed for neuropathologic analysis. Postmortem histological examination of brain sections showed loss of grey matter with the most extensive degeneration observed in the cerebellum (Figure 9B, left panel and data not shown). Numerous pyknotic nuclei were observed throughout the brain, most extensively in the granule cell layer of the cerebellum indicating a possible apoptotic mode of cell death (Figure 9B, left panel) as seen before in Tg(SHaPrP,KH→II) mice (Figure 7B). Further analysis on the cerebellum was performed by TUNEL to identify apoptotic cells. Thousands of

TUNEL-positive cells were identified in the granule cell layer (Figure. 9C, left panel) with many cells in the early to mid-apoptotic stage evident by the degree of nuclear condensation in cells staining positive for activated caspase-3 (Figure 9D, left panel).

To understand further the development of disease, the level of cell death was analyzed by TUNEL on a weekly basis after PrP^C induction at P21. A steady rise in the number of TUNEL+ cells in the first two weeks was observed, with a drastic increase in the third week (Figure. 9E), which correlated with the development of clinical symptoms. Cerebellar DNA was further analyzed for internucleosomal DNA-fragmentation. DNA extracts were analyzed at 0, 7, 14 and 21 days after PrP induction. Initially, little DNA-laddering was detected, but a substantial increase was observed within three weeks post induction (Figure. 9F). These data agree well with observations made by TUNEL-staining suggesting that apoptosis is the key mechanism of cell death and neurodegeneration in these mice.

To control for the specificity of cell death by PrP, Tg(tTA:mPrP) mice were also kept on dox throughout the duration of all experiments presented here (Figure 9A–F). Further, to rule out any pleiotropic effects of dox administration, Tg(mPrP) mice that constitutively express PrP were used as controls (Figure 9A–F) and were treated with dox in the same manner as the experimental animals. In all cases, control animals remained healthy and showed no signs of neurodegeneration (Figure 9A–F), indicating that the observed neurodegeneration is related to PrP^C expression. Therefore high levels of PrP^C

appear to lead to neurodegeneration by a caspase-3–mediated apoptotic pathway.

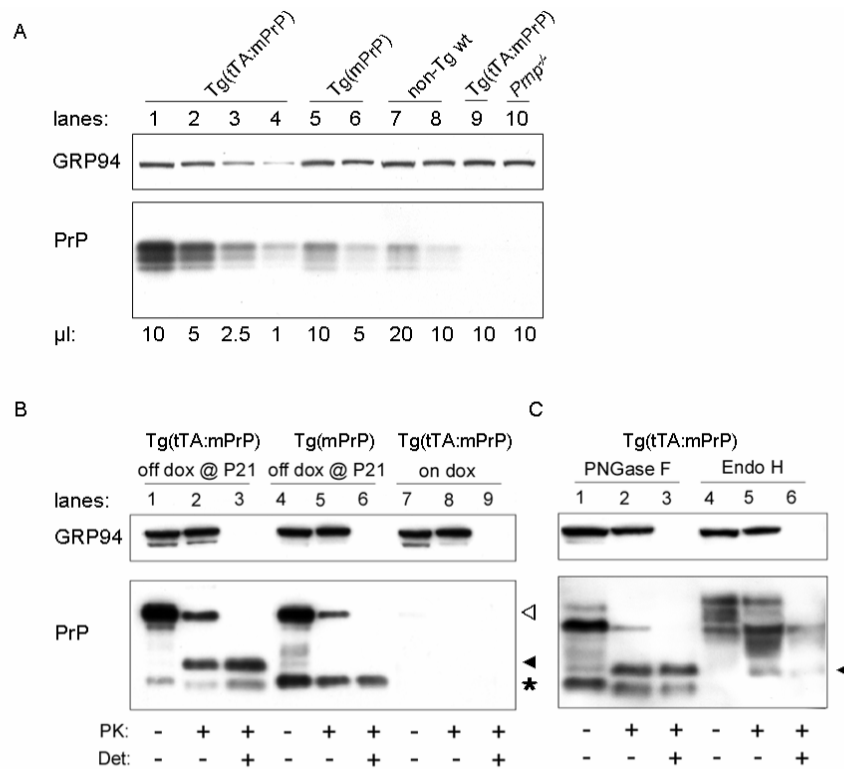


Legend Figure 9. Neurodegenerative disease in inducible Tg(tTA:mPrP) mice overexpressing PrP^C. (A) Tg(tTA:mPrP) mice were administered dox until postnatal (P) day 21 (open circles, n=27) or maintained on dox throughout the experiment (closed circles, n=14) and compared to Tg(mPrP) mice treated with dox the same way as Tg(tTA:mPrP) mice (open squares, n=14). Surviving mice were all sacrificed at approximately 600 days. (B) Histopathology in Tg(tTA:mPrP) (left) and Tg(mPrP) (center) were withdrawn from dox at P21 (left), or Tg(tTA:mPrP) mice were maintained on dox throughout (right). All mice were sacrificed at P42. Micrographs show hematoxylin and eosin (H&E) staining of formalin-fixed, paraffin-embedded coronal sections from the cerebellum. Scale bar is 50 μ m. (C) Coronal sections from panel B were also stained by TUNEL (dark brown nuclei) to determine the level of cell death. Scale bar is 25 μ m. (D) Coronal brain sections from panel B were also probed for activated caspase-3 (dark brown staining). The most significant caspase-3-positive cells are highlighted by arrows. Scale bar is 50 μ m. (E) Quantification of TUNEL in the cerebellum from Tg(tTA:mPrP) taken off dox at P21 and sacrificed at time points P28, P35, and P42. The mean was derived from counting multiple cerebellar sections normalized for surface area, the error bars display the data range (n<6). (F) Verification of apoptosis by internucleosomal DNA-fragmentation analysis. DNA was extracted from brain homogenates and DNA-laddering was analyzed. Tg(tTA:mPrP) were taken off dox at P21 and sacrificed at time points P28, P35 and P42. DNA-laddering increased substantially from brain samples taken at P42. Tg(mPrP) mice taken off dox at P21 and Tg(tTA:mPrP) mice treated with dox throughout the experiment were also analyzed; both controls were sacrificed at age P42. GAPDH was probed to control for the amount of genomic DNA.

4.6.2 Dramatic ^{Ctm}PrP expression in brains of Tg(tTA:mPrP) mice

The expression level of Tg(tTA:mPrP) mice in comparison to Tg(mPrP) mice and wt mice was determined by Western-blotting of brain homogenates. Tg(tTA:mPrP) mice exhibit ~12-16 fold overexpression compared to wt mice and ~4 fold compared to Tg(mPrP) mice (Figure 10A). Brain homogenates were further analyzed by the *topological* and *conformational* assays. High levels of ^{Ctm}PrP were detected in Tg(tTA:mPrP) mice whereas predominantly ^{Sec}PrP and its N-terminally cleaved form, termed C1 (Vincent *et al.*, 2001), were detected in

Tg(mPrP) mice (Figure 10B, compare lane 2 with 5, lane 3 with 6). Thus, simply by overexpressing wt PrP^C leads to changes in the topological isoform from predominantly SecPrP to CtmPrP, which consequently triggers neurodegeneration. To probe for differences in glycan maturation, brain samples from Tg(tTA:mPrP) mice taken off dox at P21 and sacrificed at P42 were subject to topological analysis and treated either with PNGase F or with EndoH. SecPrP and most of the CtmPrP detected was glycosylated (Figure 10C; compare lanes 1 and 4) and remained mostly resistant to EndoH treatment (Figure 10C, compare lane 2 with 5, lane 3 with 6), suggesting that both isoforms have passed the ER quality control machinery. Taken together the data suggest that overexpression of wt PrP^C can lead to a dramatic induction of CtmPrP which leads to rapid and severe neurodegeneration triggered by capase-3 mediated apoptosis.

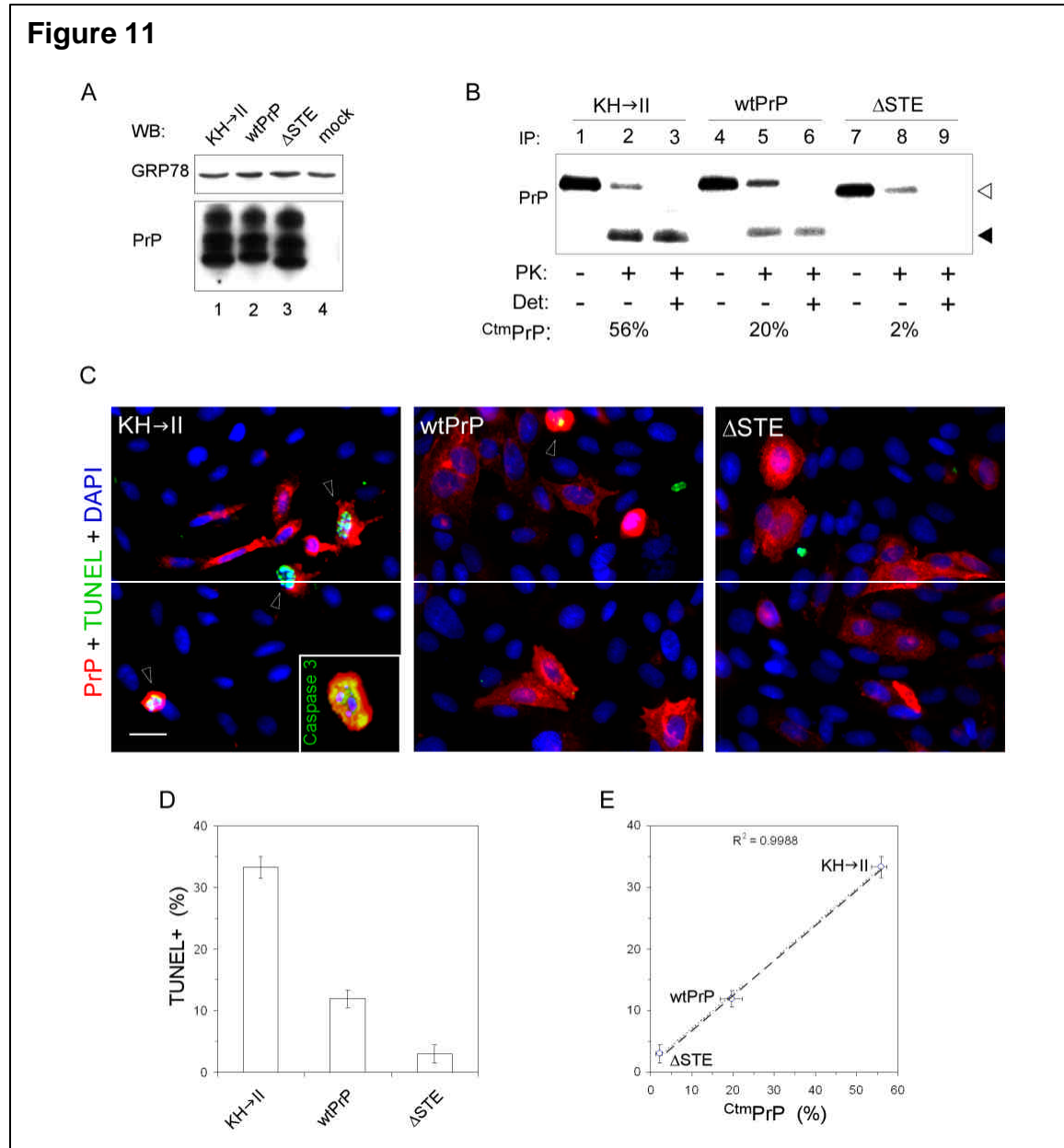
Figure 10

Legend Figure 10. Overexpression of PrP^C results in a disproportionate increase in CtmPrP expression. (A) The expression level of PrP in the cerebellum was determined at P42 by Western-blotting of normalized brain homogenates from Tg(tTA:mPrP) taken off dox at P21, lanes 1, 2, 3, 4 with 10 μl, 5 μl, 2.5 μl and 1 μl loaded respectively; Tg(mPrP) taken off dox at P21, lanes 5 and 6 with 10 μl and 5 μl loaded respectively; non-treated wt mice, lanes 7 and 8 with 20 μl and 10 μl loaded respectively; Tg(tTA:mPrP) on dox, lane 9 with 10 μl and non-treated *Prnp^{-/-}* mice, lane 10 with 10 μl. Brain homogenates were resolved and probed against anti-PrP (D18) and anti-GRP 94 (loading control). (B) Topological and conformational analysis of PrP^C from brains of Tg mice described in panel A. Whole brain homogenates were either left untreated (lanes 1, 4, 7) or digested with PK in the absence (lanes 2, 5, 8) or presence (lanes 3, 6 and 9) of Triton-X100 (Det). Samples were deglycosylated with PNGase F prior to Western-blotting with anti-PrP and anti-GRP94 (loading control). Note that the CtmPrP signature fragment remains protected from PK in the presence of detergent. Black arrowhead depicts the position of CtmPrP; white arrowhead depicts the position of SecPrP or full-length PrP in untreated samples. The asterisk signifies the position of the C1 proteolytic fragment of PrP. (C) CtmPrP maturation was investigated in Tg(tTA:mPrP) mice taken off dox at P21 and sacrificed at P42 by Endo H treatment. Brain homogenates were subjected to topological and conformational analysis as described in panel A and treated with either EndoH or PNGase F. Black arrowhead depicts the position of deglycosylated CtmPrP.

4.7 A cell culture model system: ^{Ctm}PrP triggers apoptosis in a dose-dependent manner

To investigate if the observed apoptosis in brains of Tg(SHaPrP,KH→II) mice and Tg(tTA:mPrP) mice is a *direct* consequence of ^{Ctm}PrP expression, a cell culture-based assay was established. CHO-K1 cells were transfected with either the ^{Ctm}PrP-favoring mutant KH→II, the ^{Sec}PrP-favoring mutant ΔSTE, or wt PrP. Western-blot analysis of cell lysates confirmed that expression levels and glycosylation patterns of PrP were similar (Figure 11A) in all three PrP transfectants. Next, topological and conformational analysis of metabolically labeled immunoprecipitated cell lysates were performed to determine the relative amount of ^{Ctm}PrP expression. Quantitative analysis revealed 56%, 20% and 2% of ^{Ctm}PrP in the KH→II, wt and ΔSTE transfectants, respectively (Figure 11B). Fixed cells were stained with an anti-PrP antibody and 4',6-diamidino-2-phenylindole (DAPI) to identify transfected cells and analyze their respective morphology. In the KH→II transfectants, many cells showed condensed elliptic to circular soma; some wt PrP-expressing cells showed a similar cytopathic phenotype (Figure 11C). A proportion of the cytopathic cells displayed condensed or fragmented nuclei which frequently stained positive for TUNEL (Figure 11C) or activated caspase-3 (Figure 11C, insert). Analysis of TUNEL staining showed cells expressing the KH→II mutant had significantly higher incidences of TUNEL+ nuclei compared to cells expressing the same level of wt PrP; cells expressing similar levels of the ΔSTE mutant had the least amount of TUNEL+ nuclei (Figure 11C and D). A strong correlation was identified between

C^{tm} PrP levels and cell death: higher proportions of C^{tm} PrP expression correlated with more TUNEL+ cells (Figure 11E), arguing that C^{tm} PrP triggers apoptosis in a dose-dependent manner. Furthermore, the correlative evidence shows that wt PrP has the capacity to trigger cell death, dependent on its propensity to generate C^{tm} PrP.



Legend Figure 11. Analysis of ^{Ctm}PrP-induced apoptosis in cultured cells. (A) Western-blot analysis probed with anti-PrP and anti-GRP78 (loading control) shows that all transfectants express similar levels of PrP. (B) Topological (lanes 2, 5 and 8) and conformational (lanes 3, 6 and 9) analyses of CHO-K1 cells expressing KH→II, wt PrP or ΔSTE were performed. Lanes 1, 4 and 7, untreated cells. White arrowhead indicates full-length PrP (untreated) or ^{Sec}PrP; black arrowhead indicates ^{Ctm}PrP. ^{Ctm}PrP levels are indicated as percentages of total full-length PrP from four determinations. (C) Analysis of apoptosis in PrP^C mutants. CHO-K1 cells were fixed 48 h after transfection with KH→II, wt or ΔSTE and stained by DAPI (blue), TUNEL (green) and anti-PrP (red). Arrowheads depict PrP transfected TUNEL+ cells. Scale bar, 20 μm. Insert: activated caspase-3 (green) in KH-II transfectants (red) with fragmented nuclei (blue). (D) Quantitative analysis of TUNEL+ PrP transfectants from experiments described in C. ~200 cells were counted for each transfectant per experiment. 3 determinations, mean, data range, one-way ANOVA (P>0.0001), *post-hoc* Turkey multiple comparison test (P>0.001 for all pairs). (E) ^{Ctm}PrP expression triggers apoptosis in a dose dependant manner. The relative expression level of ^{Ctm}PrP (panel B) plotted against the extent of apoptosis (panel E) shows a strong correlation (R²=0.9941).

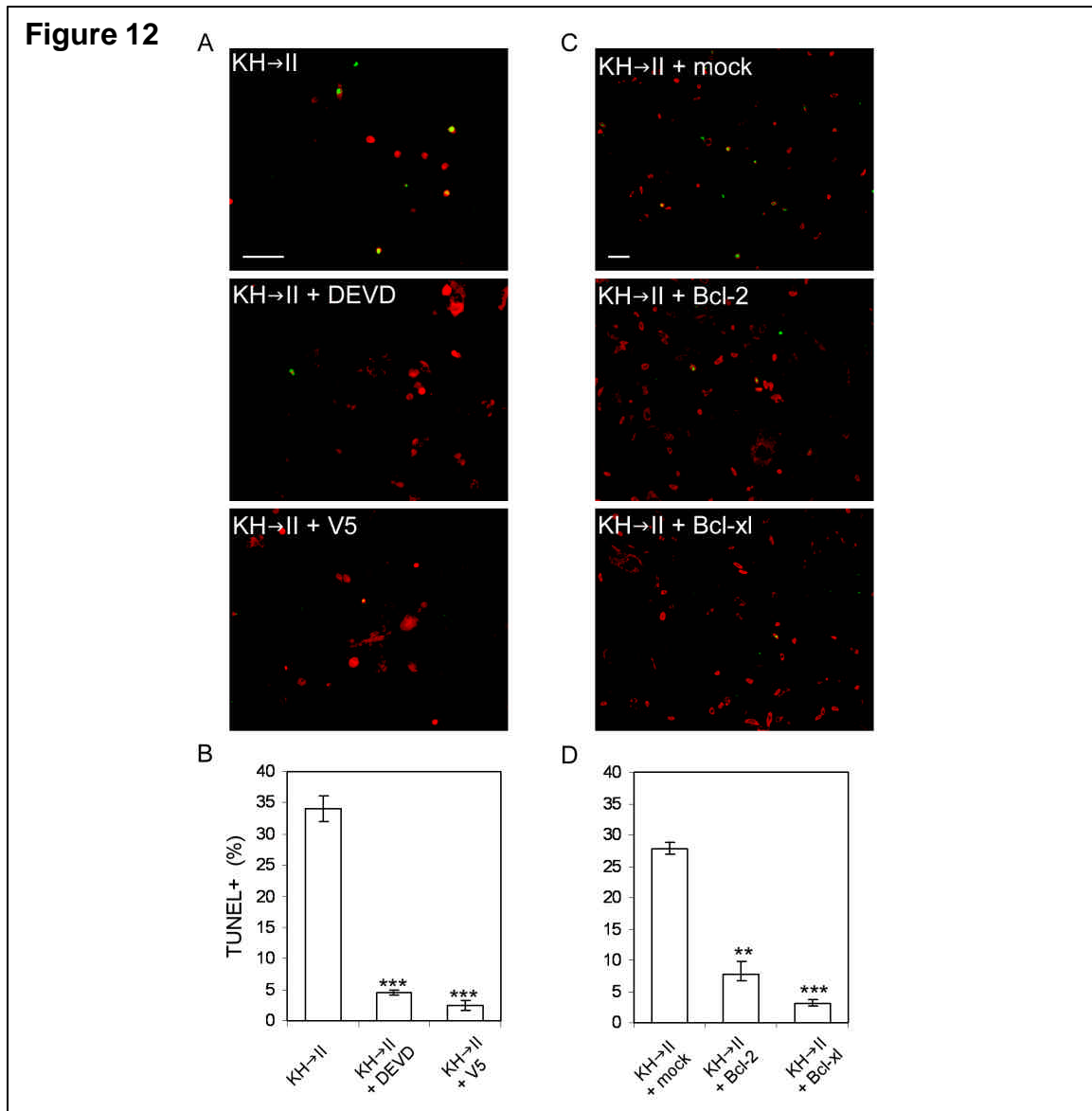
4.8 Characterization of the apoptotic pathway triggered by ^{Ctm}PrP: caspase-3 and Bax dependence

To verify the apoptotic specificity of the TUNEL staining and determine the significance of the activated caspase-3 staining, KH→II-transfected cells were treated with AC-DEVD-FMK, an inhibitor for caspase-3. The caspase-3 inhibitor substantially reduced the number of TUNEL+ nuclei, in contrast to control cells only treated with the vehicle (Figure 12A and B). Taken together, the data suggest ^{Ctm}PrP triggers apoptosis by a caspase-3-mediated pathway in a dose-dependant manner.

The involvement of the pro-apoptotic protein Bax (Oltvai *et al.*, 1993), which has been implicated previously in neurodegenerative disorders (Vila *et al.*, 2001; Lok & Martin, 2002), including some prion diseases (Chiesa *et al.*, 2005) was

investigated. To test if ^{Ctm}PrP-triggered apoptosis occurs through a Bax-dependent pathway, CHO-K1 cells expressing the KH→II mutant were treated with a cell-permeable Bax-inhibiting peptide (V5, (Sawada *et al.*, 2003)). Compared to control cells, a substantial reduction in TUNEL+ cells was observed with the Bax inhibitor (Figure 12A and B). Taken together the data suggests that ^{Ctm}PrP may trigger apoptosis by a Bax and caspase-3 mediated pathway.

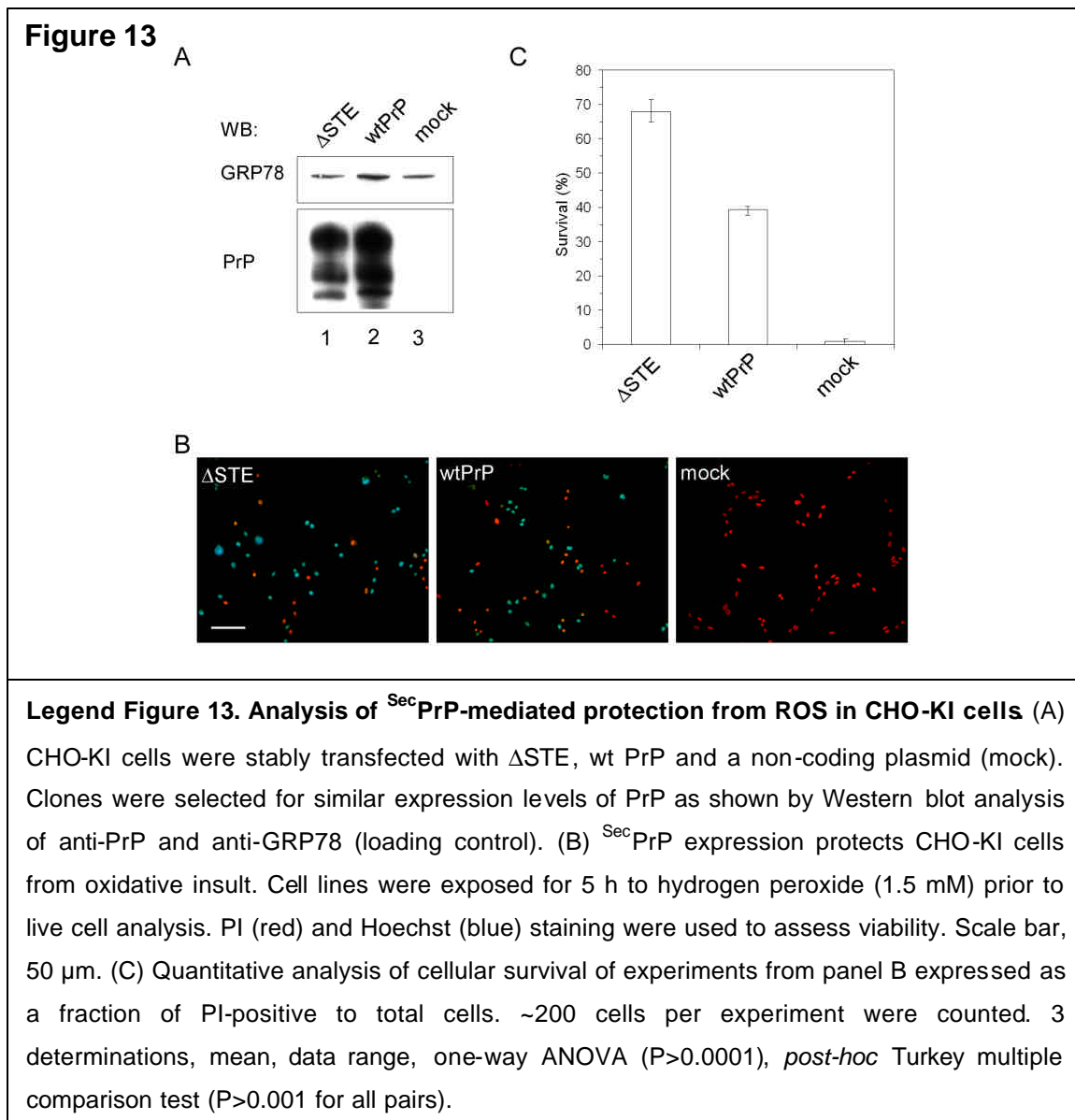
In many instances the pro-apoptotic activity of Bax can be blocked by the expression of antagonizing anti-apoptotic proteins such as Bcl-2 or other members of the BH2 family (Oltvai *et al.*, 1993, Shimizu *et al.*, 1995). Hence it was tested if ^{Ctm}PrP-mediated apoptosis could be blocked by the overexpression of anti-apoptotic molecules Bcl-2 or Bcl-XL. CHO-K1 cells expressing either Bcl-2 or Bcl-XL were clonally selected for high levels of expression (data not shown). The resulting lines were transfected with the ^{Ctm}PrP-favouring KH→II mutant, and the effect of Bcl-2 or Bcl-XL overexpression on ^{Ctm}PrP-triggered apoptosis assessed 48 h later by TUNEL (Figure 12C). Both Bcl-2 and Bcl-XL suppressed ^{Ctm}PrP-mediated apoptosis, by four- and nine-fold, respectively, compared to mock transfected cells (Figure 12D). Hence, Bcl-2 and Bcl-XL seem to antagonize ^{Ctm}PrP activity. Along with previous results, these findings suggest that ^{Ctm}PrP-triggered apoptosis may involve Bax, leading to caspase-3 activation, and ultimately, to internucleosomal DNA-fragmentation and cell death.



Legend Figure 12. Analysis of the pathway of ^{125}I PrP-induced apoptosis. (A) ^{125}I PrP-induced apoptosis is caspase-3 and Bax-dependent. CHO-K1 cells expressing the KH→II mutant were either left untreated, or treated with 100 μM of the specific caspase-3 inhibitor (DEVD) or 100 μM of a Bax-inhibitor (V5) or the vehicle alone. Experiments were carried out as in panels Figure 11C. Scale bar, 50 μm . (B) Quantitative analysis of the effect of the DEVD and V5 on ^{125}I PrP induced apoptosis was performed as described in Figure 11D. Mean, data range, paired one-tailed T-test (**, $P > 0.001$, ***, $P > 0.0001$). (C) ^{125}I PrP-mediated apoptosis can be rescued by the overexpression of Bcl-2 and Bcl-XL. CHO-K1 cell lines overexpressing Bcl-2 and Bcl-XL were assayed for ^{125}I PrP-mediated apoptosis as described in Figure 11C. Scale bar, 50 μm . (D) Quantitative analysis of ^{125}I PrP induced apoptosis in cells overexpressing Bcl-2 and Bcl-XL was performed as described in Figure 11D. Mean, data range, paired one-tailed T-test (***, $P > 0.0001$).

4.9 ^{Sec}PrP^C protects cultured cells from ROS

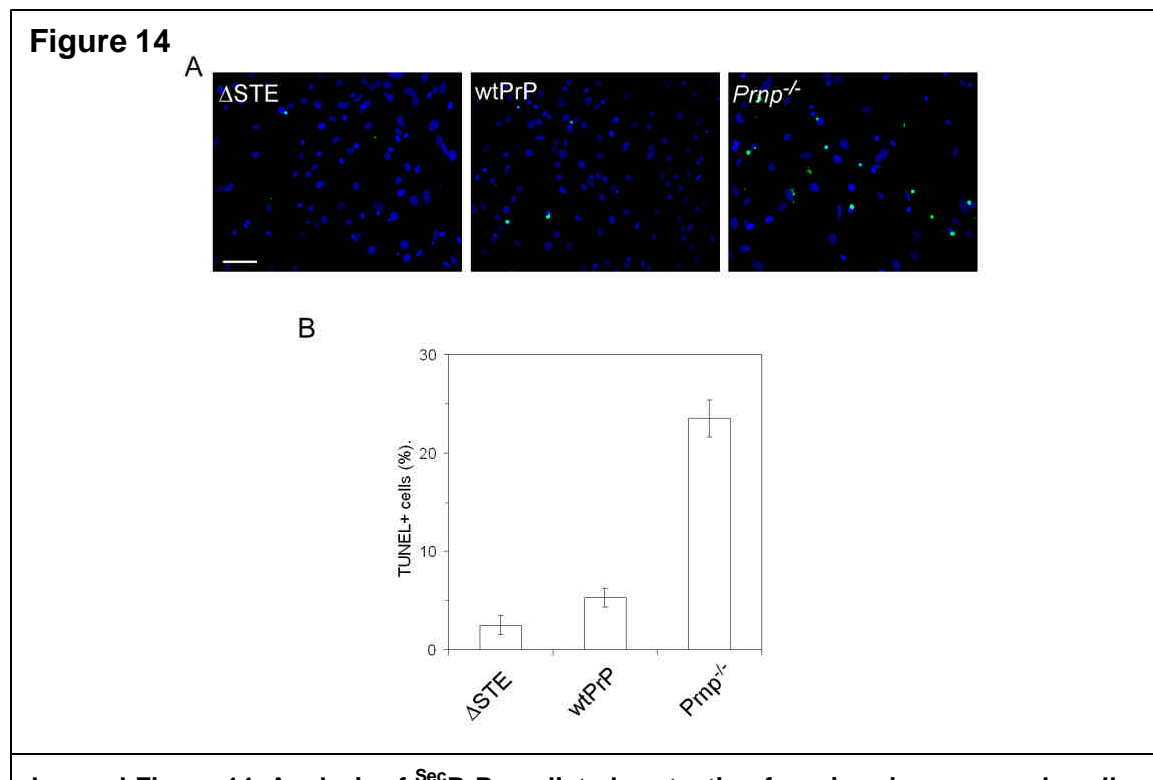
After attributing the toxic activity of PrP^C to the expression of ^{Ctm}PrP, it was examined whether ^{Sec}PrP provides protection against ROS since such a function has been proposed for PrP^C (Wong *et al.*, 2001; Brown *et al.*, 2002; McLennan *et al.*, 2004). Clonal CHO-K1 cell lines expressing either Δ STE or wt PrP^C at similar levels (Figure 13A) or a non-coding plasmid (mock) were subjected to hydrogen peroxide treatment, a broad inducer of ROS. Viability was evaluated by imaging of live cells stained with propidium iodide (PI) and Hoechst 22324 (Figure 13B). Δ STE-expressing cells had the highest viability followed by wt PrP^C-expressing cells. Mock transfectants in contrast showed barely any survival to the oxidative insult (Figure 13C). Consistent with the function proposed for PrP^C it could be found that the protective activity against ROS is likely mediated by the ^{Sec}PrP isoform. Therefore two distinct functions for PrP^C could be shown in the same cell type which is likely due to activities of distinct topological isoforms.



4.10 ^{Sec}PrP protects primary cultured neurons from ROS

Next, it was investigated whether primary granule cell neurons (GCN) derived from Tg(SHaPrP, Δ STE), non-Tg wt mice and *Prnp*^{-/-} mice would also reveal protection of ^{Sec}PrP to ROS. Primary cerebellar GCNs were exposed to kainic acid (KA) an inducer of ROS (Wang *et al.*, 2005) for 48 hours and analyzed for cell death by TUNEL (Figure 14A). Cultures derived from Tg(SHaPrP, Δ STE)

mice revealed the greatest protection with half the cell loss compared to cultures from non-Tg wt mice and cultures prepared from *Prnp*^{-/-} mice showed over all the highest vulnerability (Figure 14B). These results are consistent with the findings in CHO-K1 cells (Figure 13). The data suggest ^{Sec}PrP averts cell death from ROS. Taken together with previous results the findings provide a basis for the proposed hypothesis by revealing how PrP^C can be both toxic and protective.

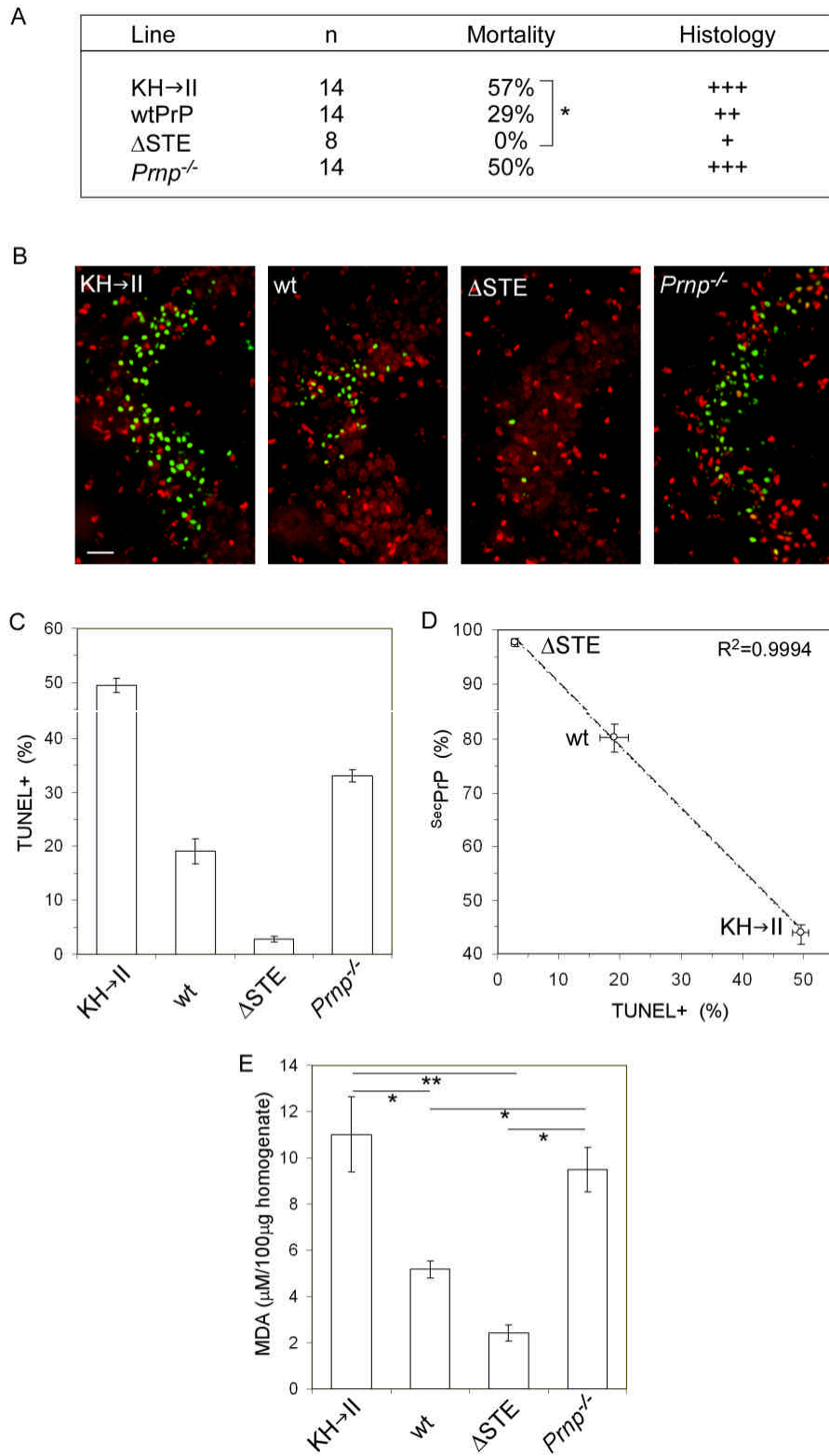


Legend Figure 14. Analysis of ^{Sec}PrP-mediated protection from in primary granule cell neurons. (A) ^{Sec}PrP protects primary cerebellar granule cell neurons (GCN) from oxidative insult. GCN cultures were prepared from 7-day-old Tg(SHaPrP, Δ STE) mice, non-Tg wt or *Prnp*^{-/-} and after three days of incubation were treated for 48 h with 100 μ M KA, fixed, then stained by TUNEL (green) and counterstained with DAPI (blue). Scale bar, 50 μ m. (B) Quantification of ROS vulnerability in cerebellar GCNs. The ratio of TUNEL+ to total nuclei was determined to establish the fraction of apoptotic cells. Multiple fields per coverslip were randomly selected for quantification purposes. Mean, SEM, (n=3), unpaired two-tailed T-test (**, P>0.001) for all comparisons to *Prnp*^{-/-} mice.

4. 11 A model system to probe both PrP^C functions *in vivo*: kainic acid-mediated neurodegeneration

The results thus far suggest ^{Ctm}PrP triggers apoptosis and ^{Sec}PrP protects cells from ROS. To understand how the two isoforms interplay *in vivo* and to further substantiate the observations made *in vitro*, mice were subjected to KA-induced seizures. KA triggers excitotoxic apoptosis in the pyramidal cell layer of the hippocampus and also leads to increased ROS which can independently trigger apoptosis (Wang *et al.*, 2005). This model system would likely enable me to test simultaneously the roles of ^{Ctm}PrP in excitotoxic apoptosis and of ^{Sec}PrP in neuroprotection from ROS.

Tg(SHaPrP, Δ STE), Tg(SHaPrP,KH \rightarrow II), *Prnp*^{-/-} and non-Tg wt mice treated with KA were monitored and, if still alive, were sacrificed 24 h later and their brain tissue analyzed for neuropathologic changes. While the extent of KA-induced seizure activity observed was comparable among all lines investigated, the mortality rate and extent of neurodegeneration were vastly different. Tg(SHaPrP,KH \rightarrow II) mice had the highest mortality rate. In contrast, none of the Tg(SHaPrP, Δ STE) mice died in response to KA treatment (Figure 15A). Brains of surviving mice were examined by histological analysis (Figure 15A) and TUNEL (Figure 15B), which consistently identified Tg(SHaPrP,KH \rightarrow II) with the highest incidence of TUNEL+ cells as quantified in the hippocampal CA3 region. In contrast, non-Tg wt mice revealed moderate numbers of TUNEL+ cells and Tg(SHaPrP, Δ STE) mice showed few TUNEL+ cells (Figure 15C).

Figure 15

Legend Figure 15. Analyzing the role of PrP^C topology in kainic acid-mediated neurodegeneration. (A) Tg(SHaPrP,KH→II), Tg(SHaPrP,ΔSTE), Tg(SHaPrP) and *Prnp*^{-/-} mice were treated with a single dose of subcutaneous KA sufficient to induce intermittent generalized tonic-clonic seizures. Mortality within the first 24 h was determined and pathologic damage was rated by examining brain sections stained with hematoxylin and eosin. Damage in the hippocampus was rated as mild (+), moderate (++) or severe (+++). ^{Ctm}PrP-expressing mice died at a significantly higher rate (*, P>0.01, Fisher's exact test) than mice expressing ^{Sec}PrP. (B) Hippocampal sections from treated mice were analyzed for apoptosis by TUNEL (green) and counterstained with PI (red). Mice expressing ^{Sec}PrP show very little apoptosis compared to ^{Ctm}PrP-expressing mice and *Prnp*^{-/-} mice. Scale bar, 10 μm. (C) Quantitative analysis of apoptosis in the CA3 region. The ratio of TUNEL+ nuclei to total nuclei was used to determine the fraction of apoptotic cells. Mean, SEM, n≤3, one-way ANOVA (P>0.0001), post-hoc Turkey multiple comparison test (P>0.001 for all pairs). (D) Neuroprotection is dependent on ^{Sec}PrP expression. Protection was assessed from the data in panel C and plotted against the propensity of PrP to be expressed as ^{Sec}PrP (Inverse fraction of ^{Ctm}PrP; Figure 11B) shows a correlation (R²= 0.9994). (E) KA-induced ROS in the hippocampus was assessed by measuring MDA levels in homogenates from mice subjected to KA. Mean, SEM, n=6, one-way ANOVA (P>0.0001), *post-hoc* Turkey multiple comparison test (*, P>0.05, **, P>0.001).

The relative contribution of ^{Ctm}PrP and ^{Sec}PrP levels to KA-mediated apoptosis was assessed by using the level of apoptosis in *Prnp*^{-/-} mice as a comparative baseline. Hence, both topological isoforms contributed to KA-mediated vulnerability (Figure 15C): ^{Sec}PrP-expression reduces apoptosis whereas ^{Ctm}PrP-expression enhances apoptosis. Most importantly, non-Tg wt mice displayed an intermediate position relative to mice favoring either ^{Ctm}PrP or ^{Sec}PrP expression in terms of both mortality (Figure 15A) and neuronal vulnerability to KA (Figure 15C) supporting the hypothesis PrP^C has the capacity to form both. Furthermore, the amount of cell death shows an inverse correlation to the propensity of the transgene to be synthesized in the ^{Sec}PrP isoform (Figure 15D). Therefore, apoptosis can be stimulated by ^{Ctm}PrP and averted by ^{Sec}PrP suggesting

neurodegeneration can result from both a loss of ^{Sec}PrP function and a gain of ^{Ctm}PrP function.

To explore the possibility ^{Sec}PrP is protecting neurons by preventing ROS mediated damage, hippocampal homogenates from KA-administered mice were analyzed for oxidative damage by measuring the amount of malondialdehyde (MDA). The lowest concentration of MDA was seen in Tg(SHaPrP, Δ STE) mice (Figure 15E) with levels comparable to untreated control animals (data not shown). Mice bearing increased cell death revealed the highest levels of MDA (compare Figure 15C and E), however MDA levels in *Prnp*^{-/-} and Tg(SHaPrP,KH \rightarrow II) mice were similar indicating a reduction in ROS is a result of ^{Sec}PrP expression and not affected by ^{Ctm}PrP expression. It should be noted that the difference in oxidative stress levels in the hippocampus was not significantly different among various untreated mouse lines (data not shown), therefore excluding the likelihood that these mice are not predisposed to increased oxidative stress levels. Furthermore, it suggests ^{Sec}PrP poses a benefit under acute ROS conditions and appears to have little impact on ROS levels under normal conditions. Taken together, these results indicate ^{Sec}PrP protects neurons from apoptosis by reducing KA-induced oxidative damage whereas ^{Ctm}PrP expression enhances neuronal vulnerability.

4.12 Probing the bifunctional hypothesis: Infectious prion disease and the role of topology

Motivated by observations that both $C^{tm}PrP$ and $SecPrP$ contribute to KA-mediated neurodegeneration, this same possibility was evaluated in mice inoculated with prions.

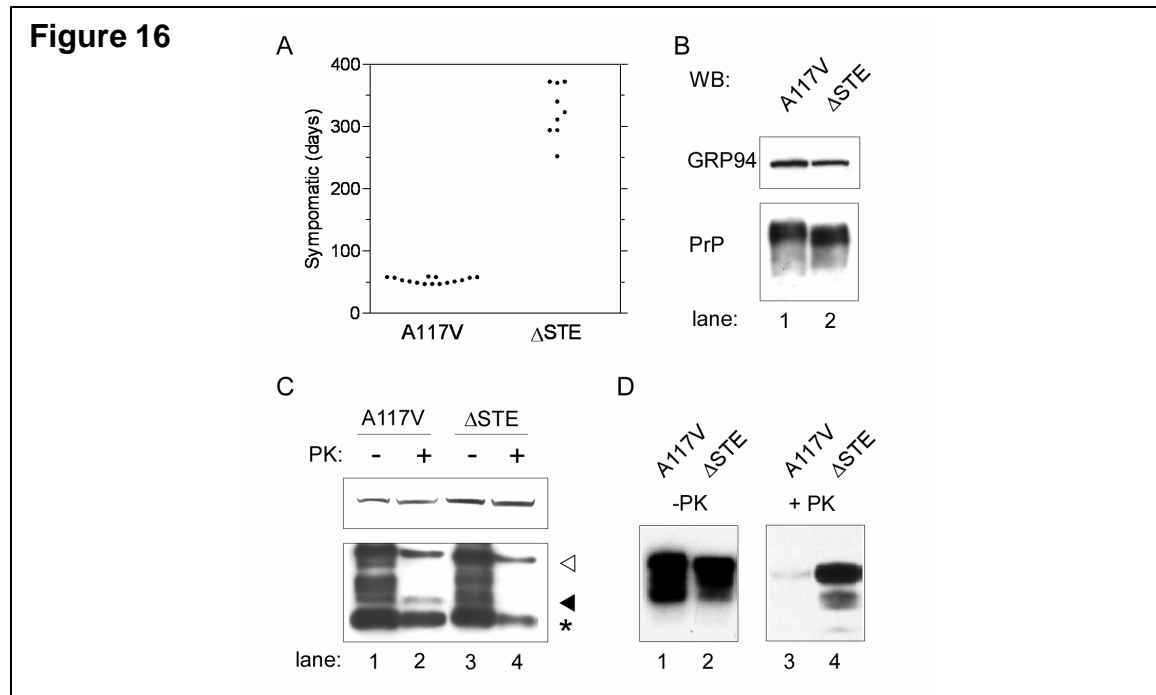
Two lines of evidence argue $C^{tm}PrP$ expression is a determinant of pathogenesis in infectious prion disease (Hegde *et al.*, 1999). First, the time point of disease onset inversely correlates with the CTM index, a measure of the absolute amount of $C^{tm}PrP$ expressed in the murine brain. Higher levels of endogenous $C^{tm}PrP$ at the time point of infection relate to shorter incubation periods. Second, upon infection with PrP^{Sc} , an increase in $C^{tm}PrP$ expression was detected. Elevation of $C^{tm}PrP$ may trigger pathogenic changes in prion disease, such as apoptosis as demonstrated in this study.

To dissect the contributions of $C^{tm}PrP$ and $SecPrP$ in the pathogenesis of infectious prion disease, Tg mice that expressed either increased $C^{tm}PrP$ or $SecPrP$ were inoculated with hamster Sc237 prions (Hegde *et al.*, 1999). To avoid interference from spontaneous neurodegeneration caused by $C^{tm}PrP$ expression, Tg mice that express $C^{tm}PrP$ to a lesser extent than the Tg(SHaPrP,KH→II) mice were used; these mice, designated Tg(SHaPrP,A117V), express PrP with an A117V mutation, develop spontaneous disease at ~572 days (Hegde *et al.*, 1998a) and clinical symptoms at ~51 days postinoculation with Sc237 prions (Figure 16A; Hegde *et al.*, 1999). In contrast, Tg(SHaPrP, Δ STE) mice, which express similar levels of PrP in the brain (Figure 16B) but do not express $C^{tm}PrP$

(Figures 6B, 6C and 16C), show no spontaneous neurodegeneration (up to 700 days of observation) and do not develop any symptoms until ~324 days postinoculation with Sc237 prions (Figure 16A; Hegde *et al.*, 1999). In comparison, Tg mice expressing wt PrP at ~2-fold higher PrP levels than Tg(SHaPrP,A117V) and Tg(SHaPrP, Δ STE) mice develop symptoms at ~55 days, and mice expressing wt PrP at a quarter of the expression levels develop symptoms at ~170 days postinoculation (Prusiner *et al.*, 1990). The data suggest disease progression is accelerated in Tg(SHaPrP,A117V) mice and attenuated in Tg(SHaPrP, Δ STE) mice, in respect to what would be expected in mice with similar wt PrP expression levels. Consistent with previous findings, the propensity of PrP^C to be expressed in the CtmPrP isoform is a key determinant of incubation time to disease onset upon inoculation with PrP^{Sc}. It should be noted that Tg(SHaPrP, Δ STE) mice lacking expression of CtmPrP still develop symptoms albeit after prolonged incubation.

Qualitative analysis of PrP^{Sc} accumulation in the brains of these ill mice revealed little PK-resistant PrP^{Sc} in Tg(SHaPrP,A117V) mice but abundant PK-resistant PrP^{Sc} in Tg(SHaPrP, Δ STE) mice (Figure 16D; Hegde *et al.*, 1999). Tg(SHaPrP,A117V) mice showed abundant PrP^{Sc} deposits in the thalamus, hypothalamus, piriform cortex and corpus callosum. In contrast, Tg(SHaPrP, Δ STE) mice showed PrP^{Sc} deposits through the entire brain with highest levels in the thalamus, midbrain, brainstem and cerebellum (Figure 17A and B). PrP^{Sc} accumulation in Tg(SHaPrP,A117V) mice was limited to brain regions close to the inoculation site as the incubation period was relatively short,

in comparison to Tg(SHaPrP, Δ STE) mice for which sufficient time was available for PrP^{Sc} to spread throughout the entire brain, which is in agreement with previous findings that accumulation of PrP^{Sc} does not correlate with pathogenesis or onset of disease (Hegde *et al.*, 1999; Chesebro *et al.*, 2005).



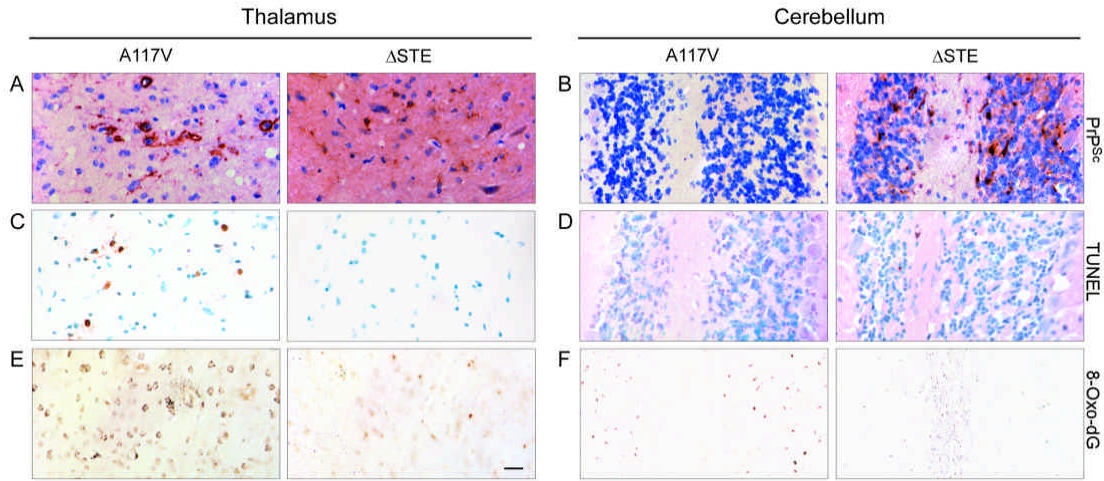
Legend Figure 16. Analysis of a dual role of PrP^C topology in transmissible prion disease. (A) The propensity to generate ^{C_{tm}}PrP dictates the time of disease onset in Tg(SHaPrP,A117V), n=15 and Tg(SHaPrP, Δ STE), n=9 mice inoculated with Sc237 prions. (B) Western-blot analysis show similar PrP expression levels in the brains of Tg(SHaPrP,A117V) and Tg(SHaPrP, Δ STE) mice. Blots were probed with anti-PrP and anti-GRP94 (loading control). (C) Topological (lanes 2 and 4) analysis of PrP in Tg(SHaPrP,A117V) and Tg(SHaPrP, Δ STE) mice. Brain homogenates were either left untreated (lanes 1 and 3) or treated with PK in the absence of detergent (lanes 2 and 4). Samples were deglycosylated prior to Western-blotting with anti-PrP and anti-GRP94 (loading control). Black arrowhead indicates ^{C_{tm}}PrP; white arrowhead indicates ^{Sec}PrP; asterisk denotes position of C1. (D) PrP^{Sc} accumulation in the brains of Tg mice inoculated with Sc237 prions. Brain homogenates were left either untreated (left panel) or treated under harsh PK conditions at 0.5 mg/ml for 1 h at 37 °C (right panel) and probed with an anti-PrP antibody by Western-blotting. Tg(SHaPrP, Δ STE) mice show marked accumulation of PrP^{Sc} compared to Tg(SHaPrP,A117V) mice.

4.13 Gain and loss of PrP^C functions: Oxidative stress and apoptosis in prion infected mice

Based on the notion that both apoptosis (Giese *et al.*, 1995; Liberski *et al.*, 2004) and oxidative stress (Milhavet *et al.*, 2000; Wong *et al.*, 2001) occur in PrP^{Sc}-inoculated subjects, a prediction was made that Tg(SHaPrP, Δ STE) mice would show little apoptosis and only signs of ROS accumulation whereas Tg(SHaPrP,A117V) mice would likely show both apoptosis and oxidative damage. Apoptosis and ROS accumulation were probed by immunohistochemistry with TUNEL and 8-hydroxy-2-deoxyguanosine (8-OHdG) respectively. In the brains of Sc237-infected Tg(SHaPrP,A117V) mice, TUNEL+ cells were found, with high levels in brain regions with PrP^{Sc} deposits, such as the thalamus (Figure 17C). Only a few TUNEL+ cells were detected in Tg(SHaPrP, Δ STE) mice, with most abundant levels in the cerebellum (Figure 17C and D). The data suggest apoptosis may play an important role in PrP^{Sc}-mediated pathogenesis in Tg(SHaPrP,A117V) mice. However, the substantially reduced apoptosis observed in Tg(SHaPrP, Δ STE) mice suggests other pathogenic mechanisms not associated with CtmPrP upregulation and apoptosis are revealed in these mice. The long incubation period in Tg(SHaPrP, Δ STE) mice suggests that gain of CtmPrP function plays a more dominant role in prion pathogenesis.

In both Tg(SHaPrP,A117V) and Tg(SHaPrP, Δ STE) mice, increased levels of 8-OHdG were observed in brain regions with the most prominent PrP^{Sc} deposits. For Tg(SHaPrP,A117V) mice, 8-OHdG was observed in several brain regions,

most extensively in the thalamus (Figure 17E and F). Increased 8-OHdG levels in Tg(SHaPrP, Δ STE) mice were found in the thalamus, midbrain, brainstem and cerebellum. In summary, the data reveal that pathogenesis in Tg(SHaPrP, Δ STE) mice have likely resulted from increased ROS which leads to neurodegeneration without triggering an apoptotic pathway involving chromosomal DNA-fragmentation. In contrast Tg(SHaPrP,A117V) mice succumbed to cell loss resulting from both apoptotic and non-apoptotic ROS related dysfunction or loss of neurons. Taken together, the data suggest that upregulation of ^{Ctm}PrP is not the sole mediator of pathogenesis. Additionally, the conversion of ^{Sec}PrP to PrP^{Sc} appears to lead to a loss of protection from oxidative insult.

Figure 17

Legend Figure 17. IHC of prion infected brains. (A and B) PrP^{Sc} staining in coronal brain sections from symptomatic Tg(SHaPrP,A117V) (left panel) and Tg(SHaPrP,ΔSTE) mice (right panel) inoculated with Sc237 prions. Tg(SHaPrP,A117V) mice only showed focal distribution of PrP^{Sc} limited to the thalamus, hypothalamus, piriform cortex and corpus callosum whereas Tg(SHaPrP,ΔSTE) mice showed diffuse deposits of PrP^{Sc} throughout the brain with high concentrations in the thalamus, cerebellum, midbrain and brainstem. (C and D) TUNEL staining in brain sections of symptomatic Tg(SHaPrP,A117V) mice show high levels of apoptosis in regions with abundant PrP^{Sc}. In contrast, few TUNEL+ cells are seen in symptomatic Tg(SHaPrP,ΔSTE) mice. (E and F) Oxidative stress-induced damage was determined by 8-OHdG staining. Tg(SHaPrP,A117V) mice (left panel) show positive nuclear or perinuclear staining in brain regions with increased deposits of PrP^{Sc}. Low levels of 8-OHdG were also detected in few unaffected brain regions, including the granule cell layer of the cerebellum. Tg(SHaPrP,ΔSTE) mice (right panel) show punctuate staining in white matter with some nuclear staining in the thalamus and cortical regions. Representative images are from the thalamus (panels A, C, E) and cerebellum (panels B, D, F). Scale bar, 50 μm.

5. Discussion

The physiologic function of PrP^C and its role in prion disease remains unclear as both neuroprotective (Chiarini *et al.*, 2002; Roucou *et al.*, 2004) and toxic functions (Westaway *et al.*, 1994; Shmerling *et al.*, 1998; Paitel *et al.*, 2003) have been described. Alongside these conflicting findings, a long-standing debate continues about whether prion disease pathogenesis results from a gain or a loss of PrP^C function or both (Brown, 2005; Harris & True, 2006). The data presented here provide a framework describing how heterogeneity of PrP^C topology can result in both pro- and anti-apoptotic functions and propose how both loss and gain of PrP^C-mediated functions could contribute to prion disease.

5.1 Conservation of PrP^C synthesis in multiple topological isoforms

It has previously been reported that PrP has been conserved throughout mammalian evolution (van Rhee *et al.*, 2003) suggesting an important function associated with PrP^C. Further sequence analysis performed in this study revealed topogenic STE and TM to be the most conserved domains within PrP. Given the notion that a single point mutation in these domains can have a dramatic impact on the ratio of topological isoforms (Kim & Hegde, 2002), it is tempting to speculate that the propensity to generate ^{C_{tm}}PrP and ^{Sec}PrP has been conserved which in turn indicates important physiological functions that may be associated with each isoform. However an alternative interpretation would be that the conservation of TM and STE domains is associated with a function distinct

from that ascribed as a topogenic determinant. Therefore the basis for the detected conservation awaits future determination.

5.2 PrP^C is synthesized as both ^{Sec}PrP and ^{Ctm}PrP under physiological conditions

In vitro studies have demonstrated the propensity of PrP^C to be expressed in three topological forms: ^{Sec}PrP, ^{Ctm}PrP and ^{Ntm}PrP (Hay *et al.*, 1987a; Hay *et al.*, 1987b; Hegde *et al.*, 1998a; Stewart & Harris, 2001). Under normal physiologic conditions the detection of PrP^C has been limited to ^{Sec}PrP and its truncated form C1 (Vincent *et al.*, 2000). *In vivo*, ^{Ctm}PrP and ^{Ntm}PrP have only been associated with pathologic conditions (Hegde *et al.*, 1998a; Hegde *et al.*, 1999; Risitano *et al.*, 2003; Stewart *et al.*, 2005); therefore it has been generally assumed that normal PrP^C consists of only ^{Sec}PrP. The data presented here suggests that PrP^C is expressed as both ^{Ctm}PrP and ^{Sec}PrP albeit ^{Ctm}PrP is expressed at very low levels as seen in normal non-Tg wt mice, which forms the basis for the hypothesis that both topological isoforms are physiologically relevant. As ^{Ntm}PrP was not detected at any instance in brains of mice it remains unclear if this is for technical reasons or a result of lack of expression in the adult tissue analyzed. The observation that both ^{Sec}PrP and ^{Ctm}PrP detected in wt PrP expressing mice are recognized and processed by the ER-folding machinery in a similar fashion is in agreement with the hypothesis that both isoforms are physiologically relevant. However, consideration should also be given to the potential idea that escaping from the quality control machinery of the ER could pose a pathologic mechanism

inherent to some secretory proteins. And indeed there is precedence that unglycosylated mutant PrP can reach the plasma membrane (Korth *et al.*, 2000) questioning the overall quality control fidelity attributed to PrP and raising the possibility that ^{Ctm}PrP could also escape the quality control mechanisms. However, it should also be noted that in most instances pathogenic and mutant PrP forms are retained in ER and degraded or accumulate in the cytoplasm (Ma & Lindquist, 2001; Stewart *et al.*, 2001; Grasbon-Frodol *et al.*, 2004). A further line of thought raises the possibility that our understanding of the quality control mechanisms of the ER are limited with unique scenarios that are yet to be defined. In light of these views further studies will be required to substantiate the finding made here if the small fraction of ^{Ctm}PrP detected under normal physiologic conditions is truly a *bona fide* folded isoform of PrP^C.

5.3 ^{Ctm}PrP dependent pathophysiological apoptosis

The detection of apoptosis in prion diseases has been described (Giese *et al.*, 1995; Liberski *et al.*, 2004) however the mechanisms underlying apoptosis have remained unclear. Also, the expression of ^{Ctm}PrP has been correlated with the development of neurodegeneration in genetic and infectious model systems (Hegde *et al.*, 1998a; Hegde *et al.*, 1999). The here presented results from transgenic mice and CHO-K1 cells suggest ^{Ctm}PrP can cause neurodegeneration through an apoptotic pathway. Tg(SHaPrP, KH→II) mice and Tg(tTA:mPrP) mice show increased expression of ^{Ctm}PrP and develop neurodegeneration with substantial loss of cerebellar granule cells. The detection of internucleosomal

DNA-fragmentation, pyknotic or fragmented nuclei and TUNEL+ cells along side with the detection of activated caspase-3 suggest cell death occurs through an apoptotic pathway. The contemporaneous detection of elevated $C^{tm}PrP$ expression further suggests apoptosis is likely triggered by $C^{tm}PrP$ expression. Furthermore, the lack of any mutation in Tg(tTA:mPrP) mice shows that $C^{tm}PrP$ production in Tg(SHaPrP, KH→II) mice is not just a result of the mutation itself and further delivers evidence that mere overexpression of PrP^C can lead to dramatic $C^{tm}PrP$ upregulation and apoptosis in the cerebellum of mice.

A direct relationship was further elucidated in cultured CHO-K1 cells and a strong correlation was revealed demonstrating the capacity of PrP to trigger apoptosis is dependent on the propensity of PrP to be made in the $C^{tm}PrP$ isoform. The expression of wt PrP^C also demonstrated a mild capacity to trigger cell death corresponding to the level of $C^{tm}PrP$ expression. It is likely that apoptosis triggered by $C^{tm}PrP$ is dependent on the activation of caspase-3 since both the activated form was detected and a significant reduction in apoptosis was observed by treatment with a caspase-3 inhibitor. Taken together the data suggests $C^{tm}PrP$ can trigger apoptosis in a dose dependent manner by a caspase-3-mediated pathway leading to cell loss and neurodegeneration. Given that $C^{tm}PrP$ has been implicated in both genetic (Hegde *et al.*, 1998a) and infectious prion diseases (Hegde *et al.*, 1999), it is likely that $C^{tm}PrP$ plays an important role contributing to neurodegeneration in these cases by triggering caspase-3 dependent apoptosis.

The implication of pro- and anti-apoptotic members of the Bcl-2 family on ^{Ctm}PrP mediated apoptosis was investigated. The overexpression of both anti-apoptotic proteins Bcl-2 and Bcl-XL significantly reduced the apoptotic potential of ^{Ctm}PrP. Moreover inhibition of Bax reduced the amount of apoptosis triggered by ^{Ctm}PrP. Hence apoptosis triggered by ^{Ctm}PrP may be Bax dependant which appears to be consistent with some experimental prion disease model systems which reveals at some instances Bax dependency (Chiesa *et al.*, 2005; Lyahyai *et al.*, 2006; Li *et al.*, 2007). Furthermore the ascribed BH2 like OR domain of ^{Ctm}PrP (LeBlanc & Roucou, 2003) could potentially interact with BH2 family members, since it has been reported that PrP can interact with Bcl-2 in a yeast two hybrid system (Kurschner & Morgan, 1995, 1996). However the relevance of these findings is questionable as the reproduction in mammalian systems has been futile (Kurschner & Morgan, 1996).

5.4 ^{Ctm}PrP dependent physiological apoptosis

A potential neurophysiologic role for ^{Ctm}PrP mediated apoptosis was highlighted in the SVZ and SE by quantitative TUNEL analysis. The SVZ and SE are two neurogenic niches where physiologic apoptosis occurs to dispose superfluous progenitor cells that fail to mature (Biebl *et al.*, 2000). Non-Tg wt mice, Tg(SHaPrP), Tg(SHaPrP, KH→II) mice all displayed similar and significantly higher apoptosis in the SVZ and SE compared to mice which do not express ^{Ctm}PrP as Tg(SHaPrP, ΔSTE) and *Prnp*^{-/-} mice, suggesting ^{Ctm}PrP may have a role triggering apoptosis in this physiological disposal process. It is surprising that

Tg(SHaPrP, KH→II) mice did not show more apoptosis than wt expressers. It could be speculated that those cells undergoing physiologic apoptosis are accustomed to the expression of ^{Ctm}PrP and are able to regulate it therefore no additional effect by increased ^{Ctm}PrP expression is observed. Consistent with the data presented here it has been reported that PrP^C can stimulate neurogenesis and leads to an increase in the progenitor population of the SVZ in wt mice in contrast to $Prnp^{-/-}$ mice (Steele *et al.*, 2006). Hence it is plausible that more excessive progenitors would need to be encountered by increased apoptosis as is seen here in this study, since no gross difference in the number of neurons or brain morphology is observed in $Prnp^{-/-}$ relative to wt mice (Bueler *et al.*, 1992; Manson *et al.*, 1994, Steele *et al.*, 2006). Taken together, the data suggest that ^{Ctm}PrP may play a role in regulating physiologic apoptosis in the SVZ and SE however under certain circumstances i.e. mutations in the STE and TM domains or infection with PrP^{Sc} can lead to pleiotropic expression of ^{Ctm}PrP which can cause neurodegeneration.

5.5 ^{Sec}PrP protects cells from ROS-mediated cell death

A neuroprotective role of PrP^C against oxidative stress has been suggested (Wong *et al.*, 2001; Brown *et al.*, 2002). Yet it remained unclear if this is specific to the ^{Sec}PrP isoform. In this study, a protective role for ^{Sec}PrP was identified in CHO-K1 cells, primary neuronal cultures and in transgenic mice. In all three model systems the ΔSTE mutant, which causes PrP^C to be almost exclusively made in the ^{Sec}PrP form, revealed the greatest protection to ROS, suggesting

that ^{Sec}PrP protects from oxidative insult and that the reduced protective capacity in wt PrP expressing cells, neurons or non-Tg wt mice emerges as a result of the increased ^{Ctm}PrP expression. Additionally, the cell culture model system shows that PrP^C can also display a protective function mediated by ^{Sec}PrP in the same cell type from the pro-apoptotic one provided by ^{Ctm}PrP.

5.6 Gain and loss of PrP^C mediated functions in non-Tg wt mice

A functional contribution of ^{Ctm}PrP and ^{Sec}PrP was identified in a model system for KA-mediated neurodegeneration. Clearly mice favoring ^{Sec}PrP expression revealed the greatest protection to the KA challenge in both terms of mortality and cell death in the pyramidal CA3 layer. The data indicates that this protection may arise from anti-oxidant properties of ^{Sec}PrP which abrogates cell death and concomitantly averts organismal mortality. In contrast, expression of ^{Ctm}PrP revealed to be most detrimental in response to KA with the highest mortality and the most dramatic apoptosis. The comparison of ^{Ctm}PrP favoring mice and *Prnp*^{-/-} mice suggests the additional cell death in ^{Ctm}PrP favoring mice is distinct from the loss of ^{Sec}PrP protection mediated cell death which appears to result from an increase in ROS. Therefore, the data can be interpreted to conclude that both topological isoforms of PrP^C may contribute to KA-mediated vulnerability: ^{Ctm}PrP triggers ROS independent apoptosis whereas ^{Sec}PrP protects from ROS dependent apoptosis. A decrease of ^{Sec}PrP expression and an increase in ^{Ctm}PrP expression are likely independent effects that can work in concert to contribute to KA-induced vulnerability suggesting that both a gain of ^{Ctm}PrP and loss of ^{Sec}PrP

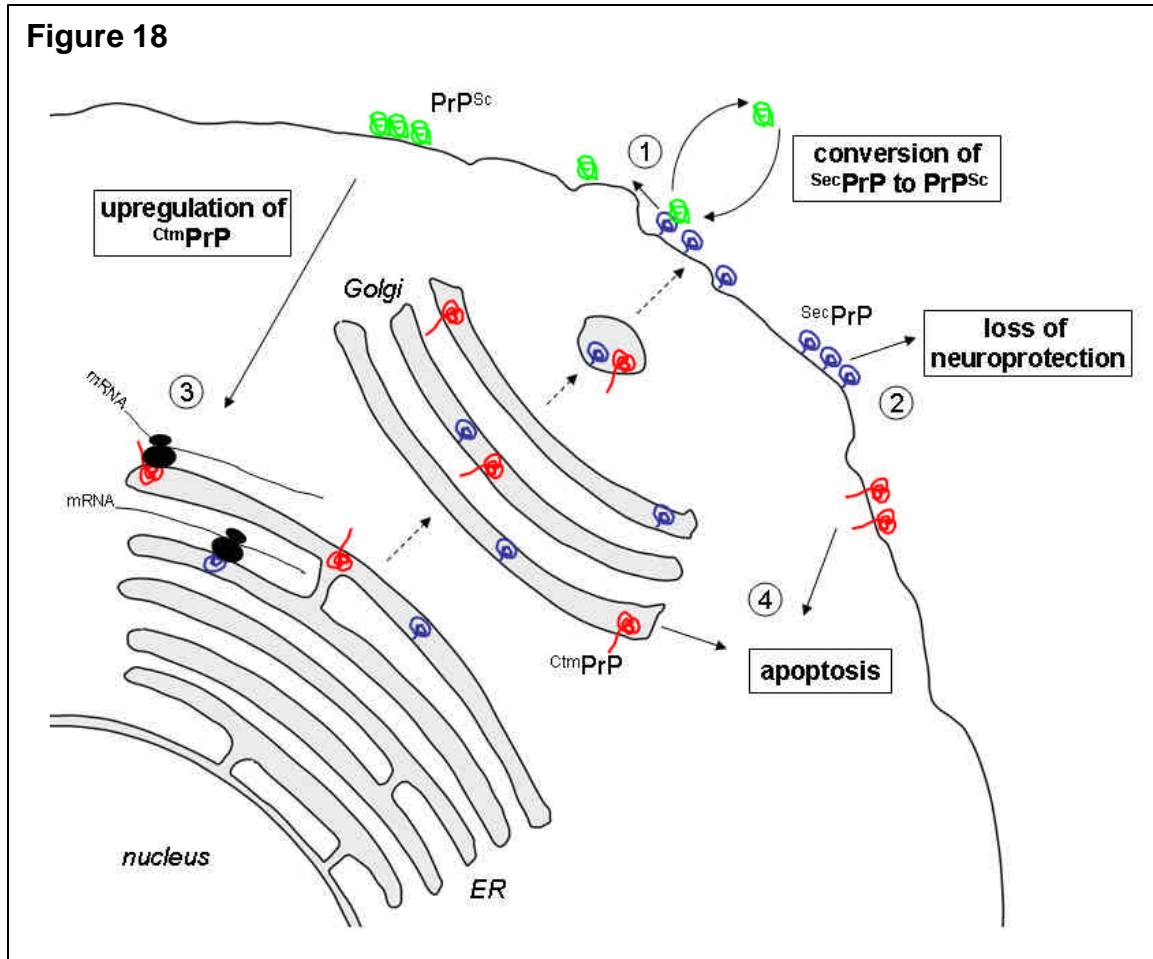
can lead to neurodegeneration. It is conceivable that differences in relative and absolute levels of $^{\text{Sec}}\text{PrP}$ and $^{\text{Ctm}}\text{PrP}$ may not be the only means to trigger independent pro- and anti-apoptotic functions of $^{\text{Ctm}}\text{PrP}$ and $^{\text{Sec}}\text{PrP}$ respectively but potentially also counteract the function of one another directly contributing to the overall outcome of cell death or cell survival which can not be readily discerned from the direct effect of each isoform in this model system.

Non-Tg wt mice recapitulated the activities of both isoforms as seen in regard to its capacity to trigger apoptosis and in regard to the protection from oxidative stress. Therefore it can be reasoned that the reduced neuroprotection of non-Tg wt mice likely results from both the reduced propensity of PrP^{C} to form $^{\text{Sec}}\text{PrP}$ and its increased propensity to form $^{\text{Ctm}}\text{PrP}$ relative to Tg(SHaPrP, ΔSTE) mice providing functional evidence that PrP^{C} displays $^{\text{Sec}}\text{PrP}$ -dependent and $^{\text{Ctm}}\text{PrP}$ -dependent functions *in vivo*.

5.7 Gain of $^{\text{Ctm}}\text{PrP}$ function and loss of $^{\text{Sec}}\text{PrP}$ function in transmissible prion disease

Finally, the data presented here suggests that both $^{\text{Sec}}\text{PrP}$ and $^{\text{Ctm}}\text{PrP}$ contribute to neurodegeneration in prion disease by loss- or gain-of-functions, respectively. To dissect the contribution of each PrP^{C} isoform in prion disease, mice favoring expression of either the $^{\text{Ctm}}\text{PrP}$ or $^{\text{Sec}}\text{PrP}$ isoform were inoculated with PrP^{Sc} ; both groups developed neurodegeneration, although at different time points and with different pathologic changes in their brains. The data suggest that Tg(SHaPrP,A117V) mice succumbed to both apoptosis as a result of $^{\text{Ctm}}\text{PrP}$

upregulation and oxidative stress-mediated neurodegeneration as a result of $^{\text{Sec}}\text{PrP}$ conversion to PrP^{Sc} . Conversely, the much-delayed pathogenesis in Tg(SHaPrP, Δ STE) mice appeared to result from the increased oxidative damage due to the loss of $^{\text{Sec}}\text{PrP}$ function. In conclusion, a model can be derived from the given data: The $^{\text{Sec}}\text{PrP}$ -to- PrP^{Sc} conversion leads to a loss of the neuroprotective function of $^{\text{Sec}}\text{PrP}$ resulting in a higher susceptibility of infected cells to ROS. Additionally, PrP^{Sc} accumulation leads to upregulation of $^{\text{Ctm}}\text{PrP}$, which triggers apoptosis (Summarized in Figure 18). Therefore, pathophysiology of infectious prion disease is possibly facilitated by *both* the apoptotic effects of $^{\text{Ctm}}\text{PrP}$ and the loss of the protective effects of $^{\text{Sec}}\text{PrP}$. These findings provide context for various studies that have proposed different mechanisms for PrP^{C} -mediated neurodegeneration including apoptosis and oxidative damage, and reconcile how both gain and loss (Brown, 2005; Harris & True, 2006) of PrP^{C} functions may occur in prion disease. Since the detection of $^{\text{Ctm}}\text{PrP}$ and PrP^{Sc} both relies on proteolysis new methods of detection for $^{\text{Ctm}}\text{PrP}$ will need to be developed to establish a direct relationship of $^{\text{Ctm}}\text{PrP}$ induction to transmissible prion disease like conformation specific antibodies that unmistakably identify the different isoforms of PrP without the need for proteolysis hence permitting *in situ* detection of $^{\text{Ctm}}\text{PrP}$ which would make it possible to probe in various disease model systems if in PrP^{Sc} affected brain regions $^{\text{Ctm}}\text{PrP}$ is induced. Furthermore, such a reagent would help to delineate the physiological role of $^{\text{Ctm}}\text{PrP}$ in the SVZ and SE.



Legend Figure 18. Model of PrP^C-mediated pathogenesis in transmissible prion disease. Shown is the default secretory pathway (dashed lines). PrP^C is cotranslationally synthesized at the ER as either SecPrP (blue) or CtmPrP (red), which is shuttled to the Golgi where further N-glycan maturation occurs, then delivered to the plasma membrane by endosomal vesicles (Gu *et al.*, 2006). During infection with PrP^{Sc} (green), conversion of SecPrP to PrP^{Sc} occurs (1) on the plasma membrane, exosomes or lysosomes (Vey *et al.*, 1996; Fevrier *et al.*, 2005). This conversion leads to a loss of neuroprotective function of SecPrP to oxidative stress (2), resulting in cell dysfunction or death without DNA-fragmentation. Additionally, an accumulation of PrP^{Sc} leads to upregulation of CtmPrP (3, Hegde *et al.*, 1999) resulting in increased apoptosis (4).

5.8 Bifunctional physiological roles for PrP^C

In this study, multiple lines of evidence converged to set forth the hypothesis PrP^C consists of two topological isoforms with independent functional roles: First, both ^{Sec}PrP and ^{Ctm}PrP were detected in brains of non-Tg wt mice. Second, both isoforms showed an equal degree of N-glycan maturation. Third, the propensity of wt PrP^C to express ^{Ctm}PrP correlated with its capacity to trigger apoptosis. Fourth, a putative physiological role for ^{Ctm}PrP mediated apoptosis was identified in the SVZ and SE of non-Tg wt mice. Fifth, the capacity of PrP^C to protect from ROS was dependant on the expression of ^{Sec}PrP. Sixth, both functional contributions of ^{Sec}PrP and ^{Ctm}PrP were observed under acute excitotoxic and oxidative stress conditions in non-Tg wt mice. Seventh, the analysis of the pathophysiologic mechanisms underlying infectious disease revealed both gain and loss of PrP^C-mediated functions identifying an engagement of both isoforms in the pathogenesis process, all supportive of the hypothesis that PrP^C naturally consists of both ^{Ctm}PrP and ^{Sec}PrP with pro- and anti-apoptotic functions, respectively and reconcile how PrP^C can be both protective and toxic (Brown, 2005; Harris & True, 2006).

5.9 Proposed novelties of this study

In this thesis several advances could be made:

First, previous studies have suggested that PrP^C is solely expressed as ^{Sec}PrP in brains of wild type mice (Hegde *et al.*, 1998a; Stewart *et al.*, 2005) and that ^{Ctm}PrP is only expressed under pathological conditions (Hegde *et al.*, 1998a;

Hegde *et al.*, 1999; Stewart *et al.*, 2005). In this study data is provided that shows under physiological conditions in addition to the ^{Sec}PrP isoform, PrP^C is also expressed as ^{Ctm}PrP albeit at extremely low levels, suggesting PrP^C can naturally be expressed as both ^{Sec}PrP and ^{Ctm}PrP.

Second, the expression of ^{Ctm}PrP has been previously linked to the onset of neurodegeneration in both genetic and transmissible prion diseases (Hegde *et al.*, 1998a; Hegde *et al.*, 1999; Stewart *et al.*, 2005). Yet the mechanism by which ^{Ctm}PrP could trigger disease remained unclear. An indication was provided by previous studies revealing that apoptosis may play a role in the manifestation of prion diseases (Giese *et al.*, 1995; Liberski *et al.*, 2004). The data in this study suggest that pleiotropic expression of ^{Ctm}PrP causes neurodegeneration by activating an apoptotic pathway in a dose dependant manner. Furthermore, the data demonstrate that ^{Ctm}PrP mediated apoptosis is likely executed by pro-apoptotic molecules Bax and caspase-3 and abrogated by anti-apoptotic Bcl-2.

Third, a previous study revealed that PrP^C may stimulate neurogenesis (Steele *et al.*, 2006) however it remained unclear why an increase in neuronal numbers or changes in brain morphology are lacking (Bueler *et al.*, 1992; Manson *et al.*, 1994, Steele *et al.*, 2006). A potential explanation for this phenomenon was provided by observations made in this study which revealed that a lack of ^{Ctm}PrP expression results in reduced apoptosis in neurogenic brain regions of the SVZ and SE. Extrapolation of the aforementioned findings suggests ^{Ctm}PrP may regulate the number of progenitor cells by triggering apoptosis establishing a potential physiologic role for ^{Ctm}PrP.

Fourth, both neurotoxic (Westaway *et al.*, 1994; Shmerling *et al.*, 1998; Paitel *et al.*, 2003) and neuroprotective (Bounhar *et al.*, 2001; Chiarini *et al.*, 2002; Roucou *et al.*, 2004) functions have been proposed for PrP^C however it has remained unresolved by which mechanism these diametrically opposed functions may unfold. In this study it was demonstrated that functional manifestation of PrP^C is dependent on the expression of the topological isoform of PrP^C. A neuroprotective function against oxidative stress was attributed to the expression of ^{Sec}PrP whereas a neurotoxic function triggering apoptosis was identified under conditions that favor the expression of ^{Ctm}PrP.

Fifth, it has previously been reported that PrP^C exhibits neuroprotective and anti-oxidant activity (Bounhar *et al.*, 2001; Brown *et al.*, 1997; Wong *et al.*, 2001). In this study it could be demonstrated that the neuroprotective activity of PrP^C is attributed specifically to ^{Sec}PrP isoform both *in vitro* and *in vivo*. Furthermore, it was demonstrated that not only does ^{Sec}PrP reduce the oxidative burden to pyramidal neurons of the hippocampus but can also avert organismal mortality.

Sixth, It is becoming increasingly clear that PrP^C plays a central role in the pathogenesis of transmissible prion disease (Chesebro *et al.*, 2005) however it has been subject of debate whether this occurs through a gain of toxic function as has been proposed for ^{Ctm}PrP or a loss of protective function associated with PrP^C (Brown, 2005; LeBlanc & Roucou, 2003; Harris & True, 2006). Previous studies have revealed that apoptosis (Giese *et al.*, 1995; Liberski *et al.*, 2004) and oxidative damage (Milhavet *et al.*, 2000; Wong *et al.*, 2001; Brown, 2005) may both occur during prion disease. Evidence presented here in this study

reveals that upregulation of ^{Ctm}PrP which has been demonstrated previously (Hegde *et al.*, 1999), correlates with abbreviated onset of disease and as shown here is accompanied by increased apoptosis and oxidative damage in brain areas with PrP^{Sc} accumulation. Conversion of ^{Sec}PrP to PrP^{Sc} and its concomitant loss of activity lead to a higher susceptibility to oxidative stress, albeit it appears that the loss of ^{Sec}PrP function is not as strong a determinant of the pathogenesis process as the upregulation of ^{Ctm}PrP associated gain of apoptotic activity. Taken together, the data presented here provide a basis reconciling how both gain and loss of PrP^C functions may occur in transmissible prion disease.

5.10 The world of PrP^C heterogeneity

The heterogeneity of PrP^C extends beyond the topological isoforms described and characterized here in this study. Glycosylation variants (Pan *et al.*, 2002), truncated forms (Vincent *et al.*, 2000), a soluble form lacking the GPI anchor (Perini *et al.*, 1996) and a cytoplasmic form have been also described. Cytoplasmic PrP can cause cell death and neurodegeneration (Ma *et al.*, 2002) however a protective role against Bax-mediated apoptosis has also been described (Roucou *et al.*, 2003). A role in natural prion disease remains to be described while studies in wt mice suggests that it may naturally occur in neurons (Mironov *et al.*, 2003). The formation of cytoplasmic PrP has been linked to both retrotranslocation of PrP from the ER (Wang *et al.*, 2005) and leaky ribosome scanning (Kang *et al.*, 2006). The notion that it has the BH2 like OR domain also exposed in the cytoplasm makes it like ^{Ctm}PrP a candidate interacting partner

with the BH2 family proteins. It will be most interesting to see if cytoplasmic PrP also plays a role in any form of prion disease and if and what type of physiological role it may exhibit.

Recently, it has also been proposed that integrase dependent proteolytic cleavage of PrP^C can produce the C1 truncated form of PrP^C that can also trigger apoptosis (Sunyach *et al.*, 2007). The data in this study do not reveal any toxic activity associated with C1, since the Δ STE mutant produces abundant C1 yet lacks any sign of toxicity. Hence future investigation will be required to identify this discrepancy.

Furthermore, over 50 different glycosylation variants have been described for PrP^C (Pan *et al.*, 2002). Whether a specific physiological and pathological role can be attributed to these forms remains unanswered. Also clarification of a potential role for NtmPrP awaits future studies.

Finally, it should be noted that despite strong evidence presented here in this study it can not be ruled out if other variants of PrP^C that escaped detection by the methods employed here in this study which may also contribute to one or several of the here made observations. It is conceivable that conditions that favor the formation of CtmPrP could potentially also favor the generation of a yet another form of PrP^C which is actually toxic and CtmPrP only an innocent bystander which may equally apply to the role proposed for SecPrP. Certainly future studies will shed light on this question and it will be interesting to see what roles all these different forms may ultimately have.

5.11 Protein heterogeneity: A new paradigm?

The focus of this study was to demonstrate the potential of PrP^C to be expressed in two topological forms that partake in independent functions. PrP^C may represent a novel class of proteins that are potentially bifunctional, but as far as is known, can have their function changed only by a change in *de novo* synthesis. Thus, the term PrP^C is ambiguous, as it does not specify *which* topological isoform is being referred to, a description of which can change either spatially or temporally, in processes that can be either physiological or pathological, in which PrP^C is involved. It is important to note that conventional proteomic analysis measuring simply the level of PrP^C expression would have missed the occurrence of multiple PrP^C topological isoforms. It is possible that proteins other than PrP^C display multi-functionality due to isoforms different in conformation but not topology, therefore making them even more difficult to detect. Therefore the question emerges whether this level of heterogeneity may be applied more universally to other mammalian or eukaryotic proteins has emerged to further increase the output of the genome. Therefore, it will be most interesting to see whether the “one gene-one protein” hypothesis will hold to the scrutiny of future experimentation.

6. Summary

The physiological function of the cellular prion protein (PrP^{C}) and its contribution to prion diseases remains enigmatic as evidence suggests both pro- and anti-apoptotic functions. The data presented here suggest PrP^{C} is expressed in two topological isoforms with unique functional manifestations and with the participation of both in the pathogenesis of prion disease. Expression of two topological isoforms were identified in wild type mice, a fully secreted isoform, designated SecPrP and a small fraction as a single spanning transmembrane isoform designated CtmPrP . By introducing mutations that favor expression in either SecPrP or CtmPrP the functional role of each form was dissected. Transgenic mice that favor CtmPrP expression develop spontaneous neurodegeneration with evidence of apoptotic cell death. Further investigation in cultured mammalian cells identified a Bax and caspase-3 dependant pathway by which CtmPrP triggers apoptosis in a dose dependant manner. In contrast, SecPrP reveals a protective role against apoptosis as seen in the hippocampus of transgenic mice challenged with kainic acid which otherwise leads to dramatic cell death by increased oxidative stress. The observation was made that CtmPrP favoring mice are most vulnerable to kainic acid mediated neurodegeneration where as SecPrP favoring mice are the least vulnerable to the same treatment. The protective role of SecPrP against oxidative stress was confirmed in cultured mammalian cells and primary cultured neurons. Finally, the contribution of each isoform was assessed in mice inoculated with prions (PrP^{Sc}). Mice favoring expression in the CtmPrP form developed symptoms at ~50 days and showed focal accumulation of PrP^{Sc} and

neurodegeneration proximal to the inoculation site with indications of both apoptotic and oxidative stress related degeneration. Mice favoring expression in the $^{\text{Sec}}\text{PrP}$ form develop symptoms at ~320 days with accumulation of PrP^{Sc} throughout the brain yet only show signs of oxidative stress related damage.

In conclusion, evidence is provided that wild type PrP^{C} has the intrinsic capacity to be expressed as either $^{\text{Sec}}\text{PrP}$ or $^{\text{Ctm}}\text{PrP}$ and that each isoform can partake in independent pathways. $^{\text{Sec}}\text{PrP}$ participates in a neuroprotective pathway against oxidative stress whereas $^{\text{Ctm}}\text{PrP}$ activates a caspase-3 dependant apoptotic pathway. Further evidence suggests that both isoforms participate in the etiology of infectious prion disease: upregulation of $^{\text{Ctm}}\text{PrP}$ which leads to apoptosis and conversion of $^{\text{Sec}}\text{PrP}$ to PrP^{Sc} and its down regulation lead to a higher susceptibility to oxidative stress, thus being able to reconcile how both gain and loss of PrP^{C} functions may occur.

7. Zusammenfassung

Prionen sind infektiöse Eiweiße, die fatale neurodegenerative Erkrankungen in Säugetieren hervorrufen können. Es wird angenommen, dass die pathologische Isoform *das sogenannte PrP^{Sc}* die Umfaltung der zellulären Isoform des Prion-Proteins (PrP^C) in weitere krankheitserregende PrP^{Sc} katalysiert. Es gibt jedoch Indizien die darauf hindeuten, dass PrP^C an der Erkrankung beteiligt ist und das PrP^{Sc} nicht unmittelbar zur Neurodegeneration beiträgt. Ein Modell des zellbiologischen Krankheitsverlaufs geht davon aus, dass PrP^C toxische Aktivität besitzt, ein anderes Modell geht davon aus, dass der Verlust von PrP^C und seiner neuroprotektiven Aktivität für die Symptome verantwortlich ist. Die Entdeckung zweier unterschiedlicher Isoformen von PrP^C könnte nun beide Modelle vereinen. *In vitro* Analyse der PrP^C-Synthese zeigt, dass PrP^C in drei topologische Isoformen synthetisiert werden kann. Zwei dieser Isoformen durchspannen die Zellmembran in entgegengesetzter Orientierung, eine mit dem C-terminus (^{Ctm}PrP), die andere mit dem N-terminus (^{Ntm}PrP) im Zytoplasma. und die dritte Form ist ein sekretiertes Protein (^{Sec}PrP).

In der vorliegenden Arbeit wird untersucht, ob die Funktion von PrP^C von seiner Faltung abhängt. Zuerst konnte gezeigt werden, dass unter physiologischen Bedingungen sowohl ^{Sec}PrP als auch ^{Ctm}PrP *in vivo* exprimiert werden. Um Erkenntnisse über die Funktion der jeweiligen Isoform zu erhalten wurden Mausmodelle und Zellkulturmodelle untersucht, die bevorzugt jeweils ^{Sec}PrP oder ^{Ctm}PrP exprimieren. Mit Hilfe dieser Modelle konnte ich eine pro-apoptotische Aktivität von ^{Ctm}PrP nachweisen, die sich unter Mitwirkung der Proteine Bax und

Caspase-3 vollzieht. Ich konnte auch zeigen, dass die Proteine Bcl-2 und Bcl-XL der apoptotischen Aktivität von ^{Ctm}PrP entgegen wirken können. Darüberhinaus zeigte sich, dass ohne ^{Ctm}PrP eine verringerte Apoptose in Gehirnregionen mit Neurogenese vorliegt. Deshalb liegt die Vermutung nahe, dass ^{Ctm}PrP die Entstehung neuronaler Vorläuferzellen regelt. Im Gegensatz zu ^{Ctm}PrP zeichnet sich ^{Sec}PrP durch eine neuroprotektive Funktion aus, die vor oxidativer Schädigung schützt. Die Isoform ^{Sec}PrP schützt Pyramidal-Zellen des Hippokampus vor Apoptose die durch erhöhte oxidative Schädigung hervorgerufen wird. Die Daten lassen die Schlussfolgerung zu, dass sowohl ^{Ctm}PrP als auch ^{Sec}PrP physiologische Funktionen besitzen.

Pathophysiologisch manifestieren sich diese zellbiologischen Prozesse wie folgt: Mäuse die hauptsächlich ^{Ctm}PrP exprimieren erkranken wesentlich schneller, wiesen weniger PrP^{Sc} auf, und zeigten sowohl apoptotische als auch oxidative Neurodegeneration. Hingegen erkrankten Mäuse, die hauptsächlich ^{Sec}PrP exprimieren wesentlich später, trotz weit verbreiteter PrP^{Sc} Akkumulation und ohne Anzeichen für Apoptose. Die Daten lassen die Schlussfolgerung zu, dass in infektiösen Prionen-Erkrankungen ^{Ctm}PrP die Apoptose einleitet, und das ^{Sec}PrP durch die Umwandlung zu PrP^{Sc} seine schützende Funktion verliert.

9. References

Aguzzi A, Heikenwalder M and Polymenidou M. **2007**. Insights into prion strains and neurotoxicity. *Nat Rev Mol Cell Biol*, **8**:552-561.

Basler K, Oesch B, Scott M, Westaway D, Walchli M, Groth D F, McKinley M P, Prusiner S B and Weissmann C. **1986**. Scrapie and cellular PrP isoforms are encoded by the same chromosomal gene. *Cell*, **46**:417-428.

Biebl M, Cooper C M, Winkler J and Kuhn H G. **2000**. Analysis of neurogenesis and programmed cell death reveals a self-renewing capacity in the adult rat brain. *Neurosci Lett*, **291**:17-20.

Blattler T, Brandner S, Raeber A J, Klein M A, Voigtlander T, Weissmann C and Aguzzi A. **1997**. PrP-expressing tissue required for transfer of scrapie infectivity from spleen to brain. *Nature*, **389**:69-73.

Bounhar Y, Zhang Y, Goodyer C G and LeBlanc A. **2001**. Prion protein protects human neurons against Bax-mediated apoptosis. *J Biol Chem*, **276**:39145-39149.

Brown D R. **2005**. Neurodegeneration and oxidative stress: prion disease results from loss of antioxidant defence. *Folia Neuropathol*, **43**:229-243.

Brown D R, Nicholas R S and Canevari L. **2002**. Lack of prion protein expression results in a neuronal phenotype sensitive to stress. *J Neurosci Res*, **67**:211-224.

Brown D R, Schulz-Schaeffer W J, Schmidt B and Kretzschmar H A. **1997**. Prion protein-deficient cells show altered response to oxidative stress due to decreased SOD-1 activity. *Exp Neurol*, **146**:104-112.

Brown D R, Wong B S, Hafiz F, Clive C, Haswell S J and Jones I M. **1999**. Normal prion protein has an activity like that of superoxide dismutase. *Biochem J*, **344 Pt 1**:1-5.

Bruce M, Chree A, McConnell I, Foster J, Pearson G and Fraser H. **1994**. Transmission of bovine spongiform encephalopathy and scrapie to mice: strain variation and the species barrier. *Philos Trans R Soc Lond B Biol Sci*, **343**:405-411.

Bueler H, Aguzzi A, Sailer A, Greiner R A, Autenried P, Aguet M and Weissmann C. **1993**. Mice devoid of PrP are resistant to scrapie. *Cell*, **73**:1339-1347.

Bueler H, Fischer M, Lang Y, Bluethmann H, Lipp H P, DeArmond S J, Prusiner S B, Aguet M and Weissmann C. **1992**. Normal development and behaviour of mice lacking the neuronal cell-surface PrP protein. *Nature*, **356**:577-582.

Bueler H, Raeber A, Sailer A, Fischer M, Aguzzi A and Weissmann C. **1994**. High prion and PrP^{Sc} levels but delayed onset of disease in scrapie-inoculated mice heterozygous for a disrupted PrP gene. *Mol Med*, **1**:19-30.

Carlson G A, Kingsbury D T, Goodman P A, Coleman S, Marshall S T, DeArmond S, Westaway D and Prusiner S B. **1986**. Linkage of prion protein and scrapie incubation time genes. *Cell*, **46**:503-511.

Caughey B, Neary K, Buller R, Ernst D, Perry L L, Chesebro B and Race R E. **1990**. Normal and scrapie-associated forms of prion protein differ in their sensitivities to phospholipase and proteases in intact neuroblastoma cells. *J Virol*, **64**:1093-1101.

Celis J E. **1998**. *Cell biology : a laboratory handbook*, San Diego: Academic Press.

Chesebro B, Trifilo M, Race R, Meade-White K, Teng C, LaCasse R, Raymond L, Favara C, Baron G, Priola S, Caughey B, Masliah E and Oldstone M. **2005**. Anchorless prion protein results in infectious amyloid disease without clinical scrapie. *Science*, **308**:1435-1439.

Chiarini L B, Freitas A R, Zanata S M, Brentani R R, Martins V R and Linden R. **2002**. Cellular prion protein transduces neuroprotective signals. *Embo J*, **21**:3317-3326.

Chiesa R, Drisaldi B, Quaglio E, Migheli A, Piccardo P, Ghetti B and Harris D A. **2000**. Accumulation of protease-resistant prion protein (PrP) and apoptosis of cerebellar granule cells in transgenic mice expressing a PrP insertional mutation. *Proc Natl Acad Sci U S A*, **97**:5574-5579.

Chiesa R and Harris D A. **2001**. Prion diseases: what is the neurotoxic molecule? *Neurobiol Dis*, **8**:743-763.

Chiesa R, Piccardo P, Dossena S, Nowoslawski L, Roth K A, Ghetti B and Harris D A. **2005**. Bax deletion prevents neuronal loss but not neurological symptoms in a transgenic model of inherited prion disease. *Proc Natl Acad Sci U S A*, **102**:238-243.

Collinge J, Whittington M A, Sidle K C, Smith C J, Palmer M S, Clarke A R and Jefferys J G. **1994**. Prion protein is necessary for normal synaptic function. *Nature*, **370**:295-297.

Curtis J, Errington M, Bliss T, Voss K and MacLeod N. **2003**. Age-dependent loss of PTP and LTP in the hippocampus of PrP-null mice. *Neurobiol Dis*, **13**:55-62.

De Armond S J, Gonzales M, Mobley W C, Kon A A, Stern A, Prusiner H and Prusiner S B. **1989**. PrPSc in scrapie-infected hamster brain is spatially and temporally related to histopathology and infectivity titer. *Prog Clin Biol Res*, **317**:601-618.

Ellgaard L and Helenius A. **2003**. Quality control in the endoplasmic reticulum. *Nat Rev Mol Cell Biol*, **4**:181-191.

Ellgaard L, Molinari M and Helenius A. **1999**. Setting the standards: quality control in the secretory pathway. *Science*, **286**:1882-1888.

Falcone D, Do H, Johnson A E and Andrews D W. **1999**. Negatively charged residues in the IgM stop-transfer effector sequence regulate transmembrane polypeptide integration. *J Biol Chem*, **274**:33661-33670.

Fassio A and Sitia R. **2002**. Formation, isomerisation and reduction of disulphide bonds during protein quality control in the endoplasmic reticulum. *Histochem Cell Biol*, **117**:151-157.

Fevrier B, Vilette D, Laude H and Raposo G. **2005**. Exosomes: a bubble ride for prions? *Traffic*, **6**:10-17.

Floyd R A and Carney J M. **1992**. Free radical damage to protein and DNA: mechanisms involved and relevant observations on brain undergoing oxidative stress. *Ann Neurol*, **32 Suppl**:S22-27.

Fons R D, Bogert B A and Hegde R S. **2003**. Substrate-specific function of the translocon-associated protein complex during translocation across the ER membrane. *J Cell Biol*, **160**:529-539.

Giese A, Groschup M H, Hess B and Kretzschmar H A. **1995**. Neuronal cell death in scrapie-infected mice is due to apoptosis. *Brain Pathol*, **5**:213-221.

Grasbon-Frodl E, Lorenz H, Mann U, Nitsch R M, Windl O and Kretzschmar H A. **2004**. Loss of glycosylation associated with the T183A mutation in human prion disease. *Acta Neuropathol (Berl)*, **108**:476-484.

Graur D and Li W-H. **2000**. *Fundamentals of molecular evolution*, Sunderland, Mass.: Sinauer Associates.

Gu Y, Luo X, Basu S, Fujioka H and Singh N. **2006**. Cell-specific metabolism and pathogenesis of transmembrane prion protein. *Mol Cell Biol*, **26**:2697-2715.

Guentchev M, Siedlak S L, Jarius C, Tagliavini F, Castellani R J, Perry G, Smith M A and Budka H. **2002**. Oxidative damage to nucleic acids in human prion disease. *Neurobiol Dis*, **9**:275-281.

Guentchev M, Voigtlander T, Haberler C, Groschup M H and Budka H. **2000**. Evidence for oxidative stress in experimental prion disease. *Neurobiol Dis*, **7**:270-273.

Harris D A and True H L. **2006**. New insights into prion structure and toxicity. *Neuron*, **50**:353-357.

Hay B, Barry R A, Lieberburg I, Prusiner S B and Lingappa V R. **1987**. Biogenesis and transmembrane orientation of the cellular isoform of the scrapie prion protein [published erratum appears in *Mol Cell Biol* 1987 May;7(5):2035]. *Mol Cell Biol*, **7**:914-920.

Hay B, Prusiner S B and Lingappa V R. **1987**. Evidence for a secretory form of the cellular prion protein. *Biochemistry*, **26**:8110-8115.

Hayat M A. **2004**. *Immunohistochemistry and in situ hybridization of human carcinomas*, Boston: Elsevier Academic Press.

Hebert D N, Garman S C and Molinari M. **2005**. The glycan code of the endoplasmic reticulum: asparagine-linked carbohydrates as protein maturation and quality-control tags. *Trends Cell Biol*, **15**:364-370.

Hegde R S, Mastrianni J A, Scott M R, DeFea K A, Tremblay P, Torchia M, DeArmond S J, Prusiner S B and Lingappa V R. **1998 (a)**. A transmembrane form of the prion protein in neurodegenerative disease. *Science*, **279**:827-834.

Hegde R S, Tremblay P, Groth D, DeArmond S J, Prusiner S B and Lingappa V R. **1999**. Transmissible and genetic prion diseases share a common pathway of neurodegeneration. *Nature*, **402**:822-826.

Hegde R S, Voigt S and Lingappa V R. **1998 (b)**. Regulation of protein topology by trans-acting factors at the endoplasmic reticulum. *Mol Cell*, **2**:85-91.

Hegde R S, Voigt S, Rapoport T A and Lingappa V R. **1998 (c)**. TRAM regulates the exposure of nascent secretory proteins to the cytosol during translocation into the endoplasmic reticulum. *Cell*, **92**:621-631.

Heitz S, Lutz Y, Rodeau J L, Zanjani H, Gautheron V, Bombarde G, Richard F, Fuchs J P, Vogel M W, Mariani J and Bailly Y. **2007**. BAX contributes to Doppel-induced apoptosis of prion-protein-deficient Purkinje cells. *Dev Neurobiol*, **67**:670-686.

Helenius A and Aebi M. **2004**. Roles of N-linked glycans in the endoplasmic reticulum. *Annu Rev Biochem*, **73**:1019-1049.

Herscovics A. **1999**. Importance of glycosidases in mammalian glycoprotein biosynthesis. *Biochim Biophys Acta*, **1473**:96-107.

Johnson A E and van Waes M A. **1999**. The translocon: a dynamic gateway at the ER membrane. *Annu Rev Cell Dev Biol*, **15**:799-842.

Kang S W, Rane N S, Kim S J, Garrison J L, Taunton J and Hegde R S. **2006**. Substrate-specific translocational attenuation during ER stress defines a pre-emptive quality control pathway. *Cell*, **127**:999-1013.

Katz F N, Rothman J E, Lingappa V R, Blobel G and Lodish H F. **1977**. Membrane assembly in vitro: synthesis, glycosylation, and asymmetric insertion of a transmembrane protein. *Proc Natl Acad Sci U S A*, **74**:3278-3282.

Kellings K, Meyer N, Mirenda C, Prusiner S B and Riesner D. **1992**. Further analysis of nucleic acids in purified scrapie prion preparations by improved return refocusing gel electrophoresis. *J Gen Virol*, **73 (Pt 4)**:1025-1029.

Kellings K, Prusiner S B and Riesner D. **1994**. Nucleic acids in prion preparations: unspecific background or essential component? *Philos Trans R Soc Lond B Biol Sci*, **343**:425-430.

-
- Kerr J F, Wyllie A H and Currie A R. **1972**. Apoptosis: a basic biological phenomenon with wide-ranging implications in tissue kinetics. *Br J Cancer*, **26**:239-257.
- Kim S J and Hegde R S. **2002**. Cotranslational partitioning of nascent prion protein into multiple populations at the translocation channel. *Mol Biol Cell*, **13**:3775-3786.
- Kimberlin R H. **1991**. An overview of bovine spongiform encephalopathy. *Dev Biol Stand*, **75**:75-82.
- Kitamoto T, Ogomori K, Tateishi J and Prusiner S B. **1987**. Formic acid pretreatment enhances immunostaining of cerebral and systemic amyloids. *Lab Invest*, **57**:230-236.
- Korsmeyer S J. **1995**. Regulators of cell death. *Trends Genet*, **11**:101-105.
- Korth C, Kaneko K and Prusiner S B. **2000**. Expression of unglycosylated mutated prion protein facilitates PrP(Sc) formation in neuroblastoma cells infected with different prion strains. *J Gen Virol*, **81**:2555-2563.
- Kretzschmar H A, Prusiner S B, Stowring L E and DeArmond S J. **1986**. Scrapie prion proteins are synthesized in neurons. *Am J Pathol*, **122**:1-5.

Kurschner C and Morgan J I. **1995**. The cellular prion protein (PrP) selectively binds to Bcl-2 in the yeast two-hybrid system. *Brain Res Mol Brain Res*, **30**:165-168.

Kurschner C and Morgan J I. **1996**. Analysis of interaction sites in homo- and heteromeric complexes containing Bcl-2 family members and the cellular prion protein. *Brain Res Mol Brain Res*, **37**:249-258.

LeBlanc A C and Roucou X. **2003**. Toxicity and protection in prions. *Science*, **301**:168-169; author reply 168-169.

Leclerc E, Peretz D, Ball H, Solfrosi L, Legname G, Safar J, Serban A, Prusiner S B, Burton D R and Williamson R A. **2003**. Conformation of PrP(C) on the cell surface as probed by antibodies. *J Mol Biol*, **326**:475-483.

Li A, Barmada S J, Roth K A and Harris D A. **2007**. N-terminally deleted forms of the prion protein activate both Bax-dependent and Bax-independent neurotoxic pathways. *J Neurosci*, **27**:852-859.

Liberski P P, Sikorska B, Bratosiewicz-Wasik J, Gajdusek D C and Brown P. **2004**. Neuronal cell death in transmissible spongiform encephalopathies (prion diseases) revisited: from apoptosis to autophagy. *Int J Biochem Cell Biol*, **36**:2473-2490.

Lingappa V R, Lingappa J R, Prasad R, Ebner K E and Blobel G. **1978**. Coupled cell-free synthesis, segregation, and core glycosylation of a secretory protein.

Proc Natl Acad Sci U S A, **75**:2338-2342.

Lledo P M, Tremblay P, DeArmond S J, Prusiner S B and Nicoll R A. **1996**. Mice deficient for prion protein exhibit normal neuronal excitability and synaptic

transmission in the hippocampus. *Proc Natl Acad Sci U S A*, **93**:2403-2407.

Lok J and Martin L J. **2002**. Rapid subcellular redistribution of Bax precedes caspase-3 and endonuclease activation during excitotoxic neuronal apoptosis in rat brain. *J Neurotrauma*, **19**:815-828.

Lowenstein D H, Butler D A, Westaway D, McKinley M P, DeArmond S J and Prusiner S B. **1990**. Three hamster species with different scrapie incubation times and neuropathological features encode distinct prion proteins. *Mol Cell Biol*, **10**:1153-1163.

Lyahyai J, Bolea R, Serrano C, Monleon E, Moreno C, Osta R, Zaragoza P, Badiola J J and Martin-Burriel I. **2006**. Correlation between Bax overexpression and prion deposition in medulla oblongata from natural scrapie without evidence of apoptosis. *Acta Neuropathol (Berl)*, **112**:451-460.

Ma J and Lindquist S. **2001**. Wild-type PrP and a mutant associated with prion disease are subject to retrograde transport and proteasome degradation. *Proc Natl Acad Sci U S A*, **98**:14955-14960.

Ma J, Wollmann R and Lindquist S. **2002**. Neurotoxicity and neurodegeneration when PrP accumulates in the cytosol. *Science*, **298**:1781-1785.

Maglio L E, Perez M F, Martins V R, Brentani R R and Ramirez O A. **2004**. Hippocampal synaptic plasticity in mice devoid of cellular prion protein. *Brain Res Mol Brain Res*, **131**:58-64.

Mallucci G, Dickinson A, Linehan J, Klohn P C, Brandner S and Collinge J. **2003**. Depleting neuronal PrP in prion infection prevents disease and reverses spongiosis. *Science*, **302**:871-874.

Manson J C, Clarke A R, Hooper M L, Aitchison L, McConnell I and Hope J. **1994**. 129/Ola mice carrying a null mutation in PrP that abolishes mRNA production are developmentally normal. *Mol Neurobiol*, **8**:121-127.

McLennan N F, Brennan P M, McNeill A, Davies I, Fotheringham A, Rennison K A, Ritchie D, Brannan F, Head M W, Ironside J W, Williams A and Bell J E. **2004**. Prion protein accumulation and neuroprotection in hypoxic brain damage. *Am J Pathol*, **165**:227-235.

Milhavet O, McMahon H E, Rachidi W, Nishida N, Katamine S, Mange A, Arlotto M, Casanova D, Riondel J, Favier A and Lehmann S. **2000**. Prion infection impairs the cellular response to oxidative stress. *Proc Natl Acad Sci U S A*, **97**:13937-13942.

Mironov A, Jr., Latawiec D, Wille H, Bouzamondo-Bernstein E, Legname G, Williamson R A, Burton D, DeArmond S J, Prusiner S B and Peters P J. **2003**. Cytosolic prion protein in neurons. *J Neurosci*, **23**:7183-7193.

Molinari M and Sitia R. **2005**. The secretory capacity of a cell depends on the efficiency of endoplasmic reticulum-associated degradation. *Curr Top Microbiol Immunol*, **300**:1-15.

Moore R C, Lee I Y, Silverman G L, Harrison P M, Strome R, Heinrich C, Karunaratne A, Pasternak S H, Chishti M A, Liang Y, Mastrangelo P, Wang K, Smit A F, Katamine S, Carlson G A, Cohen F E, Prusiner S B, Melton D W, Tremblay P, Hood L E and Westaway D. **1999**. Ataxia in prion protein (PrP)-deficient mice is associated with upregulation of the novel PrP-like protein doppel. *J Mol Biol*, **292**:797-817.

Oltvai Z N, Milliman C L and Korsmeyer S J. **1993**. Bcl-2 heterodimerizes in vivo with a conserved homolog, Bax, that accelerates programmed cell death. *Cell*, **74**:609-619.

Ott C M and Lingappa V R. **2002**. Integral membrane protein biosynthesis: why topology is hard to predict. *J Cell Sci*, **115**:2003-2009.

Paitel E, Alves da Costa C, Vilette D, Grassi J and Checler F. **2002**. Overexpression of PrP^C triggers caspase 3 activation: potentiation by

proteasome inhibitors and blockade by anti-PrP antibodies. *J Neurochem*, **83**:1208-1214.

Paitel E, Fahraeus R and Checler F. **2003**. Cellular prion protein sensitizes neurons to apoptotic stimuli through Mdm2-regulated and p53-dependent caspase 3-like activation. *J Biol Chem*, **278**:10061-10066.

Paitel E, Sunyach C, Alves da Costa C, Bourdon J C, Vincent B and Checler F. **2004**. Primary cultured neurons devoid of cellular prion display lower responsiveness to staurosporine through the control of p53 at both transcriptional and post-transcriptional levels. *J Biol Chem*, **279**:612-618.

Palade G. **1975**. Intracellular aspects of the process of protein synthesis. *Science*, **189**:347-358.

Pan T, Li R, Wong B S, Liu T, Gambetti P and Sy M S. **2002**. Heterogeneity of normal prion protein in two- dimensional immunoblot: presence of various glycosylated and truncated forms. *J Neurochem*, **81**:1092-1101.

Perini F, Vidal R, Ghetti B, Tagliavini F, Frangione B and Prelli F. **1996**. PrP27-30 is a normal soluble prion protein fragment released by human platelets. *Biochem Biophys Res Commun*, **223**:572-577.

Pitonzo D and Skach W R. **2006**. Molecular mechanisms of aquaporin biogenesis by the endoplasmic reticulum Sec61 translocon. *Biochim Biophys Acta*, **1758**:976-988.

Porter A G and Janicke R U. **1999**. Emerging roles of caspase-3 in apoptosis. *Cell Death Differ*, **6**:99-104.

Prusiner S B. **1998**. Prions. *Proc Natl Acad Sci U S A*, **95**:13363-13383.

Prusiner S B, Scott M, Foster D, Pan K M, Groth D, Miranda C, Torchia M, Yang S L, Serban D, Carlson G A and et al. **1990**. Transgenic studies implicate interactions between homologous PrP isoforms in scrapie prion replication. *Cell*, **63**:673-686.

Prusiner S B, Scott M R, DeArmond S J and Cohen F E. **1998**. Prion protein biology. *Cell*, **93**:337-348.

Riesner D. **2003**. Biochemistry and structure of PrP(C) and PrP(Sc). *Br Med Bull*, **66**:21-33.

Risitano A M, Holada K, Chen G, Simak J, Vostal J G, Young N S and Maciejewski J P. **2003**. CD34+ cells from paroxysmal nocturnal hemoglobinuria (PNH) patients are deficient in surface expression of cellular prion protein (PrP_c). *Exp Hematol*, **31**:65-72.

Roucou X, Gains M and LeBlanc A C. **2004**. Neuroprotective functions of prion protein. *J Neurosci Res*, **75**:153-161.

Roucou X, Guo Q, Zhang Y, Goodyer C G and LeBlanc A C. **2003**. Cytosolic prion protein is not toxic and protects against Bax-mediated cell death in human primary neurons. *J Biol Chem*, **278**:40877-40881.

Sadlish H and Skach W R. **2004**. Biogenesis of CFTR and other polytopic membrane proteins: new roles for the ribosome-translocon complex. *J Membr Biol*, **202**:115-126.

Safar J G, Kellings K, Serban A, Groth D, Cleaver J E, Prusiner S B and Riesner D. **2005**. Search for a prion-specific nucleic acid. *J Virol*, **79**:10796-10806.

Sailer A, Bueler H, Fischer M, Aguzzi A and Weissmann C. **1994**. No propagation of prions in mice devoid of PrP. *Cell*, **77**:967-968.

Sambrook J and Russell D W. **2001**. *Molecular cloning : a laboratory manual*, Cold Spring Harbor, N.Y.: Cold Spring Harbor Laboratory Press.

Sawada M, Hayes P and Matsuyama S. **2003**. Cytoprotective membrane-permeable peptides designed from the Bax-binding domain of Ku70. *Nat Cell Biol*, **5**:352-357.

Serban D, Taraboulos A, DeArmond S J and Prusiner S B. **1990**. Rapid detection of Creutzfeldt-Jakob disease and scrapie prion proteins. *Neurology*, **40**:110-117.

Shimizu S, Eguchi Y, Kosaka H, Kamiike W, Matsuda H and Tsujimoto Y. **1995**. Prevention of hypoxia-induced cell death by Bcl-2 and Bcl-xL. *Nature*, **374**:811-813.

Shmerling D, Hegyi I, Fischer M, Blattler T, Brandner S, Gotz J, Rulicke T, Flechsig E, Cozzio A, von Mering C, Hangartner C, Aguzzi A and Weissmann C. **1998**. Expression of amino-terminally truncated PrP in the mouse leading to ataxia and specific cerebellar lesions. *Cell*, **93**:203-214.

Stadelmann C and Lassmann H. **2000**. Detection of apoptosis in tissue sections. *Cell Tissue Res*, **301**:19-31.

Staley K, Blaschke A J and Chun J. **1997**. Apoptotic DNA fragmentation is detected by a semi-quantitative ligation-mediated PCR of blunt DNA ends. *Cell Death Diff*:66-75.

Steele A D, Emsley J G, Ozdinler P H, Lindquist S and Macklis J D. **2006**. Prion protein (PrP^c) positively regulates neural precursor proliferation during developmental and adult mammalian neurogenesis. *Proc Natl Acad Sci U S A*, **103**:3416-3421.

Stewart R S, Drisaldi B and Harris D A. **2001**. A transmembrane form of the prion protein contains an uncleaved signal peptide and is retained in the endoplasmic Reticulum. *Mol Biol Cell*, **12**:881-889.

Stewart R S and Harris D A. **2001**. Most pathogenic mutations do not alter the membrane topology of the prion protein. *J Biol Chem*, **276**:2212-2220.

Stewart R S and Harris D A. **2005**. A transmembrane form of the prion protein is localized in the golgi apparatus of neurons. *J Biol Chem*, **280**:15855-64.

Stewart R S, Piccardo P, Ghetti B and Harris D A. **2005**. Neurodegenerative illness in transgenic mice expressing a transmembrane form of the prion protein. *J Neurosci*, **25**:3469-3477.

Sunyach C, Cisse M A, da Costa C A, Vincent B and Checler F. **2007**. The C-terminal products of cellular prion protein processing, C1 and C2, exert distinct influence on p53-dependent staurosporine-induced caspase-3 activation. *J Biol Chem*, **282**:1956-1963.

Thompson J D, Higgins D G and Gibson T J. **1994**. CLUSTAL W: improving the sensitivity of progressive multiple sequence alignment through sequence weighting, position-specific gap penalties and weight matrix choice. *Nucleic Acids Res*, **22**:4673-4680.

Tobler I, Deboer T and Fischer M. **1997**. Sleep and sleep regulation in normal and prion protein-deficient mice. *J Neurosci*, **17**:1869-1879.

Tremblay P, Meiner Z, Galou M, Heinrich C, Petromilli C, Lisse T, Cayetano J, Torchia M, Mobley W, Bujard H, DeArmond S J and Prusiner S B. **1998**.

Doxycycline control of prion protein transgene expression modulates prion disease in mice. *Proc Natl Acad Sci U S A*, **95**:12580-12585.

van Rheede T, Smolenaars M M W, Madsen O and de Jong W W. **2003**. Molecular Evolution of the Mammalian Prion Protein. *Mol Biol Evol*, **20**:111-121.

Vey M, Pilkuhn S, Wille H, Nixon R, DeArmond S J, Smart E J, Anderson R G, Taraboulos A and Prusiner S B. **1996**. Subcellular colocalization of the cellular and scrapie prion proteins in caveolae-like membranous domains. *Proc Natl Acad Sci U S A*, **93**:14945-14949.

Vila M, Jackson-Lewis V, Vukosavic S, Djaldetti R, Liberatore G, Offen D, Korsmeyer S J and Przedborski S. **2001**. Bax ablation prevents dopaminergic neurodegeneration in the 1-methyl-4-phenyl-1,2,3,6-tetrahydropyridine mouse model of Parkinson's disease. *Proc Natl Acad Sci U S A*, **98**:2837-2842.

Vincent B, Paitel E, Frobert Y, Lehmann S, Grassi J and Checler F. **2000**. Phorbol ester-regulated cleavage of normal prion protein in HEK293 human cells and murine neurons. *J Biol Chem*, **275**:35612-35616.

Vincent B, Paitel E, Saftig P, Frobert Y, Hartmann D, De Strooper B, Grassi J, Lopez-Perez E and Checler F. **2001**. The disintegrins ADAM10 and TACE contribute to the constitutive and phorbol ester-regulated normal cleavage of the cellular prion protein. *J Biol Chem*, **276**:37743-37746.

- Walter P and Johnson A E. **1994**. Signal sequence recognition and protein targeting to the endoplasmic reticulum membrane. *Annu Rev Cell Biol*, **10**:87-119.
- Walz R, Amaral O B, Rockenbach I C, Roesler R, Izquierdo I, Cavalheiro E A, Martins V R and Brentani R R. **1999**. Increased sensitivity to seizures in mice lacking cellular prion protein. *Epilepsia*, **40**:1679-1682.
- Wang Q, Yu S, Simonyi A, Sun G Y and Sun A Y. **2005**. Kainic acid-mediated excitotoxicity as a model for neurodegeneration. *Mol Neurobiol*, **31**:3-16.
- Wang X, Wang F, Sy M S and Ma J. **2005**. Calpain and other cytosolic proteases can contribute to the degradation of retro-translocated prion protein in the cytosol. *J Biol Chem*, **280**:317-325.
- Weissmann C. **2004**. The state of the prion. *Nat Rev Microbiol*, **2**:861-871.
- Westaway D, DeArmond S J, Cayetano-Canlas J, Groth D, Foster D, Yang S L, Torchia M, Carlson G A and Prusiner S B. **1994**. Degeneration of skeletal muscle, peripheral nerves, and the central nervous system in transgenic mice overexpressing wild-type prion proteins. *Cell*, **76**:117-129.
- Westaway D, Goodman P A, Mirenda C A, McKinley M P, Carlson G A and Prusiner S B. **1987**. Distinct prion proteins in short and long scrapie incubation period mice. *Cell*, **51**:651-662.

- Wilesmith J W, Ryan J B and Atkinson M J. **1991**. Bovine spongiform encephalopathy: epidemiological studies on the origin. *Vet Rec*, **128**:199-203.
- Won M H, Kang T C, Jeon G S, Lee J C, Kim D Y, Choi E M, Lee K H, Choi C D, Chung M H and Cho S S. **1999**. Immunohistochemical detection of oxidative DNA damage induced by ischemia-reperfusion insults in gerbil hippocampus in vivo. *Brain Res*, **836**:70-78.
- Wong B S, Brown D R, Pan T, Whiteman M, Liu T, Bu X, Li R, Gambetti P, Olesik J, Rubenstein R and Sy M S. **2001**. Oxidative impairment in scrapie-infected mice is associated with brain metals perturbations and altered antioxidant activities. *J Neurochem*, **79**:689-698.
- Wong B S, Liu T, Li R, Pan T, Petersen R B, Smith M A, Gambetti P, Perry G, Manson J C, Brown D R and Sy M S. **2001**. Increased levels of oxidative stress markers detected in the brains of mice devoid of prion protein. *J Neurochem*, **76**:565-572.
- Wong B S, Pan T, Liu T, Li R, Petersen R B, Jones I M, Gambetti P, Brown D R and Sy M S. **2000**. Prion disease: A loss of antioxidant function? *Biochem Biophys Res Commun*, **275**:249-252.
- Yin X M, Oltvai Z N, Veis-Novack D J, Linette G P and Korsmeyer S J. **1994**. Bcl-2 gene family and the regulation of programmed cell death. *Cold Spring Harb Symp Quant Biol*, **59**:387-393.

Yost C S, Lopez C D, Prusiner S B, Myers R M and Lingappa V R. **1990**. Non-hydrophobic extracytoplasmic determinant of stop transfer in the prion protein. *Nature*, **343**:669-672.

9. Acknowledgements

First and foremost I would like to thank Vishu Lingappa from the University of California, San Francisco for providing me with the opportunity to conduct research in a very fascinating field. I am most grateful for all the years of continuous support I received with stimulating discussions on science, mankind and philosophy. I am also most grateful for the trust, support and liberty I received to venture in the world of experimentation as I pleased, so that I was forced to fully submerge myself and deal with every little aspect associated with an academic position in science.

Also, my sincere thanks goes to Jonathan Howard from the University of Cologne (Cologne, Germany) who was willing to support my endeavor coming to San Francisco. I will always have pleasant memory of the days I spent in his lab during my "Diplom" thesis.

I would also like to thank Steve De Armond from the University of California, San Francisco (UCSF, San Francisco, CA, USA) who introduced me to neuropathology and the art of detecting apoptotic nuclei.

I am also most grateful to Patricia Spilman from the De Armond lab for the continuous assistance I received with immunohistochemistry, and being a friend in those discouraging moments.

I would like to thank Stan Prusiner (UCSF) for the valuable discussions and encouragement he provided alongside with critical comments on the manuscripts. Furthermore, I would also like to thank members from his Laboratory Giuseppe Legname and Hana Serban for generously providing me with antibodies and recombinant PrP, Haydn Bell for generously providing me with peptides and Jiri Safar for stimulating discussions. My Thank also goes to Hang Nguyen for valuable suggestions on scientific writing .

I would like to thank Francis Fimantag, Chris Petromilli and others from the Hunters Point animal facility for the maintenance, breeding and typing of mice and the conductance of the animal experiments including doxycyline and prion administration.

I would also like thank Zhiqun Tanz and Steven Schreiber from the University of California, Irvine, (UCI, Irvine, CA, USA) for all their help and invaluable expertise with the kainic acid model system.

I would also like to thank Carsten Korth (Heinrich Heine University, Düsseldorf, Germany) for the many years of interesting collaboration and teaching me the how to make monoclonal antibodies. Also I am grateful for the stimulating discussions and for all the encouragement.

Furthermore, I would like to thank Manu Hedge (National Institute of Health, Bethesda, MD, USA) for providing TRAPalpha anti-sera and valuable suggestions on how to pursue my project.

I would like to thank members of the Lingappa laboratory, Toshi Yamaji, Carolyn Ott and Tom Rutkowski for the technical advice and stimulating discussions. I would like to thank Fred Cayalag for the help I received with sacrificing animals and preparing brain homogenates and May Zimmerman for assistance I received with cell culture experiments. My thanks also goes to the visiting students Mayank Mehorata and Ma'ayan Liebermann for the tutoring exposure they provided me and the help I received.

My dearest appreciation goes to my "sweetie" I-Ting Jaing for the years of emotional support in these everlasting times.

Finally, but most importantly I would like to thank my parents for the unlimited love, care and support they provided me with throughout my life without which I would have not come this far in the first place.

10. Erklärung

Ich versichere, daß ich die von mir vorgelegte Dissertation selbständig angefertigt, die benutzten Quellen und Hilfsmittel vollständig angegeben und die Stellen der Arbeit - einschließlich Tabellen, Karten und Abbildungen -, die anderen Werken im Wortlaut oder dem Sinn nach entnommen sind, in jedem Einzelfall als Entlehnung kenntlich gemacht habe; daß diese Dissertation noch keiner anderen Fakultät oder Universität zur Prüfung vorgelegen hat; daß sie noch nicht veröffentlicht worden ist sowie, daß ich eine solche Veröffentlichung vor Abschluß des Promotionsverfahrens nicht vornehmen werde. Die Bestimmungen dieser Promotionsordnung sind mir bekannt. Die von mir vorgelegte Dissertation ist von Prof. Dr. Jonathan Howard Prof. betreut worden. Die Durchführung des experimentellen Teiles dieser Doktorarbeit wurde an der University of California, San Francisco, USA unter der Betreuung von Professor Dr. Vishwanth R. Lingappa vorgenommen.

San Francisco, den 15.10.2007

11. Lebenslauf

Name Sam Saghafi

Geboren 02. Juni 1972 in London, GB

Nationalität britisch

Familienstand ledig

1977 – 1978 Vorschule London, England

1978 – 1980 Ross Elementary School, St. Louis, USA

1980 – 1982 Iran Zamin International School, Tehran, Iran

1982 – 1983 Grundschule Reiskirchen, Hessen

1983 – 1989 Gesamtschule Bonn - Beuel

Juni 1989 Fachoberschulreife mit Qualifikation für die gymnasiale Oberstufe

1989 – 1990 Harrison High School, Colorado Springs, USA

1990 – 1991 Christian Brothers College, Bulawayo, Simbabwe

1991 – 1992 Zimbabwe Distance Education College Harare, Simbabwe

Juni 1993 General Certificate of Education (Hochschulreife)

1993 – 1994 Selbstfindungs Jahr; musizierende Tätigkeiten

1994 – 2000 Biologie Studium an der Universität zu Köln
Titel der Diplomarbeit: Self-Assembly von DNA-Molekülen:
Eine formale 32-Bit Grammatik.

- Dez. 2000 Abschluß des Biologie Studiums mit der Gesamtnote sehr gut. Verleihung des Diplom Grades.
- Juli 2001 Beginn der Promotion an der Universität zu Köln bei Prof. Dr. Jonathan C. Howard
- Seit Sep. 2001 Junior Wissenschaftler an der University of California, San Francisco bei Prof. Dr. Vishwanath R. Lingappa